Detecting local surface motion of pastures on peat soils using laser scanning technology

Ze Li

TU Delft

Detecting local surface motion of pastures on peat soils using laser scanning technology

by

Ze Li

to obtain the degree of Master of Science
at the Delft University of Technology,

to be defended publicly on Tuesday January 12, 2021 at 08:30 AM.

Student number:	4903811	
Thesis committee:	Prof. dr. ir. R. F. Hanssen,	TU Delft, Geoscience and Remote Sensing
	Dr. R. C. Lindenbergh,	TU Delft, Geoscience and Remote Sensing
	Prof. dr. ir. S. C. Steele-Dunne,	TU Delft, Water Management

TU Delft

Preface

In mid-January of 2020, I was excited to start this project. One year has passed, I am about to finish it now. This preface means the end of my MSc study at TU Delft, as well as my stay at this beautiful country–the Netherlands. I have learned a lot professional knowledge during these two years, which has broaden my view on the field of remote sensing. It definitely changes the perspectives I see things and the track of my life. While many things have changed and will keep changing, one thing will not: I will continue to work in the field of science of remote sensing technology in order to make our planet be better understood.

All of these may not happen without Ramon Hanssen, who is the main supervisor of my graduation project. I would like to thank Ramon for introducing me to this topic, and his excellent guidance throughout the entire project. I have gained a lot from our discussions of solving problems. I am thankful for the guidance of Roderik Lindenbergh, who helped me with his professional knowledge in point cloud. I would also like to thank Susan Steele-Dunne for her great feedback on data processing and suggestions which I should keep in mind during my work of this project.

I would like to thank my friend Timo Bisschop for his help on field experiments and on processing of point cloud. I also appreciate the friendship with Bram Eijgenraam, with whom I understand the Netherlands much more; the friendship with Pablo Secco, with whom I did a lot sports; and the friendship with Anastasios Vogiatzis, with whom I have got a lot of fun.

I will always remember my greatest father. I would like to thank my mother, my big sister and my young brother for supporting and motivating me all the time.

Ze Li
Delft, January 2021

Abstract

Subsidence can be observed at various locations in the Netherlands. While it can be due to both shallow and deep subsurface processes, the shallow subsidence is mainly a result from compaction, oxidation and/or groundwater drainage. Moreover, for grasslands on organic soils, in particular pastures on drained peat soils, the vertical position of the ground level is subject to significant temporal variability. Temporal scales of the vertical motion are expected to vary between days and centuries, and spatial scales between millimeters and kilometers.

Unfortunately, performing precise, reliable, and representative geodetic measurements of shallow subsidence processes is very difficult for soils, as fixed benchmarks do not exist. Here we propose an in-situ measurement procedure for grass-covered soils using laser scanning, both terrestrial and airborne, using a vertically fixed reference platform. We show that for terrestrial laser scanning (TLS) it is possible to detect changes in the vertical position of soils with a systematic error of up to 2.6 mm and a standard deviation of 0.4 mm. Given a predefined level of significance of α =0.05 (confidence level of 95%) and a detectability power of γ =90%, we achieve a minimal detectable vertical deformation (MDD) of 21.1 mm in our study area. We show that the results are influenced by the grass density and length, the incidence angle of the laser beam, as well as other settings of the laser scanner. We find that the parameter settings of the method for estimating soil surface, and subsequently the subsidence, has an influence on the results and related statistics.

For airborne laser scanning (ALS), using a precisely leveled reference platform, we find that the quality of elevation estimates is still limited, requiring further considerations on the design of data acquisition surveys and the reference platforms. Our results demonstrate the ability of laser scanning technology for investigating shallow subsurface motion of grass-covered soils relative to a benchmark on a local scale. Based on the quality assessment, the detection of vertical ground level change is better understood in terms of time and probability. In future research, the factors affecting terrestrial laser scanning technology to accurately identify soils affected by vegetation, environment, and device condition, should be further studied.

Contents

List of Figures

List of Tables

1 Introduction

Subsidence, be it the sudden sinking or gradual downward settling of the ground surface, is a common problem for many areas on earth. In a general view, subsidence is an important indicator for changes of the earth, exhibiting a wide scale of temporal and spatial variability. In a local scale, people's daily lives may be significantly impacted by vertical ground motion. In the Netherlands, subsidence has been a topic of concern for decades, particularly due to the low ground elevation relative to sea level.

In this chapter, subsidence in the Netherlands is shortly reviewed in terms of its driving mechanisms. We then focus on peat soils. In section 1.4, the research aim and research questions are discussed. Finally, the outline of this report is summarized at the end of this chapter.

1.1. Subsidence in the Netherlands

As more and more land motion related damage is occurring, subsidence has gained increasing attention. In the Netherlands, subsidence results from both natural and anthropogenic causes. One of the best known man-made causes is gas extraction, e.g. in the Groningen area, which has started since 1963 (Rietveld, 1986). Realizing that properties and people's lives are vulnerable to the subsidence, many studies have been made in this area to model the pattern of land motion in order to understand and to predict potential subsidence. According to Van den Born et al., 2016, if no measures are taken to mitigate against the effects of land subsidence, then the costs of dealing with the related problems could rise to over 20 billion euros in the Netherlands by the year 2050.

Besides human activities that induce vertical motion, surface settlement due to natural causes, such as tectonic movement, soil oxidation and ground compaction, also urges researchers to stay alert. Due to sea level rise and ground level subsidence at coastal area, some villages were drowned in the past centuries (Wikipedia contributors, 2020d). This brought significant interest in understanding what is driving the subsidence in peat areas. As more and more surveys were carried out, people found subsidence can be classified as subsidence due to shallow subsurface process and deep subsurface process in terms of depth. Although no literature states an exact depth for the distinction between "shallow" and "deep", Anbazhagan et al., 2015 thought the thickness of shallow subsurface is less than 100 m. Based on this knowledge, gas extraction which happens at a depth of about 3 km below the ground level, induces the most deep subsidence in the Netherlands. The surface and subsurface in Groningen area have been investigated by a large number of studies as infrastructures are vulnerable to potential subsidence due to gas extraction.

Subsidence occurring in shallow ground layers, compared with the deep processes, is mainly found in areas with peat soil deposits. This relation can be viewed in Fig. 1.1, in which (a) depicts the soil type distribution in the Netherlands and (b) shows the locations where subsidence of shallow subsurface is observed. In this figure, a good fit between peat areas and the shallow subsurface subsidence can be observed. Colored in blue, most peat is located in mid-west and north-east area of the Netherlands. In the same area, colored in yellow and red in (b), vertical ground change due to shallow subsurface soils occurs. This relationship drives a great motive to investigate the subsidence on peat soils in this study.

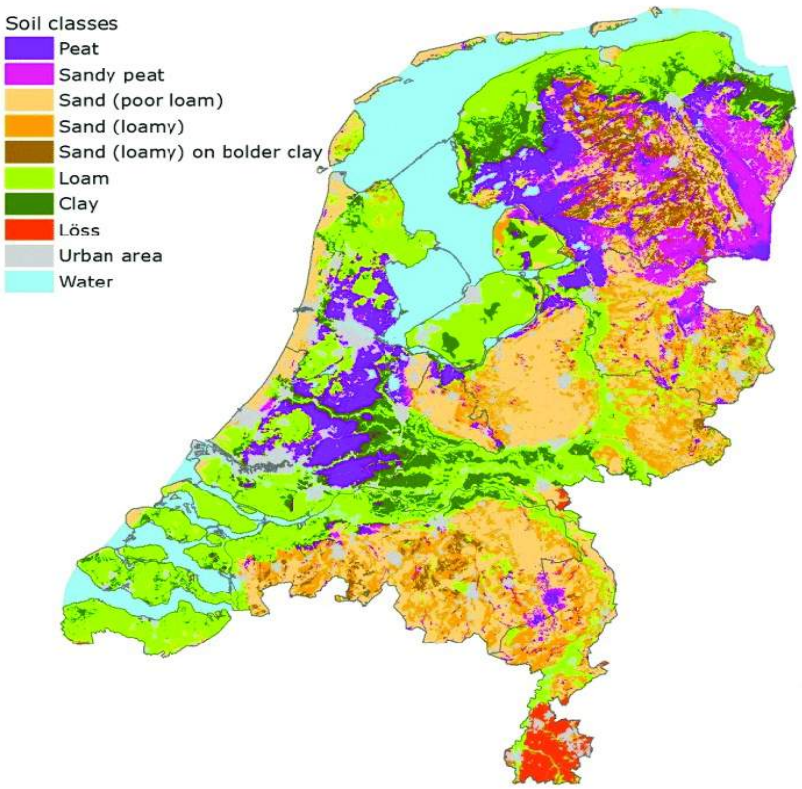

(a)

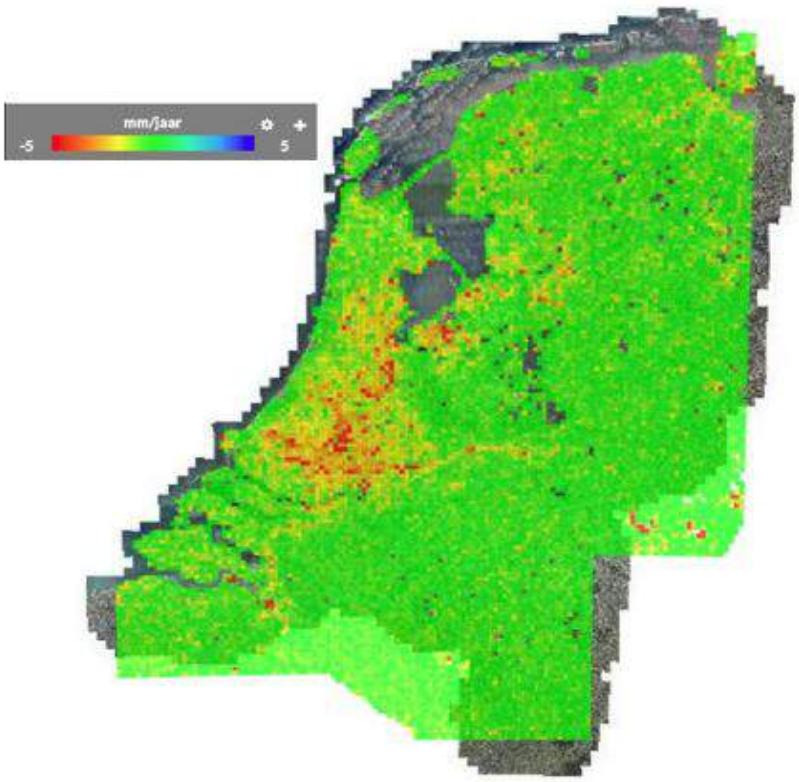

(b)

Figure 1.1: The spatial relation between soil type and subsidence of shallow surface. (a) soil map of the Netherlands, (b) spatial distribution of subsidence due to shallow subsurface process. Red pixels indicate more subsidence. These two figures show a good match of shallow subsidence and areas of peat soils. (Source: (bodemdalingskaart, 2018))

1.2. Peat soils in the Netherlands

Peat soils are an important soil type in the Netherlands, covering about 9% (about 290,000 ha) of the entire land area. As the bulk of shallow subsidence is observed over peat soils, information on the quantitative relationship between this soil type and vertical land motion is of great value.

1.2.1. Urban peat

Subsidence is causing problems in urban peat areas where buildings and other infrastructures are densely constructed. The weight of the construction leads to consolidation of the shallow subsurface. Large parts of the western Netherlands are vulnerable to land subsidence due to the high-percentage of peat land (Deltares, 2017). Several larger cities such as Rotterdam, the Hague, and Utrecht are examples located (partly) on peat soils, and soil subsidence is continuing. As a result of consolidation, oxidation, and shrinkage, these important economic areas may suffer from problems of vertical ground motion, which will cause infrastructural damages and economic loss. Built on weak peat soils, the municipalities of Gouda and Kanis are two of the urban areas in the Randstad that are currently sinking (Marlies ter Voorde, 2014). From this perspective, it is of vital importance to investigate the consequences of land subsidence in these urban areas and to provide suggestions on a plan for monitoring land subsidence.

1.2.2. Rural peat

Mainly drained and utilized for dairy farming (RECARE hub, 2020), a big part of the peat soils are valued as open landscape with a rich cultural history in the western part of the Netherlands. Peat differs from other soils due to the large quantities of organic carbon preserved, mostly in the Holocene when peat attained a thickness of up to 20 m. This leads to compaction that can be relatively great in relation to the tectonic movements (Rietveld, 1986). According to Wösten, Ismail, and Van Wijk, 1997, total subsidence due to the drainage of peat soils can be divided into three components: consolidation, oxidation, and shrinkage. All of these three causes result in reduction of peat land volume but with different rationals and/or depth where they process. Consolidation is a process that compresses the permanently saturated peat layers below the groundwater level (Weststrate, 2018). Above groundwater level, oxidation and shrinkage decrease the volume of peat as a result of organic matter loss and desiccation respectively. Especially for oxidation effect on the peat where carbon concentration of 50% of organic matter was assumed as carbon stock (Kuikman et al., 2003), subsidence of 8–-12 mm per year is induced according to (RECARE hub, 2020). As the organic soils above the groundwater level are exposed to the air, resulting in oxidation, a significant amount of land subsidence in the shallow subsurface was found on peat soils, resulting in decreasing stocks of carbon in organic matter. Besides the decomposition of the carbon, compaction of gas fields or tectonic movements and water pumping in polders also account for subsidence. Due to these factors, the long-term and irreversible subsidence of shallow subsurface is still not fully understood in terms of temporal and spatial dynamics.

1.3. Subsidence on peat

As stated above, different factors contribute to the vertical displacement of peat soils. Nieuwenhuis and Schokking, 1997 studied the effects from these three factors in the Province of Friesland, where peat and clay deposits are used extensively for agriculture and are drained to maintain a low surface water level in polder ditches. They suggested that land subsidence rates is 1 to 12 mm/year in this area. Another dramatic study on land subsidence due to shallow-depth soft soils is carried out by Asselen et al., 2018. They reconstructed subsidence over the last 1000 years and found recent subsidence rates of up to 140 mm/year averaged over an 11-year time span. They declare that, dominated by peat compaction and oxidation, the amount and rate of subsidence are variable in time and space, mainly depending on 5 conditions: 1) the Holocene sequence composition; 2) overburden thickness; 3) loading time; 4) organic-matter content and 5) groundwater-table depth.

To quantify the subsidence rate in a time interval, analyses from persistent scatterer interferometry (PSI) are used to infer subsidence rates of several millimeters per year, using coherent targets identified in the area of the Green Heart, Randstad Holland (Cuenca and R. Hanssen, 2008). In their study, InSAR (Interferometric Synthetic Aperture Radar) technology was used to calculate the height differ-

ence between two epochs, where a radar sent and received electromagnetic waves. Using two or more SAR images to compute the differences in the phase, InSAR allows to estimate land deformation with sub-millimeter precision. Taking this significant advantage of this technology, the Netherlands Center for Geodesy and Geo-Informatics (NCG) (bodemdalingskaart, 2018) applied InSAR to generate land subsidence maps of the Netherlands. The results provide a nice view on how an area varies in height in time series. In 2020, a second generation of the subsidence map of the Netherlands was generated, in which movement speed of millions of individual points are visible.

However, highly precise time-continuous InSAR points are mostly on civil infrastructure, i.e. in the urban area, where have good back-scattering points. Hence, the remaining areas, such as pastures, are missed in this analysis. There have been attempts to fill in the gaps. L. Liu, Zhang, and Wahr, 2010 and Short et al., 2011 applied this remote-sensing technique for monitoring subsidence over vegetation-covered areas. They showed that although InSAR can reach sub-millimeter scale measurement, it is limited due to interferometric phase decorrelation (Antonova et al., 2016; Beck et al., 2015). Thus, a challenging problem arises in this domain: it is difficult to evaluate vertical land motion of pastures on peat soils with high precision.

1.4. Research aim and questions

As we focus on the detection of vertical ground displacement due to shallow subsurface processes, it should be separated from deep activities. For this purpose, local reference platforms are used. Realizing that the shallow subsurface subsidence is mostly observed on peat according to subsidence map of the Netherlands and related problems, this research aims to evaluate several methods for detecting this type of subsidence on peat by applying terrestrial and airborne laser scanning technology. Elevation values in the measurements will be used to compute and analyze the distance between the ground and the reference platform. To understand how well is the detection, metrics such as the confidence level and the detectability power are introduced. This leads to our main research question:

- Is it possible to detect centimeter-level vertical surface motion of pastures on peat soils using laser scanning technology, with a predefined confidence level and a predefined detectability power?

To answer the main research question and meet the research objective, following sub-questions need to be solved:

- Where and how to set up laser scanner for elevation measurements?
- How to determine the ground surface elevation on peat areas where grass usually grows lushly with dense leaves?
- What reference platform should be designed for local scanning?
- How to evaluate the result in terms of confidence level and detectability power, and what is the minimal detectable height change using laser scanning technology on peat area?

Another important part of this study is to assess the performance of airborne laser scanning, giver the AHN3 (the Current Elevation File Netherlands) data product, at pre-installed local reference platforms. As a consequence, additional questions should be clarified:

- Will the local reference platforms appear in the AHN3 data set, and how will the related point clouds be processed?
- What is the quality of the point measurements on the platforms and ground? How to interpret the quality?

1.5. Outline

This section describes the outline of this research as a reading guide. First, subsidence in general is introduced in Chapter 1, as well as the knowledge about peat soils. Linking them together, the subsidence on peat is then described. In Chapter 2, literature about laser techniques that were applied

for subsidence detection is reviewed. Moreover, local reference platforms and experimental area are discussed in this chapter. After that, the methodology which thoroughly describes the steps to extract ground surface points and methods for estimating subsidence are introduced in Chapter 3. That chapter also describes procedures of processing ALS data. The results corresponding to the methods are shown in Chapter 4 and 5 for TLS and ALS, respectively. Finally, conclusions are elaborated in Chapter 6, with recommendation to future research in this field.

2

Background

In this chapter, subsidence background in peat area is described. To detect this vertical ground change, InSAR technology is introduced in second part of this chapter, followed by LiDAR techniques.

2.1. Peat subsidence

As stated in Chapter 1, peat, on which most subsidence due to consolidation, oxidation and desiccation of shallow subsurface are found, occupies large portion of the land of the Netherlands. It is expected that subsidence on peat in the Netherlands will continue in the coming years, which would result in sustaining negative effect or even more serious situations (Van den Born et al., 2016). In coastal area of the western Netherlands, where large part of the land is peat, it is vital to properly handle the relationship of sea level and ground surface elevation to prevent the land from the risk of flooding (Kooi et al., 1998). To forecast expected land subsidence on a coastal area where is in Polder Groot-Mijdrecht where was reclaimed in 1880 (Remkes et al., 2007), a simple dynamic model for the subsidence of peat soils due to peat oxidation was developed (Hoogland, Van den Akker, and Brus, 2012). Using this model, they predicted subsidence rate up to 8 mm/year in well aerated peat soils. However, though land use and water management are evaluated with their subsidence model on coastal peat area, the land motion of non-coastal area is not exactly the same as that of coastal area. The subsidence rates of peat of different areas differ as a result of land use history, climate of the area, density and thickness of peat layers (Schothorst, 1977). Fig. 2.1 illustrates potential relationships between subsidence and peat thickness, and relationships between subsidence and land use of mining in the Netherlands (Erkens, Meulen, and Middelkoop, 2016). Comparing Fig. 2.1 (a) and (b), the largest amplitude of subsidence (colored in red) is observed in the western areas where the thickness of peat layer is high (in red). While as the thickness decreases in surrounding areas which are shown in yellow and green, the amount of subsidence of peat decreases. Besides the effect from soil thickness, the land use also gives a positive feedback to the subsidence, meaning that more subsidence occurs at places with more mining activities. From their study, ground level in peat areas is understood from an interest perspective. However, despite the land motion picture in national perspective is recognized in a good way, subsidence in a local scale is not fully investigated. In the following sections, different techniques for studying local scale subsidence are reviewed.

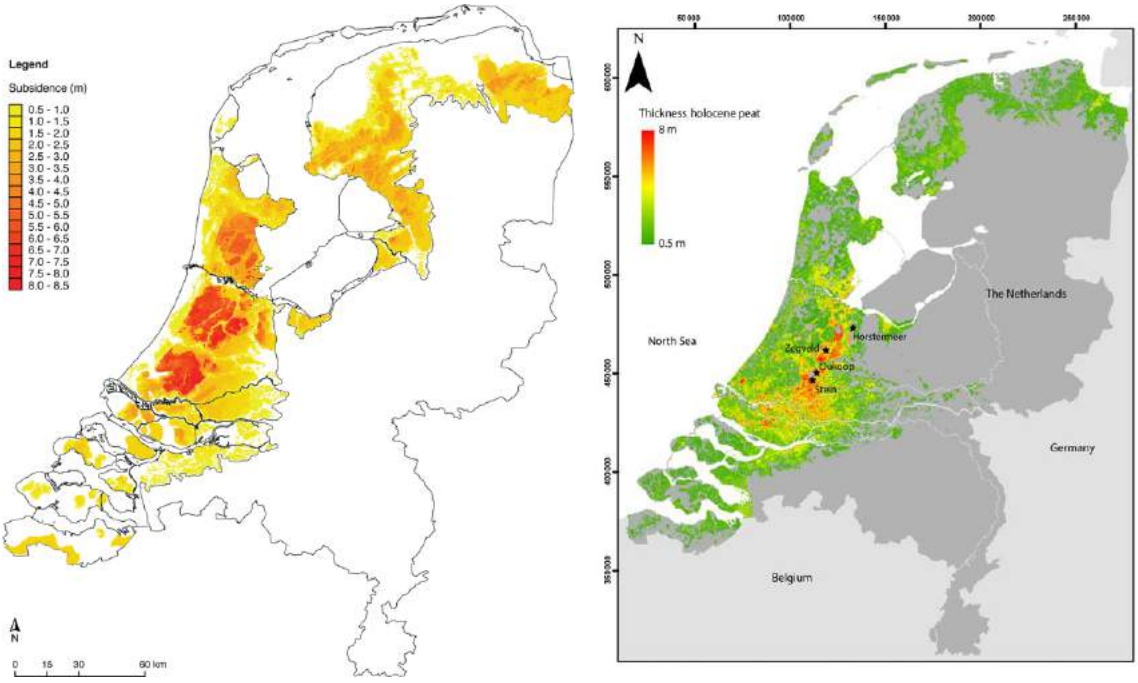

(a) (b)

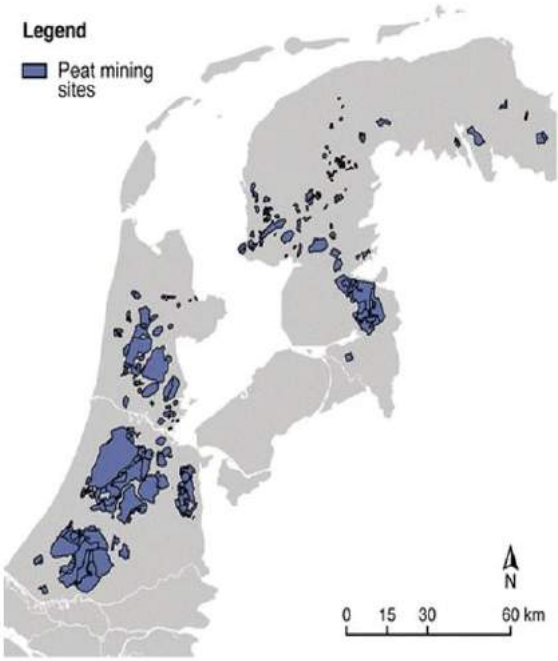

(c)

Figure 2.1: Subsidence over the peat areas of the Netherlands. (a) shows thickness of peat, (b) shows subsidence on peat, (c) shows mining sites on peat. These figures imply that there might be relationships between shallow subsidence and human activity. (Source: (Erkens, Meulen, and Middelkoop, 2016))

To better understand the subsidence on peat and to solve the problems due to subsidence, many studies were documented. As the development of remote sensing technology, different techniques were implemented for this purpose, such as InSAR (Interferometric Synthetic Aperture Radar) and LiDAR (Light detection and ranging).

2.2. InSAR

Interferometric Synthetic Aperture Radar technology is a derivative technique from SAR (Synthetic Aperture Radar), which is a geodetic method using two or more SAR images to generate maps of surface deformation. Calculating differences in the phase of the waves returning to the satellite (Massonnet and Feigl, 1998; Bürgmann, Rosen, and Fielding, 2000; R. F. Hanssen, 2001) or aircraft, this technology is able to measure millimetre-scale changes in deformation over spans of days to years (Wikipedia contributors, 2020b). Taking this dramatic advantage of high precision measurement, studies are performed in the field of investigating subsidence on peat soils. A study on Kuala Lumpur International Airport where tropical peat land is involved (Marshall et al., 2018) using InSAR method shows that reproducible ground deformation maps identifying deformation patterns across both urban infrastructure and adjacent rural plantations and tropical peat swamp can be produced. In the Netherlands, Cuenca, R. Hanssen, et al., 2011 used multi-track InSAR combining GPS and leveling to produce a velocity map of the whole Netherlands, which provides a method to estimate the land deformation. However, one limitation of this study is that the compaction rate from shallow deformation sources seems to be underestimated. In their previous study on peat related areas (Cuenca and R. Hanssen, 2008), a deformation rate around 2 mm/year was estimated, which, however, is smaller than expected value (1 cm/year). They explained partially the difference between the estimate and expectation that may due to the type of the scatterers which is a hybrid system between stable foundation objects and superficial scatterers. Stating that InSAR time series characteristics have the potential to monitor and quantify evolving peat land, more studies and evaluations need to be carried out.

2.3. LiDAR

Besides satellite-base radar technology, terrestrial and airborne LiDAR (Light Detection and Ranging) technology have gained increasingly attention in detecting range differences. As a remote sensing technique, LiDAR can measure the distance by illuminating targets and receiving the reflections with a sensor (Wikipedia contributors, 2020c). With fast development, LiDAR technology shows its superiority in detecting and monitoring local-scale surface changes due to the ability of obtaining high point density. LiDAR is mainly classified as terrestrial LiDAR and airborne LiDAR in terms of carrying platform of the sensor. This section reviews main applications in ground surface modeling using these two types of scanning technologies.

2.3.1. Airborne Laser Scanning (ALS)

Taking the advantages of high resolution remote sensing (Wehr and Lohr, 1999), Airborne Laser Scanning (ALS) is able to collect a large number of points covering large areas. This makes it possible to provide contiguous and highly detailed information about the 3D structure of the land surface environment, including the derivation of high-end Digital Terrain Model (DTM) and horizontal and vertical vegetation structure (Bramer et al., 2018). In recent years, ALS has been applied in many studies that try to model the ground surface. One example is that Wagner et al., 2004 discussed hierarchic robust filtering (Kraus and Pfeifer, 1998) of airborne laser scanning data for DTM generating in an alpine environment. They found the filter based on ALS data works well in winter but poorly in summer to properly reconstruct the forest floor. This finding provides a suggestion on the period of ALS data acquisition. Razak et al., 2013 mentioned a method that combines Global Positioning System (GPS), Total Station (TS) and ALS to construct a DTM in tropical forest environment. Their results showed that the ALS-derived DTMs allow to map and classify landslides beneath equatorial mountainous forests. They stated that for landslide mapping, the laser point density and filtered ground point density play vital roles.

In peat area, where the ground is usually covered by dense vegetation, the height changes are estimated by comparing digital elevation models (DTMs) of the two ALS surveys. The mean absolute

error can reach 0.23 m in peat swamp area where forest is also be an influencing factor. This value is likely to be enlarged if systematic offset exists (Palamara et al., 2007). Many previous studies have shown that the results of measuring the ground surface under vegetation produce DTMs of the scan areas. Using these modeled ground surfaces at two epochs, elevation difference maps are able to be generated. However, the result is affected by both the ground estimation, which leads to errors compared to the true vertical difference, and precision of the estimate which increases the uncertain of detection. In this study, a local reference platform, which is stable relative to shallow subsurface is conceived so that the change of elevation difference between the ground and the platform is able to reflect the deformation of the shallow subsurface.

For this purpose, Integrated Geodetic Reference Station (IGRS), on which precisely horizontal platform is installed, is investigated to evaluate the performance of ALS data. Buried at fundamental depth, IGRS is assumed stable at shallow subsurface layer. The ALS data on the platform of IGRS, thus, can be analyzed together with ground measurements. In principle, the uncertainty mainly comes from the point cloud of ground. This type of stations were designed by TU Delft, aiming to integrate different geodetic technologies. As they are relatively new, very less previous research on the applications has been published. More detailed descriptions of IGRS in terms of rationale, design and installment are described in Kamphuis, 2019.

2.3.2. Terrestrial Laser Scanning (TLS)

Settled closer to the targets, Terrestrial Laser Scanning (TLS) is able to scan objects in meters distance with a much higher spatial resolution, leading to high point density. Several studies (Bhardwaj et al., 2016; Marx et al., 2017; Kociuba, Kubisz, and Zagórski, 2014; Avian, Kellerer-Pirklbauer, and Bauer, 2008) have explored the applicability of TLS on monitoring the surface change in permafrost regions. Filters for extracting bare-ground points were described and a plausible subsidence rates (up to mm-scale) was derived. Their results provided an evidence that TLS can be used in dense vegetation covered area to extract the local bare ground. However, the condition of the growing grass on peat land of the Netherlands is different in aspects of vegetation type, density, length of vegetation leaves, which leads to much different assessment for vegetation error. In some studies (Fan et al., 2014; Pirotti, Guarnieri, and Vettore, 2013), this vegetation-induced elevation error in TLS surveys are investigated. They extracted ground candidates to generate DTM taking vegetation density into account. Based on the experiments, they found vegetation error (which was about 65% of the grass height for a 60 mm by 60 mm filter window) could be reduced when scanning from different directions by placing laser device at different positions, even though it will be canceled out to some extent in sequential surveys. Despite previous works have demonstrated the applicability of TLS, issues still exist and remain to be discussed for the detection of vertical ground surface displacement (Mukupa et al., 2017):

- agreed and unified method of point cloud processing;
- measurement geometry;
- design of data acquisition and quality assessment;
- environmental effects, including wind, temperature which relates to thermal expansion and contraction of the ground soils;

2.3.3. Combination of ALS and TLS

As the accuracy of laser scanning systems has been improving for years, ALS and TLS are combined to study vertical land motions (Chasmer et al., 2011; Gangodagamage et al., 2014). When using these techniques, challenges of TLS-based detection should be considered in terms of measurement geometry, registration errors, scanning directions and temporary objects (Lindenbergh and Pietrzyk, 2015). Spatial resolution should be concerned when using ALS data to study the vertical movement of the ground (Barnhart and Crosby, 2013).

While a number of studies focused on vegetation covered areas (especially on forest areas) in usage of laser technology, to our knowledge, no previous research has investigated subsidence detection on dense grass covered peat soils, especially the peat area in the Netherlands. This makes applicability

of TLS is still not fully understood. In this research, TLS and ALS data for detecting vertical land movement on peat soils are studied, which including the use of local reference platform. The overall aim of this study is to evaluate the feasibility of using laser technology to detect subsidence on local peat soils with a predefined confidence level and predefined detectability power. To achieve this goal, three methods are described in Chapter 3 section 3.1. What's more, application of moving average operator is also introduced in that chapter to reduce the sampling effect in this research. In next chapter, the study areas for TLS surveying and ALS data investigation are introduced. To obtain the quantity of subsidence in the areas, local referencing platforms for both techniques are described.

2.4. Study area and local reference platform description

As the aim of this research is to investigate the shallow subsidence, local reference platform is required to be scanned together with ground. To this end, two LiDAR technologies–terrestrial laser scanning and airborne laser scanning are used. For relatively low-cost TLS, data was obtained by implementing experiments in field. While for high-cost ALS, which collects data once per 4-5 years covering a large scope of area, data were downloaded from existing data set (AHN website, 2020). In this section, the area where TLS surveys were carried out and author-designed reference platform are described first, followed by description of areas and platforms where ALS data were investigated.

2.4.1. TLS survey area

During scanning, author-designed platform was used as reference platform. The subsidence of the ground was modeled by changing the elevation of this platform.

The experiments of acquiring TLS data were carried out in a pasture which is located in Zweth, the Netherlands. The grass in the area is quite dense and many of the grass roots are twisted. This makes the bare ground hardly exposes to the sight of view, resulting in occlusion of laser beam illuminating to soils. This may also be a reason that the wind would has less effect on laser scanning of on this field, as the wind mainly blows the upper leaves of the grass. Fig. 2.2 shows the spatial location of the experimental area in the map (in Google Earth) and visualization of the grass in the study area. It can be seen that the main vegetation type is grass, which flourishes with thick and twisted roots. The soil type of the pasture field, according to the Dutch soil map, is not totally peat even though its adjacent land in north-west is. Large quantity of organic matter is found in the subsurface which makes it show similar properties as peat in which about half of the components is organic matter. Due to this finding, the subsidence pattern of this area, especially of the shallow subsurface soils, is assumed to be the same as that of peat soils which is the aimed soil type of this research.

(a)

(b)

Figure 2.2: The location of the study area and the to-be-scanned field. Sub-figure (a) is a satellite view on the pasture, with red mark at left-top indicating the hamlet Zweth, and yellow mark and red circle at middle-bottom indicating the local study area (about 5 m^2). (b) shows a close view to the grass in the field. In our study area, the grass are thick and the leaves are long, which could cause occlusion of laser beams.

2.4.2. Reference platform in TLS surveys

A platform with a ”shoe” shape is used in this research (shown in Fig. 2.3). Two reasons that accounting for this shape design are that first, the orientation of the platform point cloud is easy to be recognized; second, it enables the registration of point clouds based on the platform. Referring to the angular position of an object in space (Wikipedia contributors, 2020e), orientation of the platform provides information of how the platform is placed in surveys, which is useful for future surveys to repeat the experiments. From perspective of registration of point cloud which is described in Chapter 3, this platform shape makes registration in a manual way possible. In registration procedure, one point cloud is moved to overlap on the other one. Hence, this shape of the platform enables corresponding points in two point clouds to be found.

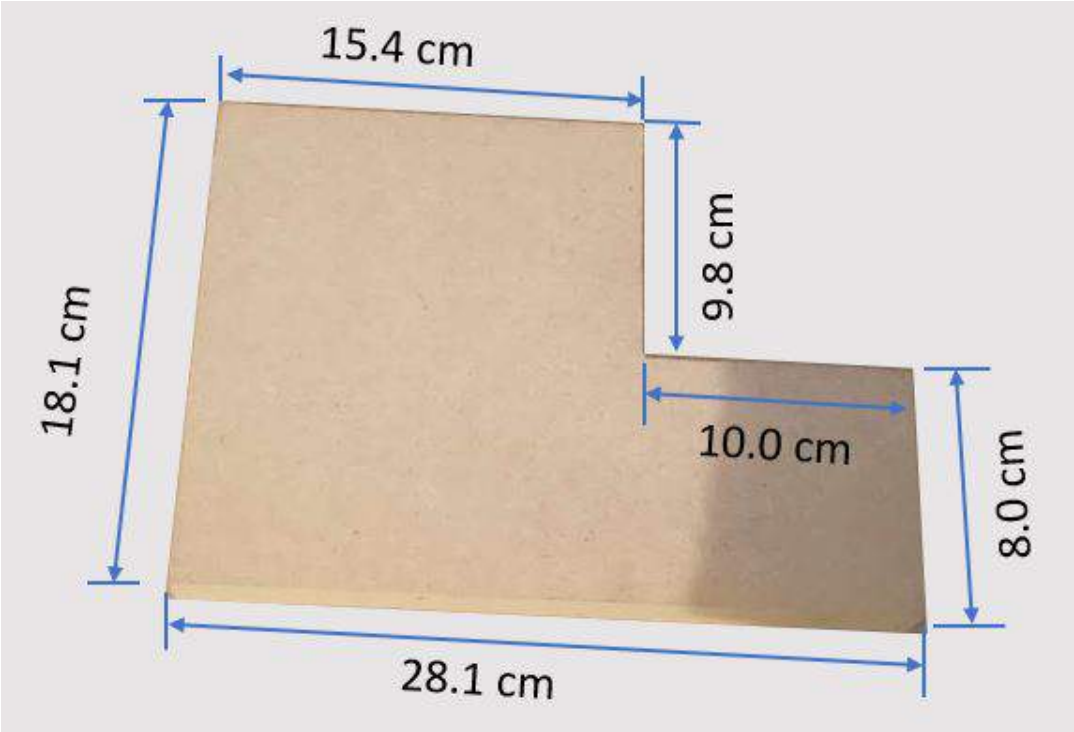

Figure 2.3: The author-designed platform (top layer) in TLS surveys. The edges of the platform are measured using a millimeter–ruler. It is used as the reference platform relative to the ground. Its shape is designed so that the shape and the orientation of scanned point cloud can be recognized.

Scanned together with the grass, the platform is seen as a stable reference between different scans. ”Stable” here means the position of platform remains unchanged during surveys. To modulate the subsidence, a wooden plate is added beneath the platform so that the vertical distance between the ground and the platform varies. In this way, the ground is assumed to subsides by a magnitude equals to the thickness of the wooden plate, which is 17.0 mm. This value is obtained by measuring the plate several times using a millimeter ruler, among which the maximal measurement is 17.1 mm and minimal measurement is 16.9 mm.

The experiments were carried out in two days, with 4 scans in each day. The time-of-flight 3D laser scanner measures the distance between sensor and objects in view, and calculates 3D coordinates (x, y, z) for the captured object points. High and low scanning resolutions ($1.6mm@10m$ and $3.2mm@10m$, respectively) were used to study the influence of resolution on the height estimate of soils. The resolution ”$1.6mm@10m$” indicates that the obtained point clouds have a point spacing of 1.6 mm at 10-meter distance from the sensor. An area of approximately five square meters around the model was scanned from three different directions by setting the laser device at three different positions. To study the effect of the grass, the area was mowed after 4 scans (in the first day), resulting in lower grass height but the roots remain unchanged. To ensure that the platform is set up at the same position in two days’ surveys, it was firmly connected to an iron tube which was inserted into ground. The build-up

and installment of the platform can be seen in Fig. 2.4. Detailed steps for achieving this goal are:

1. As a holder of the whole structure, a hollow iron tube was inserted into ground by around half of its length. It should stay unmoved during the whole field work, so that the platform on it remains stable.

2. A chassis is made up by a base plate and a stick. The stick is fastened to the based plate by an angle iron. This allows the chassis to be connected to the iron by inserting the stick into the iron tube. As a result, the reference platform can be placed on the chassis.

3. The platform which is a "shoe" shape plate made of wood is used as the reference for quantifying the height change of the ground. This platform should be flat without any ups and downs on it. Hence, the registration based on top layer of this platform can be done with less error.

4. The platform for scanning is placed on the chassis which is inserted into the iron tube in the ground. As the platform should be leveled, a spirit level is used to check the horizontality. The bubble in the spirit level points to which direction the horizontality biases. According to this information, the platform is adjusted to horizontal level by adjusting the iron tube slightly. To prevent the tube from rebounding back to original condition, small amount of soils may be needed to fill the seal between the tube and the ground.

5. The ground is not expected to subside during these two days' surveys. To modulate the subsidence of ground, the reference platform is raised up by adding a known thickness plate. Assuming the reference platform before and after using the plate is at the same elevation, the elevation of ground goes down as the relative distance between the platform and ground increases.

As long as the iron tube is stable, the position of the platform will not change when placing on the tube. Another benefit of this structure is that the reference platform can be take away after the first day's survey, while leaving the iron tube in field. This prevents the wooden platform from distorting due to water vapor released from the vegetation during the night and rain in case.

When scanning the study area at different positions, the laser device need to be moved and reset up. The device height is not necessarily the same in each scan but high laser sensor allows more laser to penetrate the grass leaves because of smaller incidence angle (Coveney and Stewart Fotheringham, 2011; Fan et al., 2014; Lindenbergh and Pietrzyk, 2015). Thus, gathering measurements by different manipulators does not affect the consistency of the point clouds.

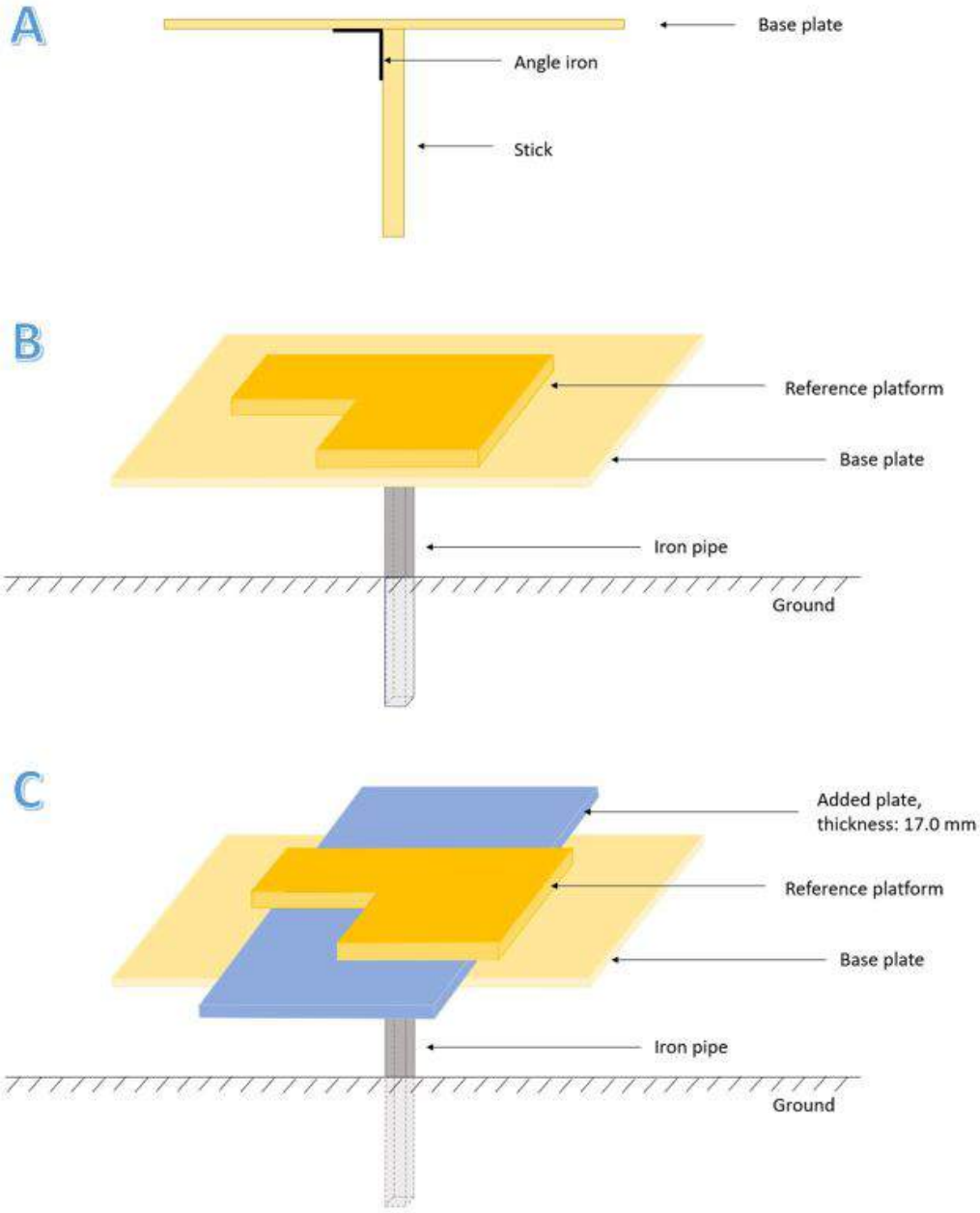

Figure 2.4: Illustration of making a stable reference platform. (A) shows the chassis which is made up by a base plate, stick and an angle iron. (B) shows the platform which is placed on the base plate. (C) shows the subsidence of the ground is modulated by adding a plate beneath the platform for scanning (top layer). This group of figures demonstrates how the platform is set and how the plate which modulates the subsidence is placed in the field experiments.

2.4.3. Area for studying ALS data

ALS data studied in this research is AHN3 data. They are inspected in very local areas where IGRS, shorted for Integrated Geodetic Reference Station, are located. Fig. 2.5 shows the location of all IGRS in Groningen area. These geodetic measurements at these stations provides surveillance and study on the ground motion.

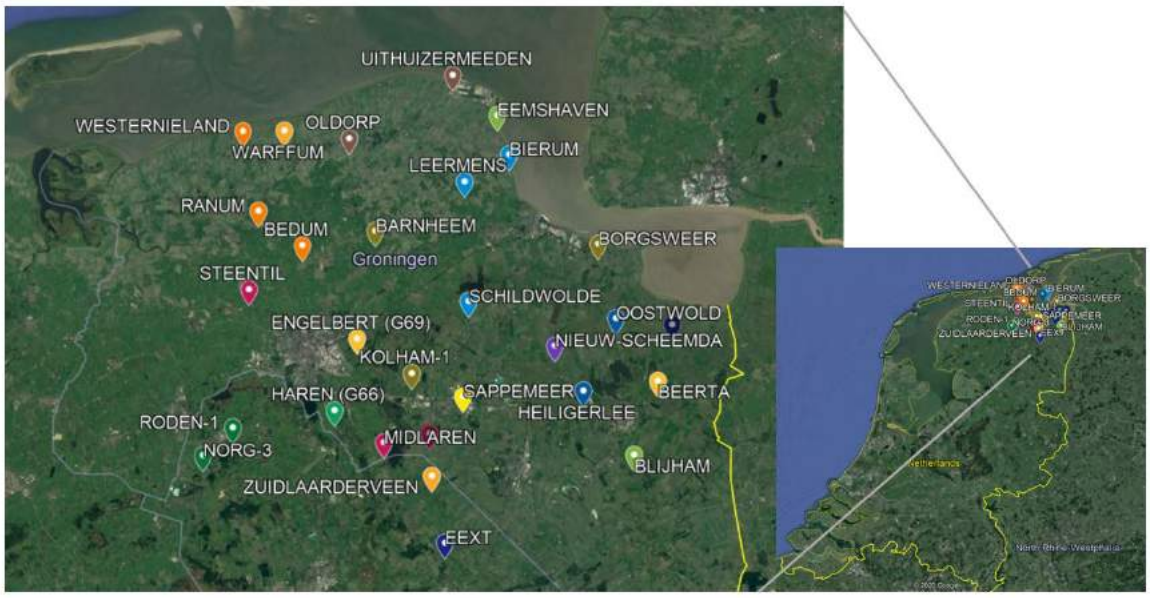

Figure 2.5: Location of IGRS in Groningen area. This figure shows spatial distribution of IGRS covering the most area of Groningen. They form a net so that vertical land motion of this area can be studied by integrating multiple geodetic measurements.

AHN-3 is the third generation of the Actueel Hoogtebestand Nederland (AHN) project, which concerns the acquisition of high-resolution altimetry data over the entire Netherlands using airborne laser scanning. Showing capabilities in different aspects, such as monitoring the infrastructures like dikes, investigating how the river bank changes over time, AHN data are acquired in order to have a better and thorough management on the soils and water (AHN website, 2020). Data acquisition of AHN3 is expensive in terms of both economy and time. Thus, flight plan is made considering different information of boundaries of target scanning areas, specifications of the data such as point density and point distribution (AHN website, 2020). A full circle of scanning work may last for 3-4 years to collect points over the entire country. AHN3 data in local scale are scarce, with 6-10 points per square meter. Even though this number can increase a bit when the flight lines overlay, the increment is small.

2.4.4. Reference platform for ALS data–IGRS platform

The reference platform used for investigating ALS is the platform on IGRS, which is also called Ground Control Point (GCP). Co-locating reference points for multiple geodetic techniques, IGRS is mainly composed of GPS antenna, GPS receiver, a platform on which markers are made, radar reflectors and a pole to connect them as an entire body. In the work of Kamphuis, 2019, these parts of the reference station are described thoroughly. Developed by joined team of the TU Delft, NAM (NAM, 2019) and 06-GPS (06-GPS, 2019), the setup of IGRS is motivated by the problem that the geodetic interpretation of deformation estimates, which are derived from spatio-temporal location measurements obtained by multiple geodetic observation techniques, is limited by the differences in their sampling methods of physical processes (Kamphuis, 2019). Thus, the main purpose is clarified as to couple GNSS, leveling and preferably other geodetic measurements (e.g. LiDAR, Total Station), with InSAR measurements into a well defined geodetic datum. Fig. 2.6 (a) illustrates the implementation of an IGRS in field. Its base is buried at the fundamental depth and assumed to move in company with the ground as a whole.

To find a stable platform relative to shallow subsurface, the platform (shown as "Top plate" in Fig. 2.6 (b)) of IGRS is going to be used in this research. This horizontal platform is leveled using a total of 6 permanent markers, of which 4 are located on the horizontal plate and 2 are located at the far tip of either reflector (see Fig. 2.6 (c)). The 4 markers on the horizontal plate can be used to detect a tilt of the IGRS in any direction. The 2 markers at the far tips of the reflectors can be used to detect any change in tilt of the reflector with respect to the IGRS.

This chapter answers sub-question related to the design of reference platform. Once the study areas are clearly defined, and the reference platforms are well prepared, we could acquire data of TLS and ALS for processing, which is described in Chapter 3.

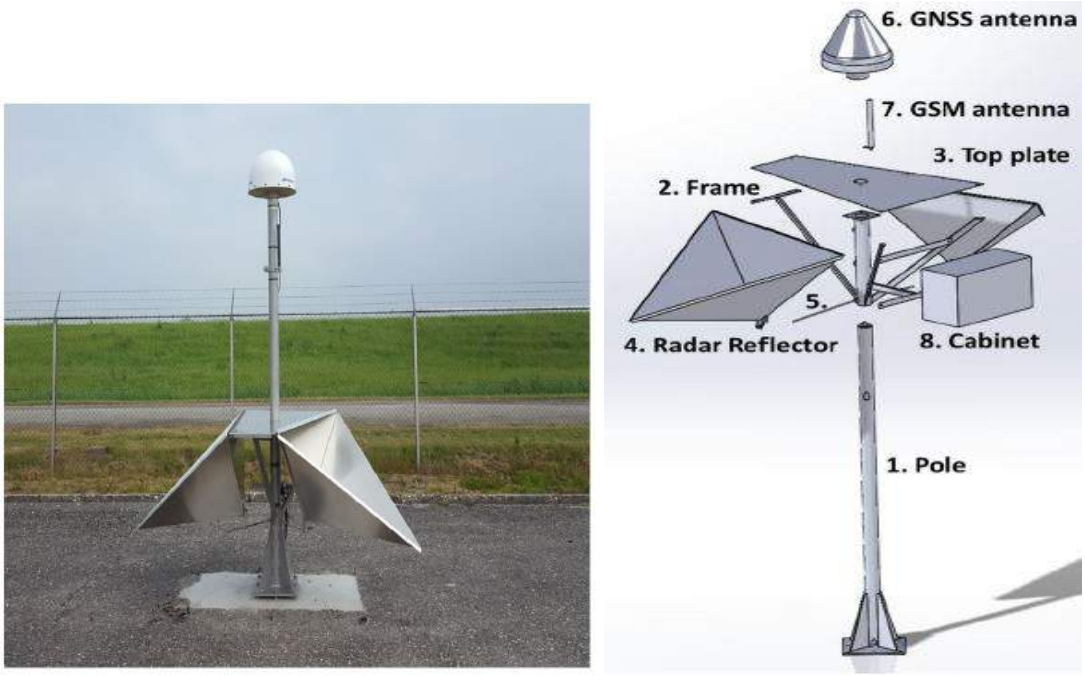

(a)

(b)

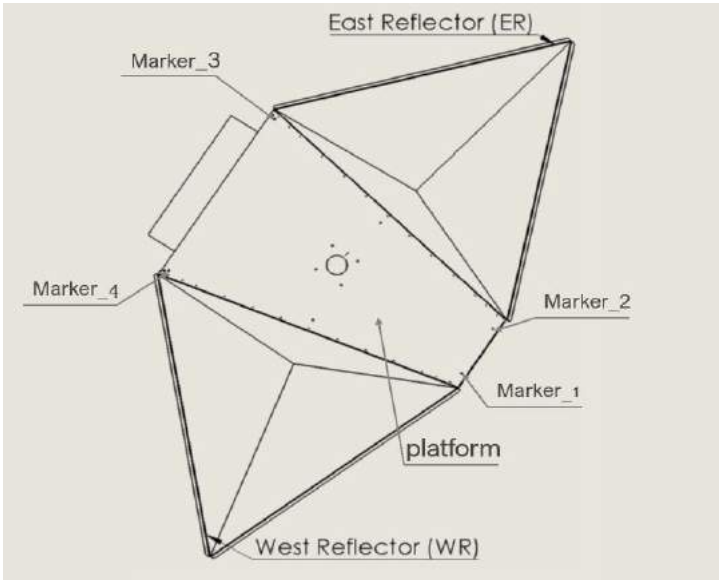

(c)

Figure 2.6: Setup of IGRS. (a) show an IGRS in field. On the top is a GNSS receiver, supported by a pole which sticks into the subsurface. The plate is at the middle with two radar reflectors at each side. The entire outfit fixed relative to the ground. (b) shows IGRS platform and the radar reflectors on both sides. The long edges have a length of about 130 cm. 4 markers are seen on the platform and 2 on either the reflectors. (Source: (Kamphuis, 2019))

3

Methodology

In this chapter, methods of estimating the subsidence of the ground surface using TLS data are presented first, as well as the processing of data sets. In this part, we start with data acquisition of TLS, followed by pre-processing of the gained point clouds in order to do further computation on subsidence. After methodology of evaluating the results of TLS, investigation of ALS data is described.

3.1. TLS based subsidence estimation

Terrestrial Laser Scanning technology is able to scan targets with high point density and high accuracy with up to millimeter bias. Here we aim to estimate ground subsidence relative to local reference platform taking the advantages of TLS. In this section, methodology of acquiring TLS data by field experiments, estimating ground subsidence and evaluating the results are given. Finally, we will evaluate the ability of TLS for achieving our aim.

3.1.1. Data acquisition

In this study, eight scans were obtained by terrestrial laser scanner in two days.

For TLS data, to investigate the influence of the resolution and grass, 4 different positions were chosen to set up the laser scanner. As shown in Fig. 3.1, laser scanner was deployed at two positions in the first surveying day to scan the study area from a different direction. At each position, a low-resolution scan and a high-resolution scan were captured. Comparison of the subsidence estimate based on low and high resolution provides a hint on the selection of resolution in studies in such vegetation environment, this will be discussed in Chapter 4. In each scan, incidence angle of 80 degree was used so that a large area is scanned. Also, we scan the area with 360-degree rotation of the laser scanner, which ensures the area of interest is in the field of view when laser device is placed at different positions. This setting ensures the whole study area to be included in the view of scanning while excluding uninterested area. In the meanwhile, it is noted that the laser device should not be too close to the platform to avoid occluding as the smallest incidence angle of the scanner is 55 degree. The platform was put at a low height when the laser scanner was placed at the first position. After first two scans (with high and low resolution setting), the laser device moves to the second position. The platform and the area of interest are then scanned from a different direction to reduce occlusion due to the grass (Fan et al., 2014). To modulate the height change of the ground surface under the assumption that the platform is stable, a 17.0 mm plate is added beneath the platform (see Fig. 2.4). Then the platform and the area of interest are scanned when the laser is at the second position. Until now, we have 4 scans with different settings of platform or resolution (see Appendix A).

After each scan, a point cloud containing a full area of interest is stored in the laser device. By exporting the data into a point cloud processing software, the area of interest can be extracted. Fig. 3.2 illustrates the setup of the experiment of one scan and the resulted point cloud of the area of interest for further processing. We can see the relative position of the laser scanner (on the tripod) and the local reference platform. The shape of the area of interest is defined by author, for the sake of two main

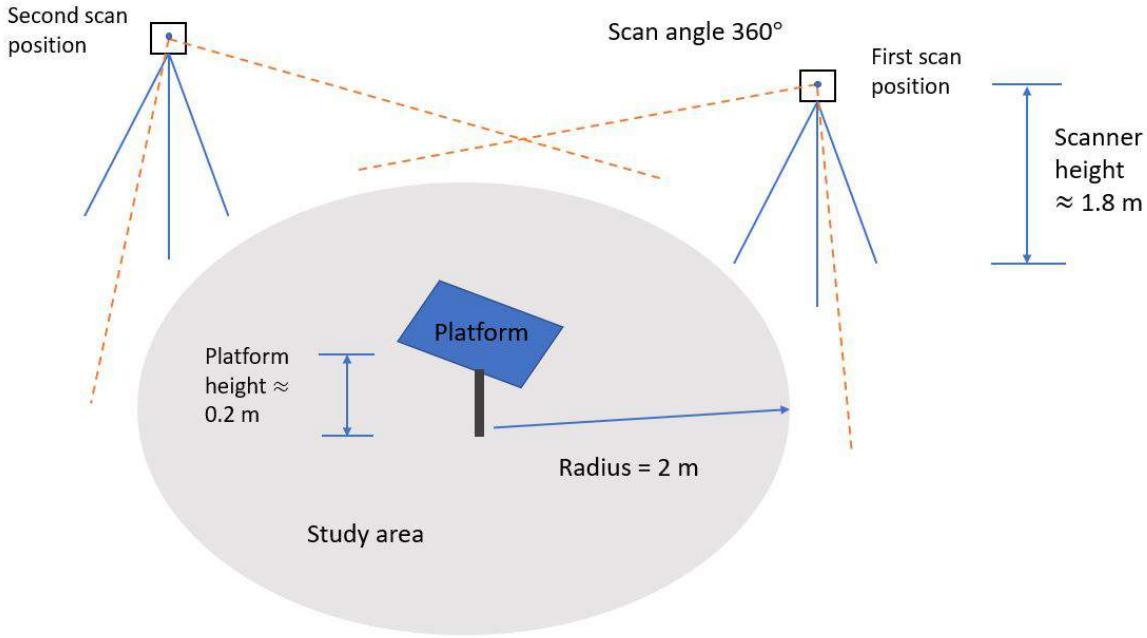

Figure 3.1: Two different scan positions in one surveying day. When scanning in the other surveying day, the laser device was set up at similar positions. The grey shape indicates the study area and the blue shape in the middle indicates the platform which connects with the iron tube. During scanning, the laser rotate by 360 degrees to obtain the area around it. The study area is then extracted from the large point cloud in data processing procedure.

considerations:

1. occlusion due to grass. The ideal situation for scanning the grass covered ground is from the direction right above the area, which reduces the occlusion effect when laser beams illuminate the targets at distance. However, this is limited by the practical installment of the device in field, as a result, the laser device has to be installed and stabilized on ground beside the platform. To reduce the occlusion effect from grass, a small area should be scanned.

2. the relationship between reference platform and ground. To study the vertical motion of the ground relative to the reference platform, the area should be more or less centered at the platform. This circle shape controls the effect of the distance between platform and ground points from different directions.

On the second surveying day, another 4 scans were captured. The settings were same except that the grass surrounding the platform was mowed. This allows to compare the height change between point clouds with different grass heights, which seems a way to study the influence of the grass on subsidence estimation. It is remarkable that the platform remain unchanged during the two surveying days so that the detected height change is totally due to the added plate. This is ensured by putting the platform on an iron tube which is inserted half length into the ground.

3.1.2. Registration and clipping of TLS point clouds

The point clouds obtained from each scan were stored under the coordinate system which centered at laser scanner. To estimated ground subsidence referencing to the same platform, point clouds from all scans should be registered into the same coordinate system. Besides, as laser scanner scans a large area, clipping is needed to obtain only the study area.

Registration

TLS point clouds are registered based on the platform of each scan. This can be done in three steps:

(a)

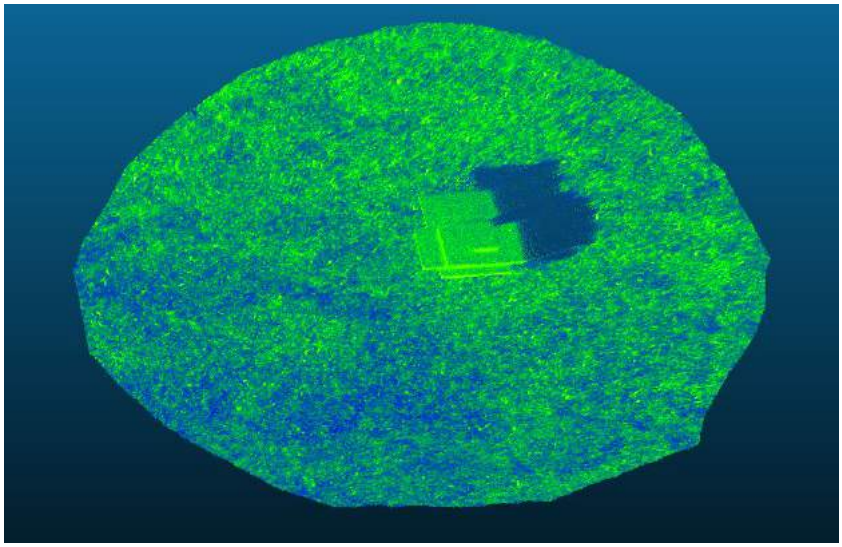

(b)

Figure 3.2: Picture of how the ground and the platform are scanned in one scan and the extracted point could of the area of interest. (a) shows a side view of the experiment while the laser scanner is working. (b) show the point could of the small area of interest which is extracted from the raw point cloud covering relatively large area around the platform.

1. First, the points standing for the platforms are extracted. To obtain a clear extraction for each platform, the distinct corners of each platform can be used.
2. Then taking the platform of the first survey as reference platform, all other platforms are transformed and rotated so that they are overlapped on the first platform. Each overlapping pair produces a transformation matrix and a rotation matrix.
3. The matrices are applied to the other part of the point cloud besides the platform. By doing so, every point cloud is registered to the coordinate system of the first point cloud.

To reach a highly accurate registration, the transformation and rotation operation should be carefully performed to make it overlap with the reference platform as much as possible. The Root Mean Square Error (RMSE) of registration is a parameter to evaluate the quality. In this research, it can achieve to sub-millimeter level. After registration, the platforms have the same height, the only difference between each two scans is vertical difference of the ground which is deemed subsidence relative to reference platform.

Clipping

The point cloud in each is obtained over a large area containing the small area of interest. Due to the considerations mentioned in section 3.1.1, this local area is extracted from the whole point cloud. As all the point clouds are registered and geo-referenced, the same area of interest in each scan is able to be clipped.

The clipped area is about 5 m^2 including the platform and ground. They are extracted and stored separately. For the subsidence of the ground, we can analyze the ground point clouds. The procedures of registration and clipping are depicted in Fig. 3.3. The ground point cloud is similar as Fig. 3.2 (b), but without the platform.

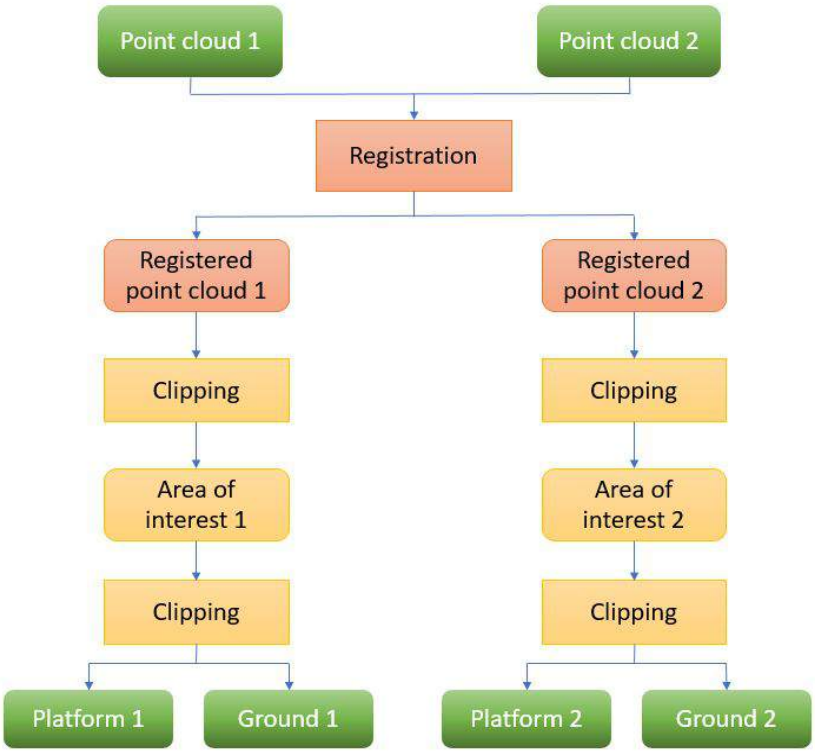

Figure 3.3: Work flow of registering and clipping the point cloud. The results are platform point clouds and ground point clouds. This workflow shows the procedures of obtaining separate point clouds of ground and platform. The point clouds of ground are used to acquire the height change of the ground, and point clouds of platform are registered so that they have the same elevation in order to fulfill the assumption that it is stable.

3.1.3. Pre-processing

We aim to determine whether the vertical movement of the soils is able to be detected, and to what extend it can be quantified. Thus, it is required to properly identify the soils surface. This is challenging thanks to densely covered grass. One way to overcome this problem is to select the local lowest point (Fan et al., 2014; Marx et al., 2017) to represent the soils. However, the single lowest point of the whole area is not simply used because on the first hand, the area is not perfectly flat so that it may be falsely on behalf of the soils; on the other hand, it is likely to be the outliers due to edge effect (Fan et al., 2014) when laser beam hits the edges of the grass leaves. Klapa and Mitka, 2017 defined edge effect as a measurement error resulting from the reflection of the laser beam on the adjacent walls, or by its breaking on the edges. This leads to a portion of the laser beam continue to another surface resulting in longer time-of-flight. Edge effect could result in either underestimated or overestimated height measurement. Fig. 3.4 shows how edge effect leads to incorrect measurements. If leaves like "grass leaf 1" (upper leaves) dominate when exposing to the laser scanner, and there are very few leaves at lower position, edge effect leads to over-estimation in height measurement. In contrast, if leaves like "grass leaf 2" (lower leaves) dominate, edge effect leads to under-estimation in height measurement.

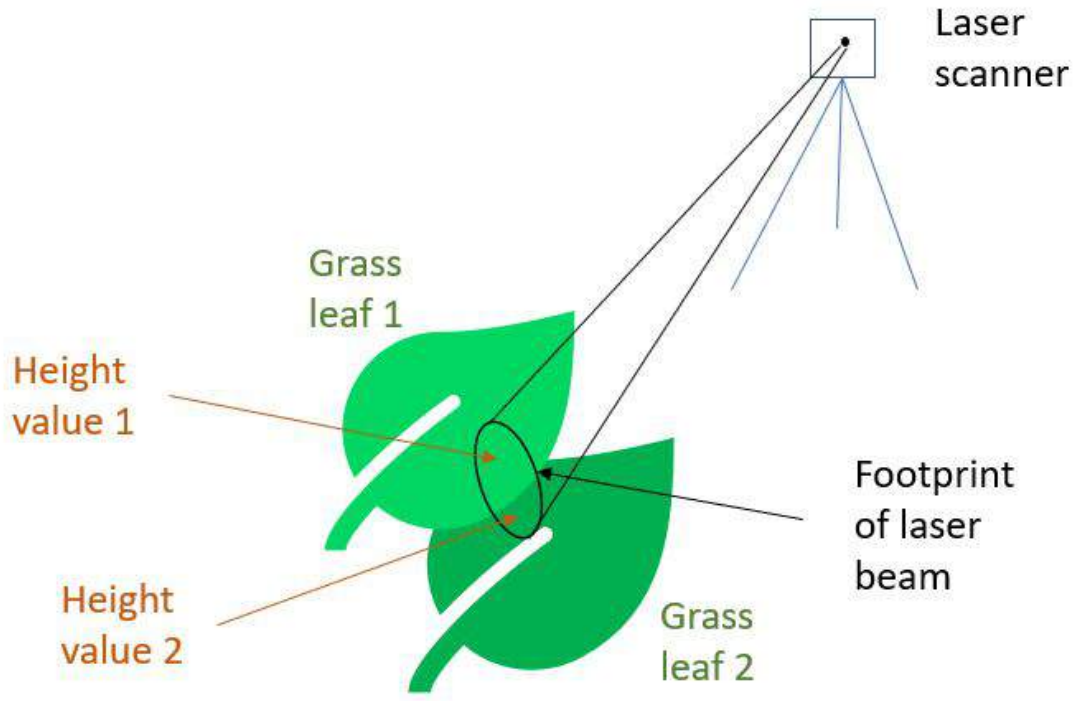

Figure 3.4: Illustration of edge effect when a laser beam hit areas of more than one leaves. In this figure, two grass leaves have different heights. When laser beam scans at this position, coordinates of points are determined by averaging the measurements (height value 1 and height value 2) in two areas. This results in incorrect positioning in space (Klapa and Mitka, 2017).

Once we have point clouds of ground, four steps are undertaken to express the elevation of the ground of study area in a detailed scale: 1) the entire study area is equally divided into 900 windows using a 30×30 grid, resulting in each window size of $10.00cm \times 10.00cm$ large; 2) the lowest 0.5% of the points within each window are then selected; 3) delete the lowest 20% of the selected points considering the possible edge effect from the grass and outliers; 4) taking the average of z-values of final collected points in each window as the elevation estimate of that window. By this way, the area is reliably represented even the ground surface is not flat. Fig. 3.5 illustrates the steps. Amongst them, step 3) is considered because edge effect is likely to happen frequently (Fan et al., 2014), which may result in a lower z-value of a point. To make it clear of what size of the window and how many lowest points in each window are the best option, different sizes of windows and different amount of points are tested. Finally, we decide to set the window size $10.00cm \times 10.00cm$ (30×30 grid) large to balance

the number of windows and obtained laser points in each window. The reason for this setting is that as the window size decreases, the number of windows increases. We have more representatives of the study area, resulting in more detailed expression. In the meanwhile, as the window size decreases, we have less laser collections in each window, which results in a low number of effective representatives of the soils in each window. Using $10.00cm \times 10.00cm$ window size, we have several hundred of window samples and enough point collections. Besides, we use the lowest 0.5% points of the total number of points in each window instead of higher percentage or a certain number of points. This is because that this percentile results in a relatively good estimate of the subsidence (with errors in sub-millimeter scale) when different number or percentage of points are tried. It makes sense, since a certain number of points can not fairly represent the window as each window has different amount of point collections, and larger percentage would bias from the concept of "lowest points".

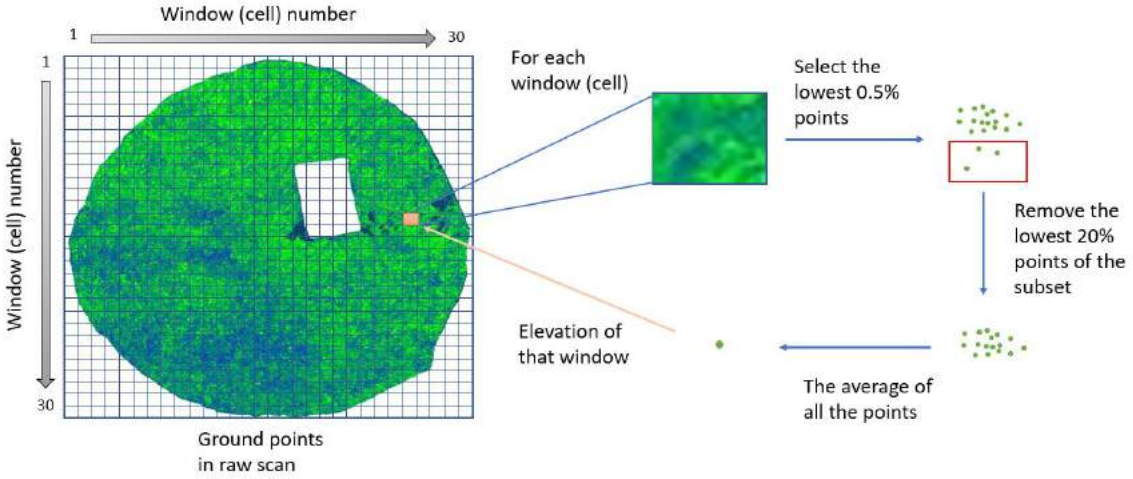

Figure 3.5: Illustration of steps for selecting the soil candidates. The white hole in the point cloud is due to the extraction of platform. For each small cell, the lowest 0.5% points are selected. This percentage is chosen because it produces the closest subsidence after trying multiple percentages from 0.1% to 90%. Among these selected points, the lowest 20% of them are removed to prevent possibly existing outliers. After that, taking the average of the elevation values of remaining points as the candidate of this cell. Repeat the procedures for all the cells. Thus, the soil candidates of this survey are selected.

It is significant to realize that the soils may be absolutely shielded by the thick roots of the grass at some spots. The roots are twisted and have formed a hard surface which performs as a solid surface adhering on the soils so that it has the same movement as the ground. In this study, the soils surface is defined as this author-called "root surface" at some spots where the laser is completely interfered by the grass root.

To analyze the effect of vegetation, error bar (or uncertainty bar) of the soil candidates in each window is introduced. The error bars used in this study are lines through the soil representatives indicating the uncertainties of the computed soil candidates. They tell how the lowest 0.5% points in a window distribute by the mean and standard deviation. The half length of one error bar is about $1.96\sigma_s$, with σ_s the standard deviation of the collected lowest 0.5% points in a window and 1.96 the coefficient meaning 95% confidence interval. Fig. 3.5 shows the estimated representatives of the soils and their error bars of two surveys in study area. The windows in this figure are organized by traversing every non-empty windows row by row from top to bottom (see Fig. 3.5 the gridding of ground point cloud). This can be noticed from the distribution pattern of the window elevations in Fig. 3.5 (a) and (c). The mean elevation of the soil candidates shows an increasing trend from this figure, which may be explained as: 1) the ground elevation in the study area is not flat; 2) however, this is more likely due to the occlusion from the grass, since these windows with higher elevations are farther from the laser scanner than other windows. Despite most soil candidates distribute in range $[-1.95m, -1.99m]$, some large and low evaluations are observed in the figure due to the above-mentioned grass effect. From the enlarged error bar Fig. 3.5 (b), the 95% confidence intervals of the soil estimates from each window can reach down to sub-millimeter or millimeter level. The high precision implies that the selected

lowest 0.5% points in each window vary in height by very small scale, indicating that the method for selecting the soil representatives is acceptable. Nevertheless, this figure also demonstrates that the height estimates of the soil representatives vibrate from window to window even for those neighboring windows, indicating the roughness of the area as well as the ”root surface”.

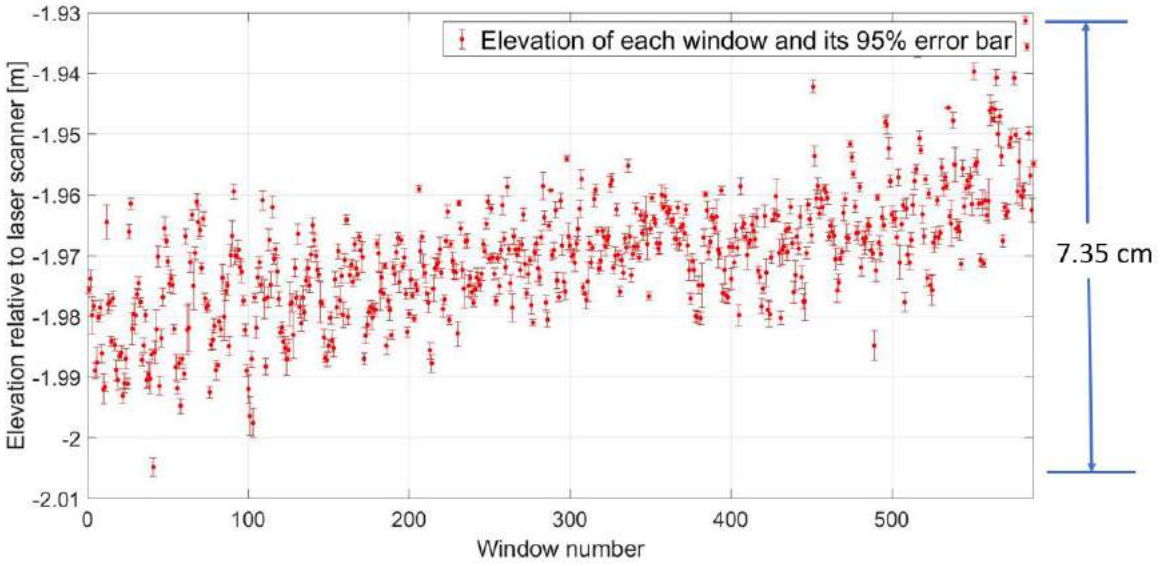
Elevation of each window and its 95% error bar
Elevation relative to laser scanner [m]
Window number
7.35 cm

(a)

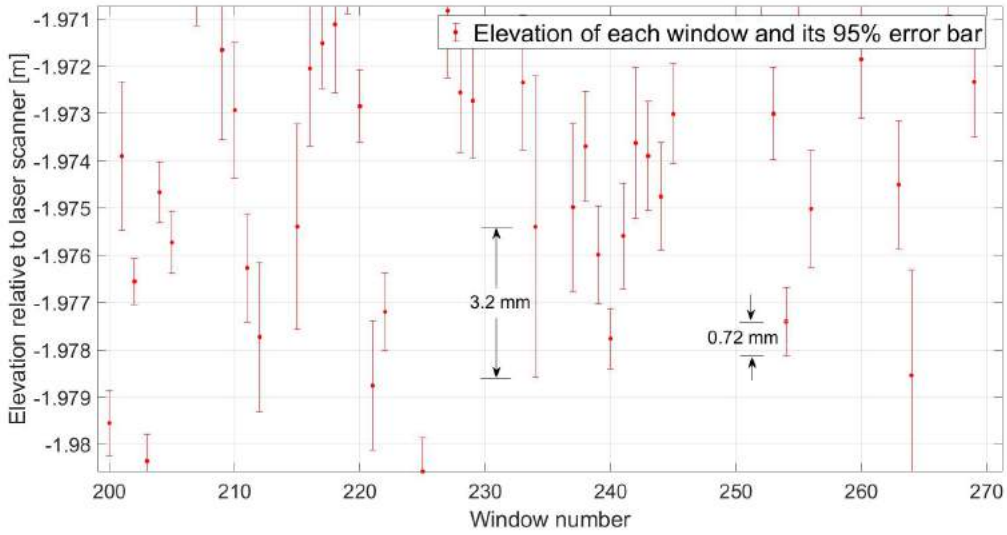
Elevation of each window and its 95% error bar
Elevation relative to laser scanner [m]
Window number
3.2 mm
0.72 mm

(b)

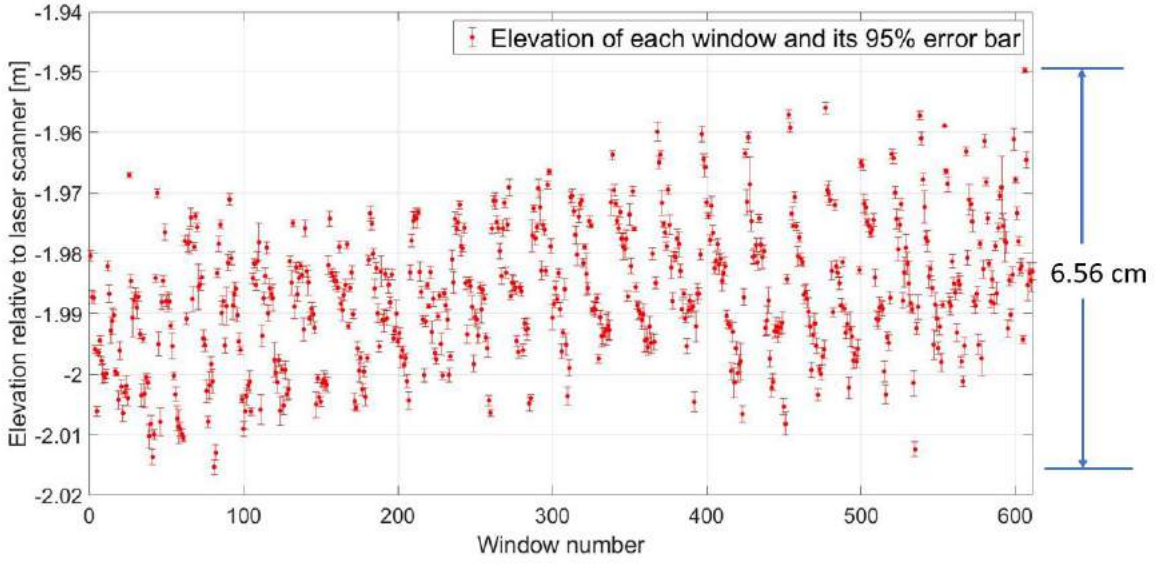
Elevation of each window and its 95% error bar
Elevation relative to laser scanner [m]
Window number
6.56 cm

(c)

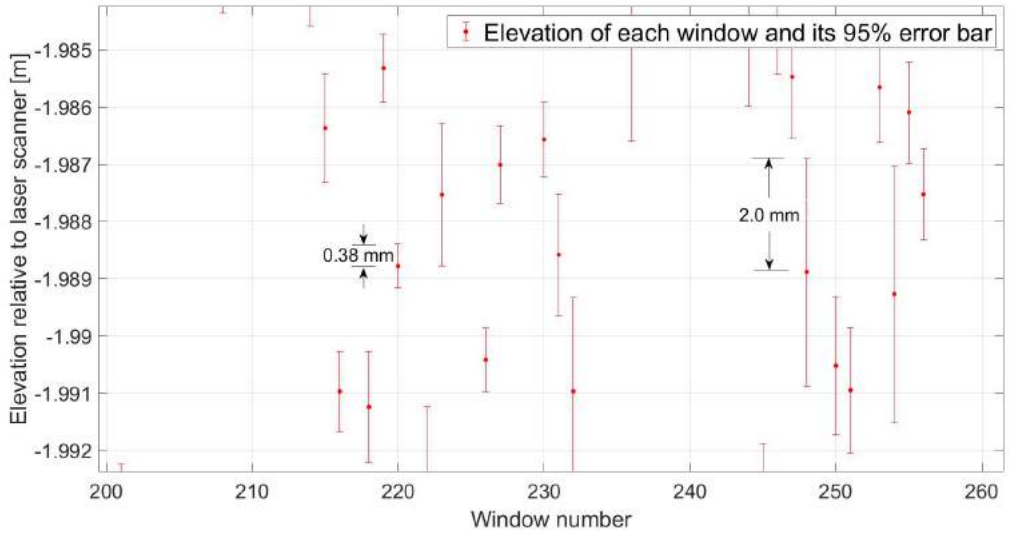

(d)

Figure 3.5: The error bar of the representatives of the soils in each window, with window size $10.00cm \times 10.00cm$ and the lowest 0.5% of all the points in each window. The representatives of in each window is calculated by taking the mean of z-values of the selected lowest points and the length of the bars are determined by the standard deviation of the distribution of those z-values. Elevation of different windows are different even though they are adjacent, implying that grass has different effects on the select lowest points in these windows. They are arranged by traversing every non-empty window row by row. (a) shows error bar of all non-empty windows of survey 1. From this figure, we see that elevations of different windows vary, with 7.35 cm at largest. The trend from left to right and up-and-down hills in between are resulted from the way of organizing windows row-by-row. The values of windows are irrelevant. High values may due to the terrain or grass. (b) shows enlarged error bars of some windows of survey 1 to show the amplitudes clearly. From the error, the uncertainties of elevation estimates of windows are different, ranging from 0.72 mm to 3.2 mm in this enlarged figure. (c) shows error bar of all non-empty windows of survey 3. The largest elevation difference among windows can reach 6.56 cm. (d) enlarged error bars of some windows of survey 3. The uncertainties of elevation estimates of windows vary from 0.38 mm to 2.0 mm in this enlarged figure.

3.1.4. Window pair

A "window pair" is defined in this study as the two windows having the same position but different height measurement. It is explained using the registered point clouds of survey 1 and survey 3. After registration and clipping (described in section 3.1.2), the only difference between these two points clouds is the height values of the ground surface, namely, in Z-dimension. The overlap of the point clouds in horizontal dimension enables to segment the area by the grid (described in 3.1.3) in exactly the same way. In other words, each of the windows in survey 1 produced by gridding corresponds one identical window in survey 3 at the same location. It can be seen in Fig. 3.6, the two ground point clouds of two surveys are shown at right side, with zoom-in picture of several windows. For example, one window pair in this figure is the windows with elevation value Z_5 and Z'_5. They are the same in $X-Y$ dimension but different in Z dimension. The height difference between them is computed by subtraction. The other window pairs in this zoom-in figure are $[Z_6, Z'_6]$, $[Z_7, Z'_7]$, $[Z_9, Z'_9]$, $[Z_{10}, Z'_{10}]$ and $[Z_{11}, Z'_{11}]$. Besides the window pairs, empty windows which have no measurements are also shown in this figure.

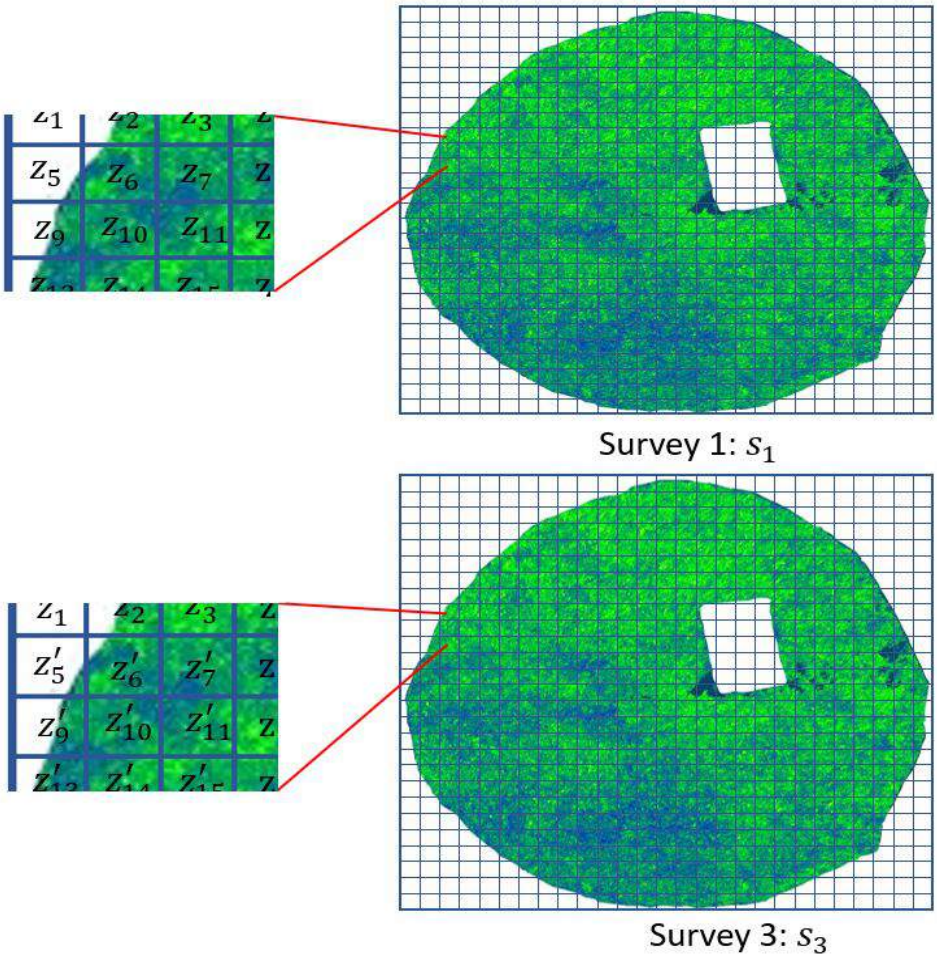

Figure 3.6: Window pairs of two surveys. Each window (cell) in survey 1 corresponds a window in survey 2. They are at the same horizontal position but different height, indicated by letter z and z', respectively.

3.1.5. Best Linear Unbiased Estimator

This section introduces a way of estimating the subsidence of the ground surface using Best Linear Unbiased Estimator (BLUE). As part of Gauss-Markov theorem which states that satisfying the Ordinary Least Squares (OLS) assumptions keeps the sampling distribution as tight as possible for unbiased estimates, BLUE has the tightest possible distribution of all unbiased linear estimation methods (Harville, 1976; Frost, Jim, n.d.). Thus, the result of BLUE has the smallest variance among all unbiased linear

estimators (Goldberger, 1962). BLUE is used when two criteria are met: 1) the observation is a linear function of the unknown variable and 2) The expectation of the unknown equals the unknown itself. In the following context of this section, it is demonstrated how BLUE is applied to estimate the modulated subsidence and why the method meets the criteria of applying BLUE. It should be noted that thresholds (95% confidence level) for filtering out too large and too small soil candidates in the study area are set to remove very large and very small measurements. For the windows pairs which show elevation difference surpassing the thresholds, they are removed out considering that they may induce more biases than other window pairs.

For each window pair, the height difference between two corresponding windows is

$$d_i = Z_i - Z'_i, \tag{3.1}$$

where d_i is the height difference between a window pair with index i, it is computed by the subtraction between two elements in the window pair which are 1) Z_i, z-value of a window of the ground measurements at epoch 1 and 2) Z'_i, z-value of the other window in the window pair, which is from the ground measurement at epoch 2.

This lead to the expression of the height change between the two ground measurements by doing subtraction for every window pairs. This can be written in mathematical way

$$d = s1 - s2, \tag{3.2}$$

where $s1$ and $s2$ are two vectors in which are the height estimates of all the windows in ground point cloud 1 and ground point cloud 2, and d also a vector denoting the height difference between each window pair. Thus, they have the same size. Taking the computed difference of the window pairs between two surveys as derived observations, a functional model of BLUE can be constructed by equation

$$E(d) = Ax, \tag{3.3}$$

where x is a quantitative value meaning a potential subsidence, A design matrix and $E(d)$ the expectation of height difference of window pairs. A is a all-ones vector with a size the same as d. This equation can be simply explained as that the height difference of the two surveys is deemed subsidence of the ground. Thus, the criteria for applying BLUE are met. As the variances of the soil representatives of each window in two scans are able to be computed from the extracted lowest 0.5% points, the variance of each window pair indicating the height change is known as the sum of the variance of separate windows. Based on this relationship, the stochastic model of BLUE is constructed as

$$D(d) = Q_{dd}, \tag{3.4}$$

where $D(d)$ and Q_{dd} are the co-variance matrix of the derived observations d. They are diagonal matrix evaluated as the variances of window pairs, with each element in them is the sum of variances of two individual windows of a window pair. Applying BLUE, the unknown subsidence and its variance are estimated by equations

$$\hat{x} = (A^T Q_{dd}^{-1} A)^{-1} A^T Q_{dd}^{-1} d \tag{3.5}$$

and

$$Q_{\hat{x}\hat{x}} = (A^T Q_{dd}^{-1} A)^{-1}. \tag{3.6}$$

It is noticeable that the height difference of a window pair may be zero if the two windows have same z-value due to the situation when the soil representative in the higher window is evaluated too low and the lower window is evaluated too high (see Fig. 3.5). If this situation occurs, the height difference of this window pair can be considered as an outlier, as a result, it is removed from the derived observation vector. This reduces the influence of the uncertainties for subsidence estimation, which may be from incorrect extraction of soil candidates. Comparing this result to the foreknown thickness of the added platform which is deemed as the modulated subsidence in this research, an error is computed. Thus, how much the subsidence estimate biases from the truth is known.

3.1.6. Histograms of soil candidates

The height change (i.e., subsidence) between two surveys can be estimated in principle using histograms derived from the two surveys. The distance between two peaks of histograms reflects the height difference. Taking survey 1 and survey 3 as an example, their point clouds are processed by the method of local-lowest-points which is described in section 3.1.3. This produces two vectors, each of them contains the soil candidates of the study area. The height distribution of soil candidates can be displayed in histograms (see Fig. 3.7). The height values of the soil candidates on the x-axis refer to the distance to the reference platform which keeps unmoved. The main message of this figure is the changing probability of the soil candidates at different z-values. A roughly normal distribution can be observed from the figures, implying that there is a higher probability to determine the height of the soil surface at the elevation that reaches the peak of probability distribution. The outliers among candidates may be found at two sides of each figure, which could be affected by the grass. As the soil surface in this study is defined as the solid surface of the grass roots that thickly covers on the bare ground, the height with highest probability is estimated as the grass root surface. The height distributed at left may be caused by grass edge effect or occasionally deep penetration of laser beam, and the distribution at the right part of the figure indicates that the laser beams are likely to hit on the upper stems or leaves of the grass.

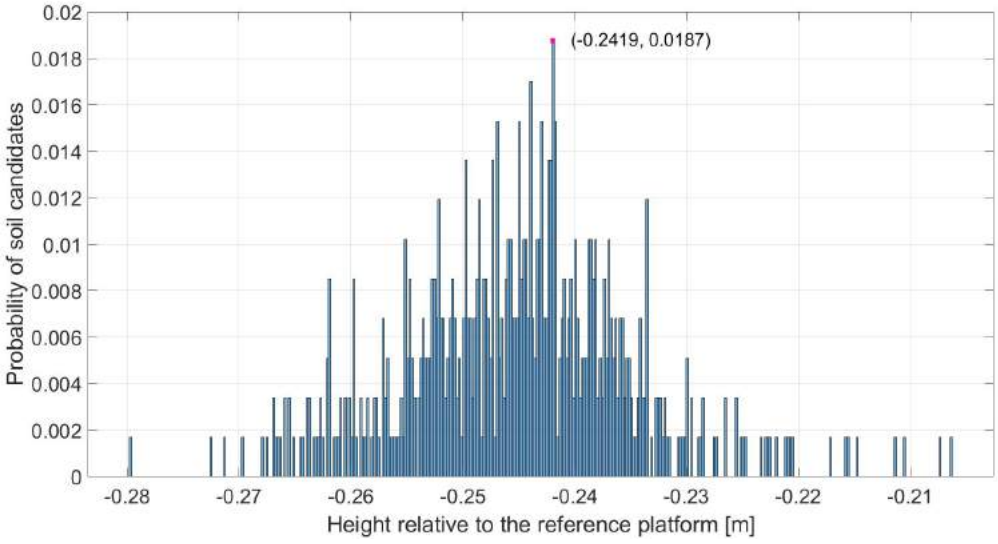

(a)

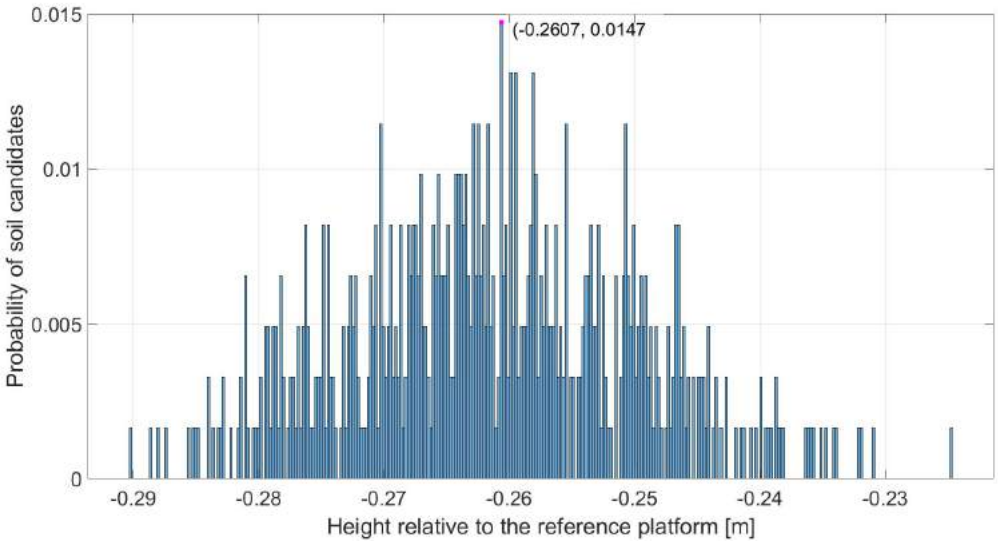

(b)

Figure 3.7: The histograms of soil candidates of survey 1 and survey 3, with bin width 0.2 mm. X-axis indicates the vertical distance relative to the reference platform. Y-axis indicates probability of the vertical distance. (a) show the height distribution of soil candidates of survey 1, (b) show the height distribution of soil candidates of survey 3. The histograms have roughly normal distribution in shape, which means there is higher probability that the elevation of soil measurements is located closer to the middle of the histograms. From these two histograms, the difference between the peaks which indicates elevation difference can be computed.

The subsidence is able to be assessed by calculating the height difference between the peaks of the two histograms. Drawing the histograms in one figure gives a clear view of the disparity of the peaks. From the figure, we can see the quantity of the difference of the probability peaks. This quantity is estimated as the subsidence from survey 1 to survey 3. The quality of the estimation mainly depends on two factors: first, the accuracy of selecting soil candidates using local-lowest points in each window; second, bias when using the peak of a histogram to represent the height of soil surfaces.

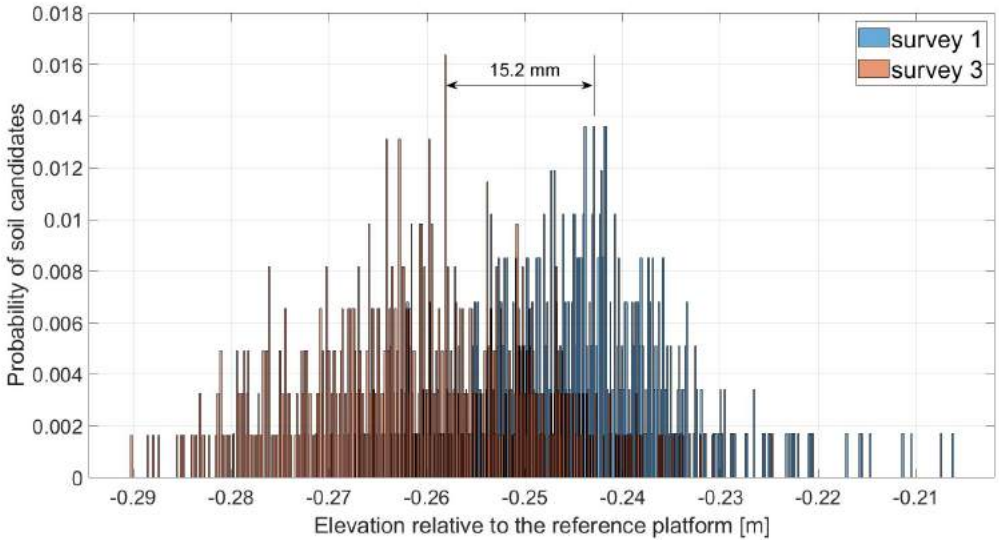

Figure 3.8: The histograms of soil candidates of survey 1 and survey 3 showing together in one figure to show the disparity of their distributions. Referencing to the same reference platform, the height difference between two peaks implies elevation difference of two surveys. From this figure, we can derive a 15.2 mm ground displacement, which is close to the actual value 17.0 mm.

3.1.7. Convolution

In this research, the author employs the convolution operator from another viewpoint: applying convolution operator on two one-dimension vectors. In Digital Signal Processing, convolution is a mathematical tool that uses two signals to produce a third signal (Smith et al., 1997). Likewise, thinking that replacing the two time series signals by two elevation series vectors, the convolution operator is applicable to find potential relationships between the two vectors.

The two vectors for doing convolution operation are derived from histograms of the elevation distribution (as described in section 3.1.6). Among the elements, only the elevations with a non-zero probability are selected to form the elevation vector. Once the vectors are determined, the operation of convolution is executed by two steps:

1) every element in vector 1 traverses all the candidates in vector 2 to do subtraction between each two of them. This generates an ergodic vector containing all the height differences between candidates in survey 1 and survey 3. For example, a vector with length m traverses a vector with length n could result in a $m \times n$ vector by this way. Fig. 3.9 illustrates how the convolution between two vectors works.

2) A probability distribution of the height difference can be constructed using this derived new vector.

By investigating the probability distribution of the elevation differences in the derived vector, the subsidence from survey 1 to survey 3 can be estimated.

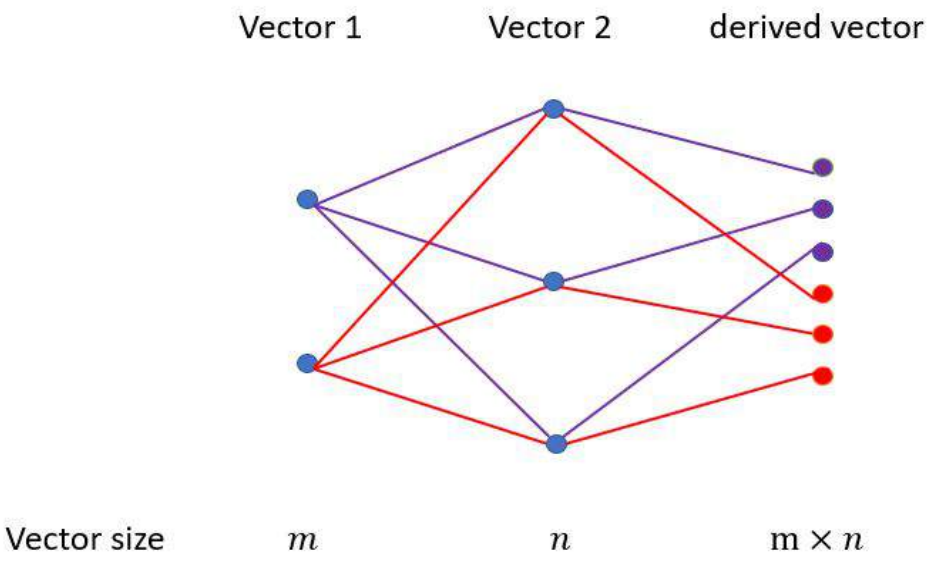

Figure 3.9: The traversing sketch between two vectors. In this example, vector 1 has two elements and vector 2 has three elements, resulting a derived vector with $2 \times 3 = 6$ elements. The "purple" lines indicate the operation between the first element of vector 1 and all elements in vector 2, "red" lines indicate the operation between the second element of vector 1 and all elements in vector 2.

3.1.8. Moving Average

Moving average is a calculation to analyze data points by creating a series of averages of different subsets from a full data set. It can be applied to the selected soil candidates. The reason for applying moving average here is to reduce the grass effect which biases the value of representatives of the soils. Thus, it allows to reduce the grass effect on subsidence estimate and to increase the detectability power. The way of using moving average is illustrated in Fig. 3.10. It can be separated into three steps:

1) take the cell with sign z_6 as the center, another eight cells implying height values are selected in the left figure before doing moving average;

2) take the mean of these selected nine cells, resulting in a new elevation value of the cell located at the center of the selected cells, namely, z_6;

3) repeat step 1) and step 2) for all other cells except those located on the edge of the gridding.

This produces a new derived gridding in which the elevations of all cells are changed. In this study, after having the results obtained from the methods depicted above, moving average is subsequently applied to the soil candidates, leading new results to be observed. Comparison between the results of with and without doing moving average will be done to assess the quality of moving average operator.

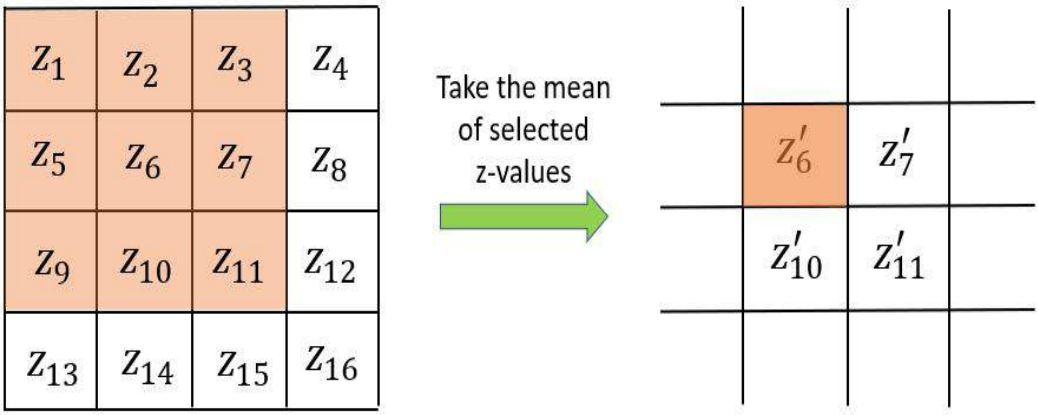

Figure 3.10: A simple example explaining how moving average operation works in this study. Two gridding at left and right indicate the data before and after applying moving average operator. The letters with subscript numbers in a small grid indicate z-value of the grid. The arrow between two griddings means the way of using moving average operator for selected z-values.

3.1.9. Assessment

A way to evaluate the quality of subsidence estimate is to investigate the bias from the truth and its standard deviation. The factors that affect the accuracy of measurements and estimate itself are also analyzed. Furthermore, to determine the probability of detecting a subsidence, the detectability power is calculated (T. T. Liu et al., 2001).

In this research, the detectability power is a measure of the ability to detect a quantity of subsidence of the soil surface. It is expressed as a percentage γ within the context of hypothesis testing. The addition of detectability power and Type II error equals 1. Distinguished from the Type II error which describes the error that occurs when one accepts a null hypothesis that is actually false, detectability power is used to imply to what extent a subsidence can be detected. This gives a hint of predicting the time span between two surveys for a vertical land motion to be detected with a reliable probability. In the following section, the method of doing hypothesis testing is described.

Hypothesis testing

The two important components of a hypothesis testing are null hypothesis stating there is no relationship between two variables and alternative hypothesis stating there is a relationship between them. In light of this research, the null hypothesis and alternative hypothesis are constructed as:

- Null hypothesis H_0: no subsidence
- Alternative hypothesis H_a: b millimeter subsidence

In alternative hypothesis, the variable b is defined as the magnitude of the subsidence.

Under the condition of null hypothesis, we can estimate the subsidence and the residuals in equations

$$\hat{x_0} = 0 \tag{3.7}$$

and

$$\hat{e_0} = d - E(d) = d - A\hat{x_0} = d, \tag{3.8}$$

where $\hat{x_0}$ is the estimated subsidence under the null hypothesis, and $\hat{e_0}$ the residuals. Overall Model Test (OMT) is then used to check the consistency of the collected observations and the underlying mathematical model. It uses the weighted sum of squared residuals as a test statistic, in which the residuals are compared to the a-prior co-variance matrix of the random errors. The test statistics of

the overall model test T_q has so-called "chi-square" distribution when the observations are normally distributed (which is assumed for the distribution of soil candidates, see Fig. 3.1.6). T_q is expressed as

$$T_q = \hat{e_0}^T Q_{dd} \hat{e_0} \sim \chi^2(m-n, 0), \tag{3.9}$$

where $\hat{e_0}$ is the residuals of estimates, Q_{dd} the co-variance matrix of the derived observation (i.e., the soil candidates), and $m-n$ the degree of freedom of chi-square distribution with m the number of observations and n the number of unknowns. To decide whether the null hypothesis should be rejected, the critical value K_α is introduced. K_α is selected based on a so-called "level of significance" α, which is a small probability that make $P(T_q > K_\alpha) = \alpha$. Fig. 3.11 shows the relation between critical value K_α and level of significance α in a "chi-square" distribution. Since we select a level of significance α, the critical value K_α can be determined. In practice, a value of 0.05 is usually chosen for α. Subsequently, we can decide to reject the bull hypothesis H_0 if: $T_q > K_\alpha$.

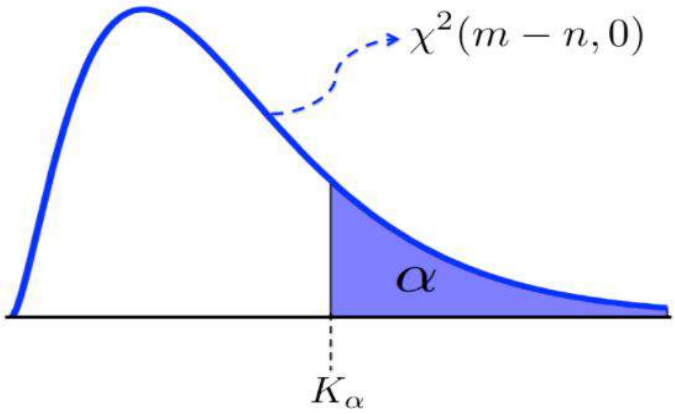

Figure 3.11: A sketch depicting the relation between critical value K_α and level of significance α in a "chi-square" distribution χ^2. $m-n$ is the degree of freedom. (Source: Delft University of Technology, n.d.)

Once the null hypothesis is rejected, the alternative hypothesis is considered with the only different aspect, i.e., the amount of subsidence. Using the confidence level of 95%, the probability of detecting b millimeter subsidence mentioned in alternative hypothesis can be computed. As the null hypothesis is constructed based on height differences of the window pairs (which is defined in section 3.1.3), its standard deviation σ_d is able to be calculated. The coefficient for searching the detectability power is computed by the following equation

$$C = (b - 1.96\sigma_d)/\sigma_d, \tag{3.10}$$

where b is the quantity of subsidence in alternative hypothesis, σ_d the standard deviation of the height difference between two surveys. The 95% confidence level is indicated by $1.96\sigma_d$. It is noticeable that this C corresponds to an area under the one-tailed standard normal curve. The area corresponding the C value can be found in the table in Appendix B, which can be expressed in percentage. Then, the detectability power is determined by adding this area by 50%.

3.2. ALS data investigation

In this section, ALS data are analyzed at some local stations. ALS data used in this study is the Current Elevation File Netherlands (AHN) which is digital elevation map for the whole Netherlands. Organized by the water boards, the provinces and the Ministry of Infrastructure and Water Management, AHN data is mainly used for managing water and flood defense. As laser technology develops, multiple generations of AHN data are acquired with more detailed information and preciser measurements. In this study, the third generation (AHN3) is used for evaluating the performance of ALS data at local areas where IGRS are installed. As the downloaded ALS data contain a broad land, they should be

clipped to focus on the study area. Scanned from airborne sensor, AHN data in local scale are very scarce, with 6-10 points per square meter.

The processing method is described by a working flow, which is a general procedure for analyzing ALS points at IGRS. The way of data acquisition and factors that affecting the result accuracy are given in the follow subsections. What's more, filtering of the measurements manually is illustrated.

3.2.1. Working flow

In this study, AHN3 data covering some local areas wheres IGRS are located are analyzed. There are 30 IGRS have been installed in Groningen area to monitor and detect the potential land motion due to subsurface process. 24 of them, which are installed before the AHN flight over that area are studied. For the other six IGRS, five of them have been installed after the acquisition of AHN3 data, and one IGRS is not clearly seen for some reasons. At these locations, IGRS stations are not visible. The procedure of processing obtained data is illustrated in Fig. 3.12. Once an integrated geodetic reference station is selected to be investigated, one should judge that if the AHN data are obtained after installation of that IGRS. If not, it is not possible to have AHN data on IGRS. If the IGRS is operational after the AHN flight, then corresponding AHN3 data in that area should be downloaded according to the so-call "map number" in AHN official website. As AHN data covering the whole Netherlands are segmented into a lot of pieces in terms of acquisition time, map number is used to code these pieces. Considering flight time and spatial aspects, map number also gives information on the direction of the flight. Each piece of AHN data shrouds a large area where everything in sight is illuminated. Therefore, clipping of data is needed in order to have only a small IGRS-contained local area. The size of the area for clipping is defined by user based on study purpose, thus, the area at each station is extracted manually and differs from each other. The principle to do the manual selection is that selecting an area of 25 to 84 m^2 centered at IGRS, depending on how flat the area is. If the ground is flat, larger area was extracted. While if the ground is not flat since the IGRS is installed on grass land, smaller area was extracted. In this context, many situations are that only the concrete floor where IGRS are installed are clipped (see figures in Appendix D). The concrete floor is usually flat so that the collected ALS points do not have too much variation in height. For those IGRS that are located on very small concrete area, the surrounding grass land is included in clipping procedure, resulting in a larger standard deviation of the ALS measurements of the ground. By importing the clipped data into processing tool, for example Mat-Lab, the points on the platform of IGRS and points on the ground are extracted as subsets. Note that the ability of ALS is limited in accuracy, inducing isolated points from the platform. To filter out the isolated points, manually selection is necessary. Similarly, it is also true for ground points. Nevertheless, the situation for the ground measurements is more complex due to uneven terrain and vegetation. Once the points are selected, statistics are then computed and analyzed. In next section, the influencing factors for ground measurements are discussed, following by the method of removing outliers from the main point group.

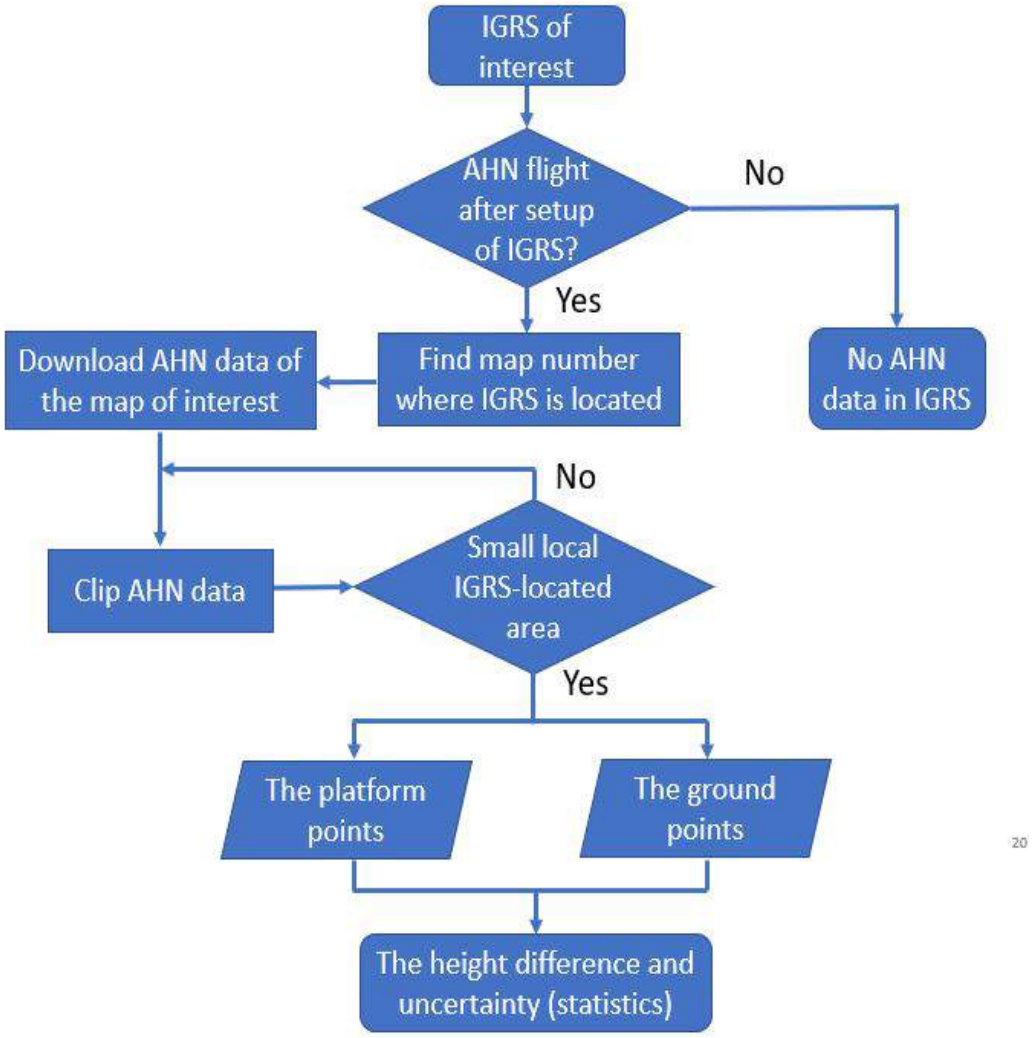

Figure 3.12: The procedure of processing AHN3 data at IGRS. This is a procedure from choosing an IGRS station to estimating the relative height difference between ground and reference platform.

3.2.2. The factors inducing outliers

Calibration

Errors may happen when two fly strips calibrate with each other. Fly strip is a term indicating the area swept by laser in an ahead-planned flight lane. In flight lane, as the fly strip is limited with respect to its width, multiple strips have to be used to cover a large area. One problem from using more than one strips is that the objects at the edge of one strip, such buildings, houses and roads, have to be displayed completely without distortion of shape and height. To solve this problem, the fly strips usually overlap each other somewhere between 20 and 35% (AHN, n.d.). To connect these fly strips in use of the overlaps, calibration is needed. Three main sources of misfit in calibration and related misfits are shown in Fig. 3.13 and Fig. 3.14:

- roll. As shown in Fig. 3.14 (A), the roll behaviour of the plane causes misfit of the saddle-back lines. Despite a horizontal difference is viewed in the figure, the bias between two objects in practice also contains a vertical component because the strip is rotated according to the roll axis instead a transformation offset.
- pitch. Fig. 3.14 (B) shows how a rotation in according to the pitch axis affects the match of the fly strips. This occurs when the plane tilts forwards or backwards. Still, a misfit in horizontal and vertical dimension is found due to instability in pitch axis.
- yaw. Another pattern of misfit is found when the heading of the plane varies when calibrating two fly strips (see Fig. 3.14 (C)). The yaw manifests a shift of the flight lanes, resulting in different shapes of a fly stripe at front and back sides.

Due to the misfits of the fly strips, calibration errors are inevitable. In practical processing, objects with prominent shape and clear view in the obtained point clouds are often used for calibration, because these objects appearing in two strips allow easy matches of them.

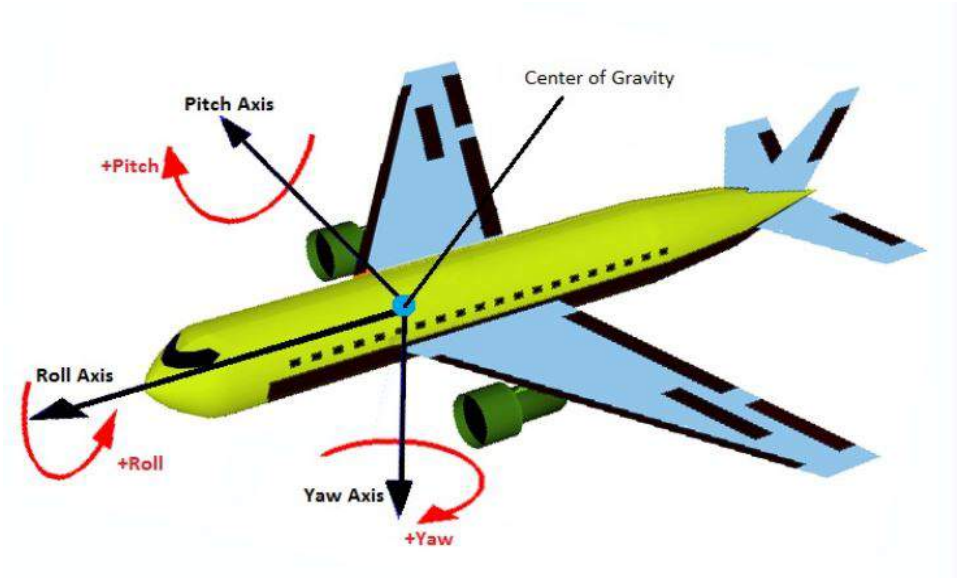

Figure 3.13: Three patterns of the motion of the plane when obtaining AHN data. (Source: (Tekno-Port, n.d.))

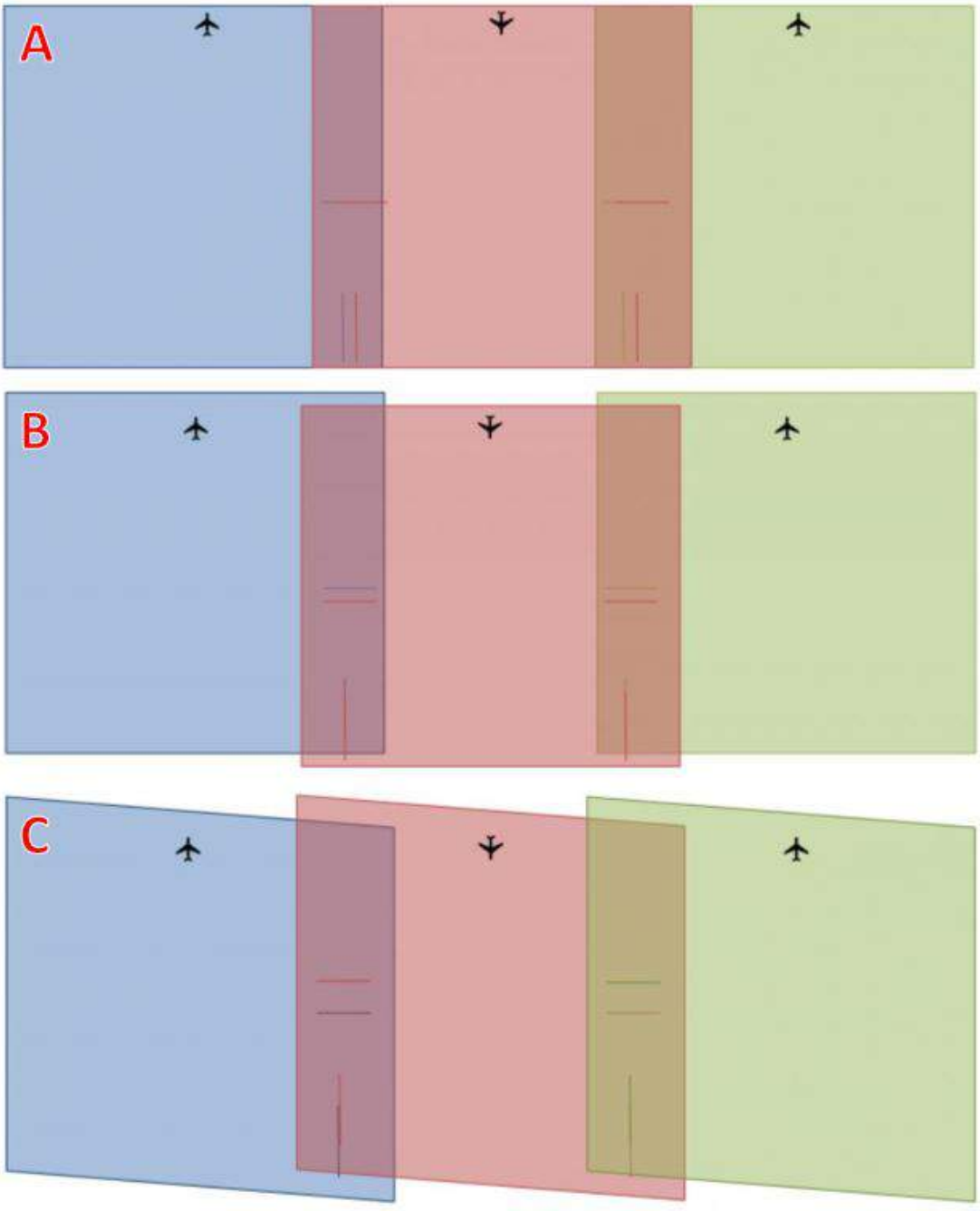

Figure 3.14: The diagrams demonstrate different misfits resulting in calibration errors. Shapes with different colors means different fly strips and the lines in the overlapping part imply the saddle-back roofs that are used as the targets for calibration. (A) shows the misfit due to rolling of the plane when fling for measuring. (B) shows the misfit due to pitch of the plane. (C) shows the misfit due to yaw behaviour. (Source: (AHN, n.d.))

Terrain and vegetation

Calibration errors or outliers occur when connecting two or more flight strips. For the object inside one strip, the outliers may result from different sources. One aspect is the inaccuracy of laser scanning. In order to hit the ground surface, the energy of laser must be strong enough. However, when the energy of laser increases, the frequency of laser beam decreases. To meet the request for minimal points to be collected, there is a balance between energy of laser and frequency. This is especially concerned for the ground measurement when terrain fluctuates. In this study, the local ground surface is assumed to be generally flat at IGRS so that the the standard deviation of ground measurements is able to be computed. This is true especially for those that are installed on concrete and with concrete surrounding area. Under this assumption, the terrain that may vary at some spots leads to outliers. If the ground is found with a slope, a modification will be applied to adjust it to the horizontal surface. This allows the statistical computation of the elevation points distribution. This will be discussed further in the result chapter.

Besides the terrain, vegetation is another important source of the outliers for ground measurements by ALS. Even though AHN3 data have been processed taking into account the grass, outliers are still possible if the grass is dense and high.

3.2.3. Remove outliers

Filtering out the outliers is done manually. The points at IGRS are investigated using processing platform, for example, MatLab in this study. Fig. 3.15 provides an example of how the points of local ground surface and IGRS in AHN3 distribute, together with a picture of the station. The coordinates of the points are shown in local coordinate system (EPSG:28992). Knowing the IGRS structure (see Fig. 3.15 (a)) as a-prior knowledge, different components of IGRS can be recognized and subsequently, the points of each part can be selected. However, outliers may exist in both platform point group which are the points on the platform and ground point group which are the points on the ground surface. As the reference platform of IGRS is precisely leveled, the points on it should be located at the same elevation level. Thus, the elevation that most platform points located is considered as the platform surface, resulting that other points as outliers. Only non-outlier points are selected as the derived platform point subset. This method is also applied to ground points selection although the ground surface is not as horizontal as IGRS platforms. However, realizing that the ground points are affected by the terrain and vegetation, higher elevation difference is acceptable, meaning that the height difference in ground point group is allowed as long as no height jumps. In Fig. 3.15 (b), the point at middle bottom is considered as an outlier because its height isolates from the main ground point group.

(a)

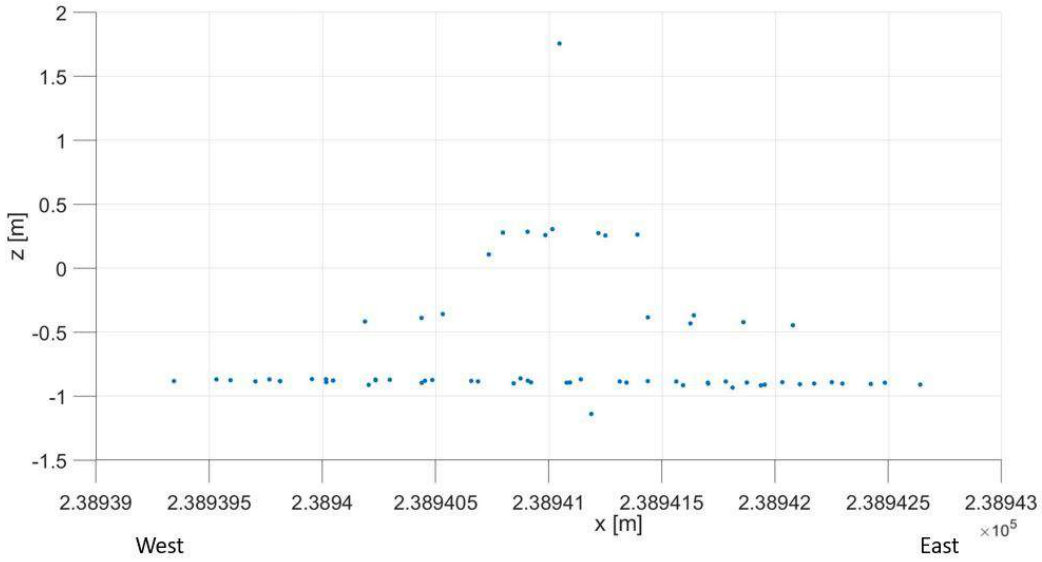

(b)

Figure 3.15: The picture of IGRS Engelbert (a) and its point cloud (b) from AHN3 data. This point cloud is shown in x-z dimension to highlight the elevation of the points. The horizontal reference system is Amersfoort / RD New - Netherlands - Holland - Dutch (EPSG:28992). Variation of x-values from left (small) to right (large) indicates the direction from West to East on Longitude perspective. We recognize different components of IGRS based on this point cloud, as each part of the station has different elevation and they reflect laser beams of ALS. (Picture (a) source: (Satellite Radar Lab TU Delft, 2019))

This chapter introduces how the laser scanner was placed in TLS experiments. To determine soil candidates, local-lowest points in each small window are selected. For surveys obtained at two epochs, methods of BLUE, histograms and convolution operator are applied to estimate ground subsidence. After that, the way of determining uncertainties of ALS data at IGRS is introduced. In next chapter, the results obtained using these methods to TLS data are shown and discussed. In Chapter 5, the results of studying ALS data are introduced.

4

Subsidence estimation based on TLS data

In this chapter, results of applying the methods to estimate the subsidence from multiple survey pairs are given and discussed. The influence of using moving average operator is analyzed by comparing to the results without using that operator. Finally, the quality assessment in terms of detectability power is described. It should be noted that the vertical land motion is modulated by changing the vertical distance between the ground and the platform by adding a plate beneath the platform. As a reminder, the thickness of the added plate in the experiments is 17.0 millimeter.

4.1. Vertical change estimation and evaluation

In this section, vertical land motion is first estimated using BLUE. The results are then used to compute the probability of the detection. After that, results of the other two methods, histograms and convolution operator, are given.

4.1.1. Estimation form BLUE

Vertical change between the point clouds of two surveys is estimated using Best Linear Unbiased Estimator. Taking survey 1 and survey 3 as an illustration, a vertical change of 17.4 mm is estimated. Affected by the quality of selection of the soil candidates in each survey, the result differs from the truth by only 0.4 mm, implying that the method of local-lowest-points for representing the soils is applicable. Besides, the precision (or standard deviation) of the estimation reaches sub-millimeter level (0.3 mm). This means that the uncertainty of the estimation is small. In other words, there is 95% chance that the error obtained from BLUE locates in the range 0.3 mm $\pm$0.6 mm. When speaking of a window pair, we mean two windows which have the same (x, y) coordinate in two surveys. The term "window" in this research is defined as a frame which indicating a local area in the point cloud to select the 0.5% lowest points. The result demonstrates that the size of the window and the quantity of the selected points work well in representing the soil surface in this example.

We tried this method for eight surveys conducted, which are numbered from 1 to 8. Amongst them, survey 1 to survey 4 were carried out in the same day when the grass was long, while survey 5 to survey 8 were carried out in another day when the grass was short. What's more, high resolution was used by laser scanner in singular-number surveys, while low resolution was used in even-number surveys. Tab. 4.1 shows the results of the subsidence estimate using various combinations of singular survey numbers. It implies generally the performance of high resolution laser scanning in this grass covered area. We have mentioned that applying BLUE for survey 1 and survey 3 results in a 0.4 mm error and 0.3 mm standard deviation of the subsidence estimate. As a comparison, the results of survey 5 and survey 7, in which the grass was short after mowing, show a much higher bias from the true subsidence but a smaller standard deviation. For survey 1 with long grass and survey 7 with short grass, a ground subsidence of 19.2 mm is estimated with standard deviation of 0.3 mm. As there are very

small differences in standard deviation, the main effect of grass is on the height change computation. Deviating from original thought that long leaves of grass lead to more occlusion of laser beam, the smallest error is obtained from the first computation in the table. Unexpected from the result of short grass scanning, the computation on second combination gives the largest error. Besides, from the first two combinations of surveys, we see that the subsidence estimates are not same. This is surprising because the surveys for applying BLUE were obtained under the same grass condition, either long grass or short grass. The reason for explaining the bias might be that scanning a low grass covered area from different positions can lead to different extents of occlusion. In other words, the penetration depth from different scan directions can differ a lot in a low grass covered area. This finding differs from the conclusion made by previous study (Fan et al., 2014) which stated that scanning from different position reduces vegetation error. For a more general case when two surveys were obtained at different grass condition, the third combination of surveys results in a 2.2 mm error. From these comparisons, we can conclude that the grass have an influence on the representation of the ground, thus, on vertical motion. However, how the result varies along the grass length remains unclear.

Table 4.1: Subsidence estimation using BLUE for different survey combinations. For each survey combination, the true ground elevation difference is equal to the thickness of the plate (17.0 mm). This "true" value is measured several times using a millimeter ruler, among which the maximal measurement is 17.1 mm and minimal measurement is 16.9 mm. We conducted eight surveys in total, which are given serial numbers from 1 to 8. Amongst, survey 1, 3, 5, 7 were conducted using high resolution ($1.6\ mm@10m$), while survey 2, 4, 6, 8 were conducted using low resolution ($3.1\ mm@10m$).

Survey combination	True subsidence	Grass leaves	Estimate [mm]	Bias [mm]	Standard deviation [mm]	Resolution
Survey 1 and survey 3	17.0	Both long	17.4	0.4	0.3	high
Survey 2 and survey 4	17.0	Both long	17.3	0.3	0.4	low
Survey 5 and survey 7	17.0	Both short	14.4	2.6	0.2	high
Survey 6 and survey 8	17.0	Both short	14.9	2.1	0.2	low
Survey 1 and survey 7	17.0	One long, one short	19.2	2.2	0.3	high
Survey 2 and survey 8	17.0	One long, one short	18.8	1.8	0.3	low

Tab. 4.1 also provides the subsidence estimate from survey combinations using low laser resolution ($3.1mm@10m$) while remaining other settings the same. Similar as the result of survey 1 and survey 3, the result of BLUE using survey 2 and survey 4 gives the smallest error among low-resolution surveys. Even though the quantity of estimated subsidence from survey 6, 8 and survey 2, 8 are a bit better in terms of subsidence estimate compared to the result of survey 5, 7 and survey 1, 7, The standard deviations of estimate are same. The results in this table are also proofs that the grass has a dramatic influence on the subsidence estimate using terrestrial laser scanning technology. Comparing these two tables, we can see that the performance of TLS on study area is better in use of low resolution. This could be because low resolution allows larger spacing interval of points, resulting in higher chance to illuminate the soils under the grass. Fig. 4.1 shows the study area after mowing and a close view on the mowed grass. In (b) we can see that the grass is so densely covering on the ground that the soils are hardly exposed to sight. This figure could also provide an illustration that scanning the ground from different directions may result in different penetration depth, especially for densely short grass.

(a)

(b)

Figure 4.1: The grass in the study area after mowing. (a) shows a general view of the mowed area together with laser scanner. The spatial relationship of the area, the platform and the scanner are seen. (b) takes a close look at the mowed ground. After mowing, the grass is shorter, exposing its roots to the coming laser. However, the bare soils are still seriously shielded as a result of the roots.

4.1.2. Hypothesis testing on estimated value

In last section, the results of subsidence estimate from multiple survey combinations are given. This provides information of how BLUE performs in our environmental setting. However, this is not enough considering the quality of the soil representatives (see Fig. 3.5). There is a chance that the estimated height change of the ground is not due to subsidence, but instead, incorrect measurements. Therefore, it is of importance to know to what extent the detection is subsidence. To this end, detectability power is used as a descriptor to evaluate the possibility of detecting a certain amount of height change.

Null hypothesis

To compute detectability power, hypothesis testing should be conducted. Utilizing the hypothesis testing to the result of BLUE allows to calculate the probability of the detection for such an estimated subsidence. In this research, the null hypothesis is that no subsidence occurs in the scanning area. As the residuals are computed based on BLUE, the test statistics T_q which is the weighted sum of squared residuals, is calculated. This value is compared with the critical value K_α which corresponds to a (usually chosen) significance level 0.05. Using the result of survey 1 and survey 3 as an example, the null hypothesis is rejected as the test statistic T_q is larger than critical value K_α.

Alternative hypothesis

The construction of alternative hypothesis is described in section 3.1. Using the result of survey 1 and survey 3, an alternative hypothesis that there is a 17.4 mm subsidence can be constructed. The graphic relation between null hypothesis and alternative hypothesis is depicted in Fig. 4.2. As we choose 0.05 significance level, and the standard deviation (σ_d) of the height difference (H_0) of window pairs between survey 1 and survey 3 is calculated as 6.5 mm, K_α is calculated as $1.96 \times 6.5 = 12.7mm$. Thus, the distance between K_α and μ_2 can be calculated. Subsequently, the coefficient that implies the area in between K_α and the green dashed line in the figure can be inspected in probability table shown in Fig. B.1. Recalling Eq. 3.10, the coefficient can be calculated as

$$C = (17.4 - 1.96 \times 6.5)/6.5 = 0.7169. \tag{4.1}$$

The probability corresponding to the coefficient can be found in table (figure) B.1. After that, detectability power γ_0 implying the area under H_a and at the right side of K_α can be calculated, which is 75.80%.

This means that there is a probability of 75.80% to detect a vertical change of 17.4 mm in our implemented experiments. It gives a significant message that if the 17.4 mm subsidence obtained in a previous time period can be detected with 75.80% probability, one can thus design a longer time interval for next experiment in order to detect the vertical land motion with a good probability. Reflected from the detectability power, we know that a subsidence of 17.4 mm is how likely to be detected. If we want to recognize the vertical land motion before it reaches 17.4 mm, for example 15 mm, it is in principle detected with a small probability. In other words, if we assume the subsidence of 17.4 mm is accumulated in a time span of one year, we could design our next survey for subsidence detection in a longer time interval so that we can recognize the subsidence with still a high power of detection. This is important for planning a survey to prevent meaningless work that no subsidence is detected or too much subsidence has occurred.

We have known how possible an amount of subsidence could be detectable from detectability power. Similarly, if we aim to know the minimal detectable subsidence with a certain detectability power, e.g., 90%, the following equation derived from Eq. 3.10 can be used:

$$b_{90} = C_{90}\sigma_d + 1.96\sigma_d, \tag{4.2}$$

where C_{90} is the coefficient corresponding to 90% detectability power in a normal distribution curve (see section 3.1.9), σ_d is the standard deviation of the height difference between two surveys, 1.96 indicates the 95% confidence level and b_{90} means the minimal detectable subsidence with 90% detectability power. From the probability table shown in Fig. B.1, we can find the coefficient of 90% probability is 1.281. Thus, the minimal detectable subsidence is computed, which is

$$b_{90} = 1.281 \times 6.5 + 1.96 \times 6.5 = 21.1mm. \tag{4.3}$$

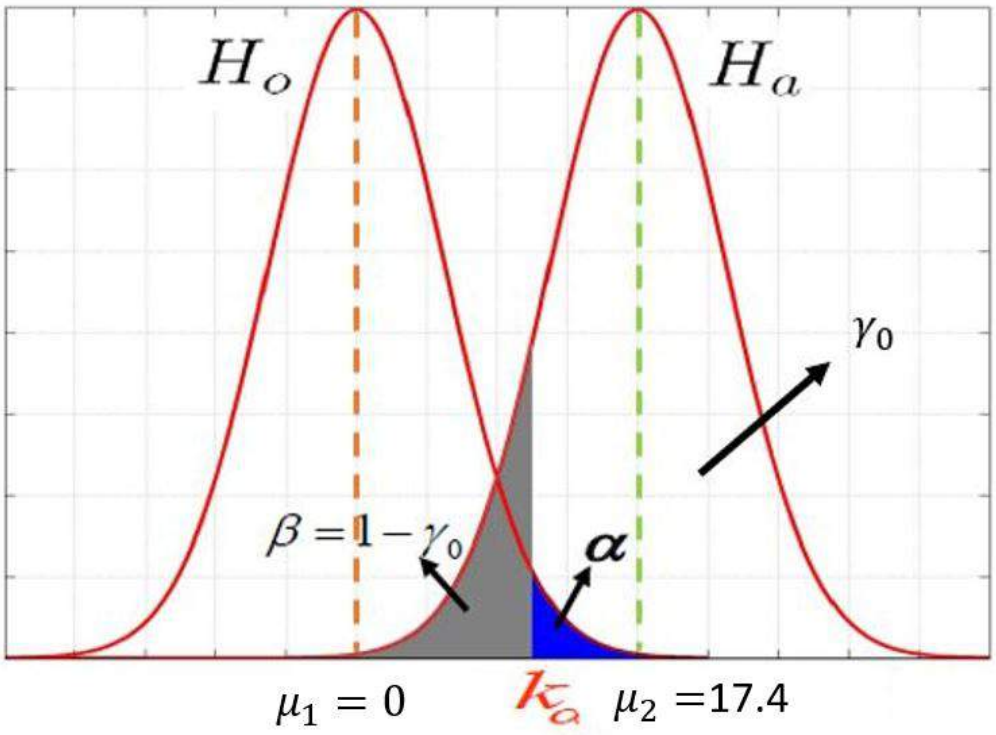

Figure 4.2: The graphic relation between null hypothesis H_0 and alternative hypothesis H_a. The subsidence value in both hypothesis are shown as μ_1 and μ_2 respectively. In this figure, α indicates Type I error or significance level, β indicates Type II error and γ_0 indicates the detectability power under critical value K_α.

We also computed the detectability power for other survey combinations besides survey 1 and survey 3. Tab. 4.2 shows detectability power of different subsidence estimates under both high and low resolution scanning conditions. It is greatly noticeable that for different subsidence estimates, with either large error or small error, the probability of detection for that subsidence is dramatically high. This is because:

1. the distribution of elevation difference of window pairs (see section 3.1.4) has a small standard deviation, which is around 4.0 mm for different survey combinations. This results in a slim probability distribution of both null hypothesis and alternative hypothesis (see Fig. 4.2).

2. the distance between the peaks of null and alternative hypothesis (see Fig. 4.2), namely, the subsidence, is much larger than the standard deviation of null hypothesis (or alternative hypothesis) .

Table 4.2: Detectability power of different survey combinations. This implies under different conditions with respect to grass length and resolution, the power for detection is high. This is because the selected soil candidate in each window has small standard deviation.

Survey combination	Subsidence estimate from BLUE [mm]	Detectability power [%]
Survey 1 and survey 3	17.4	75.80
Survey 2 and survey 4	17.3	75.49
Survey 5 and survey 7	14.4	96.71
Survey 6 and survey 8	14.9	95.25
Survey 1 and survey 7	19.2	89.80
Survey 2 and survey 8	18.8	91.15

4.2. Histogram

Reflected from the height distribution of the soil candidates, the vertical change is able to be obtained. Fig. 4.3 to Fig. 4.14 show the histograms of different survey pairs, with each survey pair distinguishing by orange and blue colors. In the figures at left side, x-axis shows the elevation of the soil candidates referencing to the platform, with bin-width 0.2 mm, and y-axis indicates the probability of each elevation value. Adding a normally fitted line to each histogram, the figures at right side have the same x-axis but different y-axis which means the numbers of soil candidates. The organization of survey numbers are the same as the survey combinations used in Tab. 4.2. Amongst these figures, histograms in Fig. 4.3 to Fig. 4.8 are obtained from scans using high resolution ($1.6mm@10m$), while Fig. 4.9 to Fig. 4.14 are obtained from scans using relatively low resolution ($3.1mm@10m$). It can be obviously observed that an offset exists between two histograms in each figure with respect to elevation. By observing this elevation offset between the two peaks of the histograms, the subsidence of different survey combinations can be estimated. However, limited by the total amount of soil candidates, the number of soil candidates at each elevation is small. This results in a step distribution of the histograms bins, which can be seen in all figures. Despite this limitation, roughly normal distributions of the soil candidates are still observed.

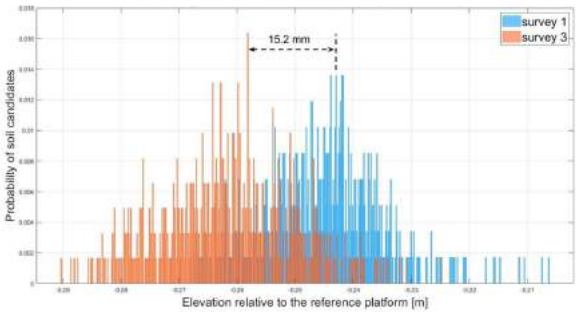

Figure 4.3: Histograms of soil candidates of survey 1 and survey 3. Height difference between peaks of two histograms is 15.2 mm.

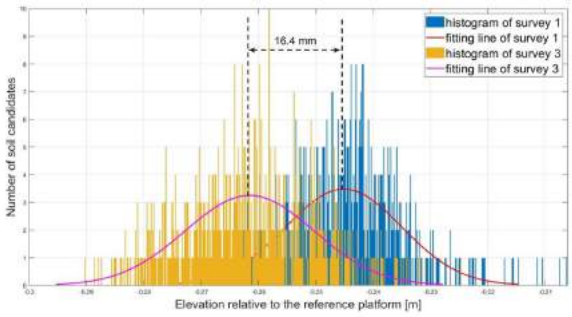

Figure 4.4: Histograms of soil candidates of survey 1 and survey 3, and the normally fitting lines of the histograms. Height difference between peaks of two histograms is 16.4 mm.

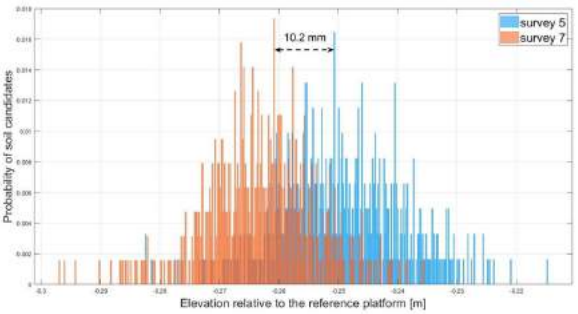

Figure 4.5: Histograms of soil candidates of survey 5 and survey 7. Height difference between peaks of two histograms is 10.2 mm.

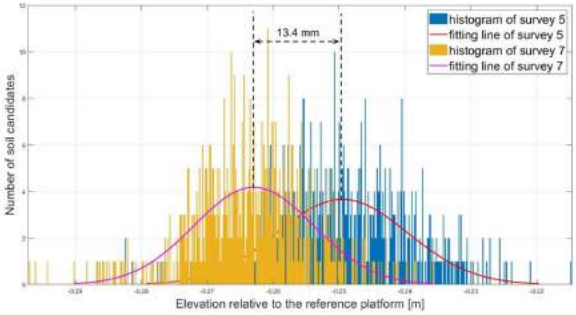

Figure 4.6: Histograms of soil candidates of survey 5 and survey 7, and the normally fitting lines of the histograms. Height difference between peaks of two histograms is 13.4 mm.

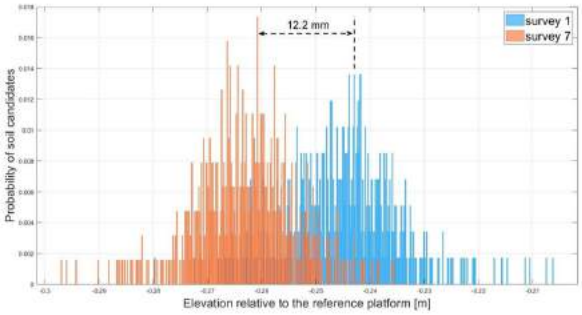

Figure 4.7: Histograms of soil candidates of survey 1 and survey 7. Height difference between peaks of two histograms is 12.2 mm.

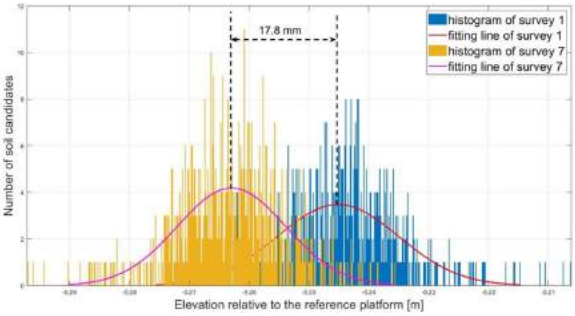

Figure 4.8: Histograms of soil candidates of survey 1 and survey 7, and the normally fitting lines of the histograms. Height difference between peaks of two histograms is 17.8 mm.

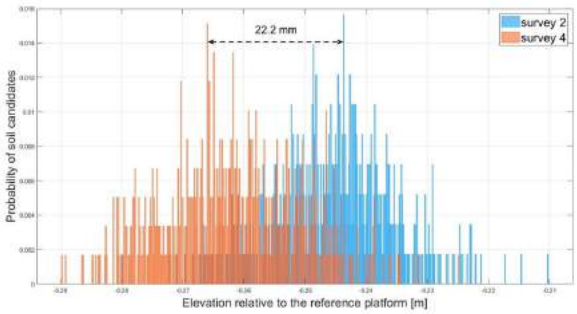

Figure 4.9: Histograms of soil candidates of survey 2 and survey 4. Height difference between peaks of two histograms is 22.2 mm.

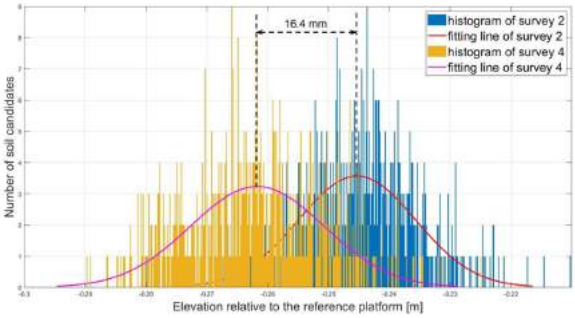

Figure 4.10: Histograms of soil candidates of survey 2 and survey 4, and the normally fitting lines of the histograms. Height difference between peaks of two histograms is 16.4 mm.

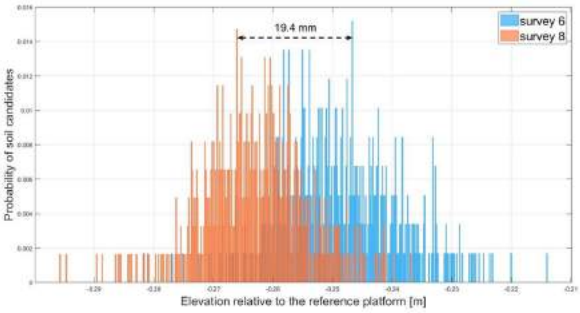

Figure 4.11: Histograms of soil candidates of survey 6 and survey 8. Height difference between peaks of two histograms is 19.4 mm.

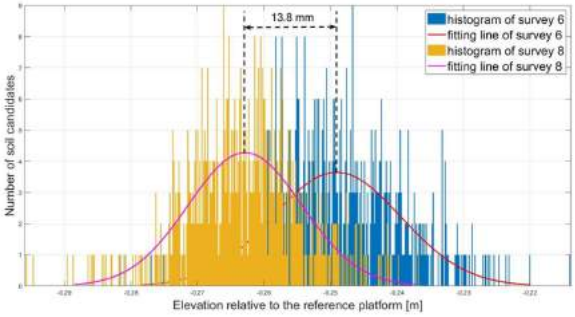

Figure 4.12: Histograms of soil candidates of survey 6 and survey 8, and the normally fitting lines of the histograms. Height difference between peaks of two histograms is 13.8 mm.

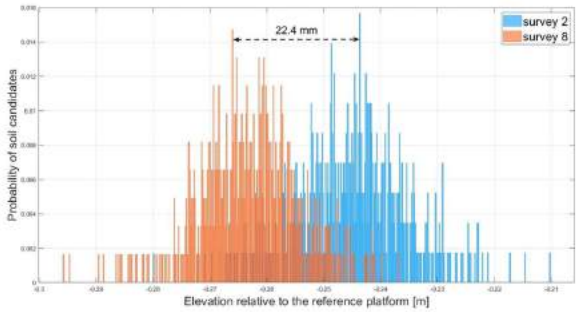

Figure 4.13: Histograms of soil candidates of survey 2 and survey 8. Height difference between peaks of two histograms is 22.4 mm.

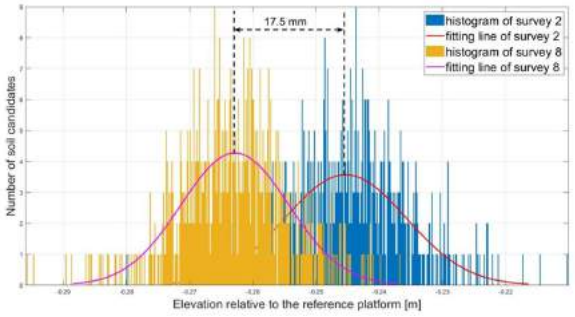

Figure 4.14: Histograms of soil candidates of survey 2 and survey 8, and the normally fitting lines of the histograms. Height difference between peaks of two histograms is 17.5 mm.

4.2.1. Estimating directly from the histograms

The results of the subsidence estimation from both histograms and histogram fitted lines are shown in Tab. 4.3. It is interesting to notice that if estimating directly from histograms, high resolution scans result in underestimation, while low resolution scans result in overestimation. The biases of these estimates reach up to 6.8 mm, which is large compared with the results of BLUE (shown in Tab. 4.2). Comparing the results of survey 1, 3 with the results of survey 5, 7, the estimate of subsidence becomes worse when the grass was mowed. However, opposite variation is observed when comparing the results of survey 2, 4 with the results survey 6, 8.

To conclude, it is difficult to estimate the grass-covered land motion in vertical dimension directly from the histograms. The subsidence varies a lot when grass or scanner position changes.

Table 4.3: Subsidence estimation from histograms directly and from normally fitted lines of histograms. Survey 1, 3, 5, 7 are obtained with high resolution scanning. Survey 2, 4, 6, 8 are obtained with low resolution scanning. True subsidence means the modulated amount of subsidence which is a known value.

Survey pair	True subsidence [mm]	Estimate from histograms [mm]	Estimate from fitted lines [mm]
Survey 1 and survey 3	17.0	15.2	16.4
Survey 2 and survey 4	17.0	22.2	16.4
Survey 5 and survey 7	17.0	10.2	13.4
Survey 6 and survey 8	17.0	19.4	13.8
Survey 1 and survey 7	17.0	12.2	17.8
Survey 2 and survey 8	17.0	22.4	17.5

4.2.2. Fitted line of histogram

The fitted lines of histograms in the figure are generated by normally fitting the histogram bins. As the elevation differences estimated from fitted lines are obtained by comparing the peaks of the lines, the results are different from the results that estimated directly from the histograms. This discrepancy is reflected in the figures and the table. It is widely observed that the estimates using the fitted lines of histograms are closer to the truth. For some survey pairs, the results improve significantly. According to the estimation using fitted lines, it seems that shorter grass (survey 5 and survey 7, survey 6 and survey 8) deteriorates the quality of laser scanning compared to long grass (survey 1 and survey 3, survey 2 and survey 4), which is unexpected as short grass induces less occlusion to our knowledge. This can be seen for both high resolution scans and low resolution scans in Tab. 4.3. For example, fitted lines of survey 1 and survey 3 give the best estimate (with 0.6 mm error), while fitted lines of survey 5 and survey 7 give the worst estimate (with 3.6 mm error). However, taking one survey from scans with long grass (survey 1) and one survey from scans with short grass (survey 7), the result is in between the best and the worst, with 0.8 mm error.

4.2.3. Discussion

From the figures and tables, we see biases in subsidence estimate. The reason for the bias could be because the peak of a histogram does not express the soil surface with a high accuracy. From the distribution of soil candidates in Fig. 4.3, there are three peaks showing the highest probability in the blue histogram. The elevation difference of 15.2 mm is obtained using the peak of the left histogram and the middle peak of the right histogram, ignoring the other two peaks. The reason of this choice is because this peak may balance the other two peaks which is either larger or smaller. However, this may lead to a lower or higher soil surface estimate which will make the soil surface estimate inaccurate.

According to the result of the histograms, we conclude that it is difficult to make a reliable estimation of the height change of the grass covered ground. Affected by the grass length, the result varies unpredictably. The result can be improved by fitting lines to the histograms, which produces errors from 0.6 mm to 3.6 mm in our experiments.

4.3. Convolution

Based on the histograms of the soil candidates, the result of convolution tells how the height differences between each two soil candidates in two surveys distribute (see section 3.1.3). From the height difference distribution, the height difference with highest probability is deemed as the subsidence between two surveys. Fig. 4.15 shows the results obtained from convolution lines which look like roughly normal distributed curves, with a mean and standard deviation. The smaller the standard deviation, the slimmer the convolution curve. The shapes are not unexpected because the soil candidates of the two surveys has roughly normal distribution in height, which would also result in a normally distributed distribution of the height differences between them when each element in soil candidate set 1 traverses the elements of soil candidate set 2. From these curves, subsidence is estimated as the elevation difference when probability reaches the peak. For different survey pairs, various estimates and standard deviations are obtained. As each survey pair has different settings, the results provide information on the influence

of these settings. Tab. 4.4 summarises the statistics of the results in terms of the estimated height change and corresponding standard deviation. From this table, the error of the vertical change of the point cloud is relatively small in this research, ranging from 0 mm to 2.9 mm. Similarly as the results of histograms, the effect of resolution is not clear based on this table. Also, the same influence of the grass is observed in this table as that in Tab. 4.3, which states that short grass deteriorates the accuracy of the estimation. However, when looking at the precision of the subsidence estimate (i.e., standard deviation), we can find that short grass performs a bit better. This is because short grass allows the scans of the ground points to be more centrally distributed in elevation. However, the increase in standard deviation is small. Besides, the standard deviation in the table does not show any evidence to demonstrate which resolution is better.

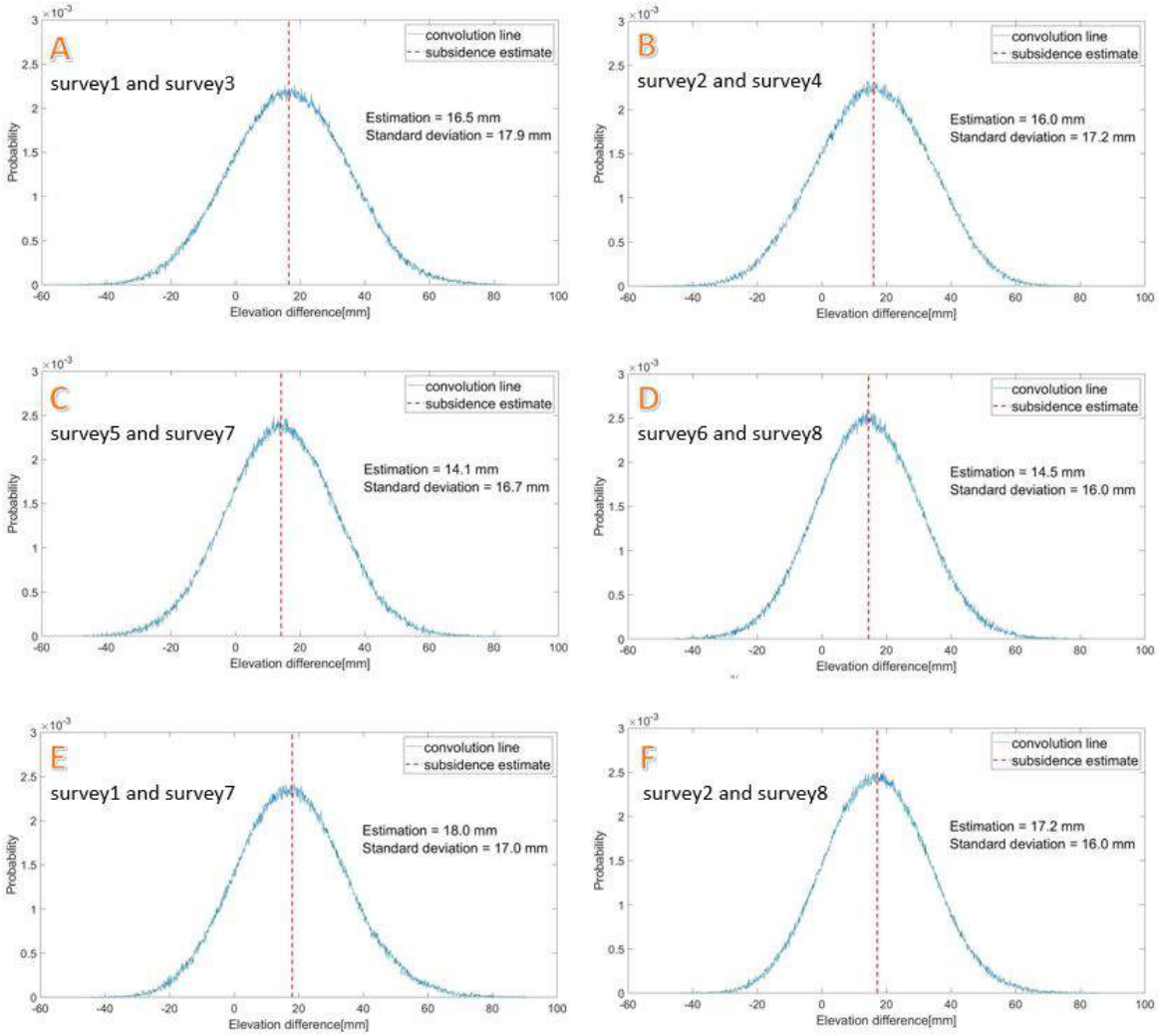

Figure 4.15: Convolution of soil candidates of different survey pairs. X-axis is the height difference and y-axis the probability of the occurrence of that height difference. The red dashed line indicates subsidence estimate. (A) convolution of survey 1 and survey 3. (B) convolution of survey 2 and survey 4. (C) convolution of survey 5 and survey 7. (D) convolution of survey 6 and survey 8. (E) convolution of survey 1 and survey 7. (F) convolution of survey 2 and survey 8.

The advantage of using convolution operator is recognized that the height change can be viewed directly at x-axis where the curve reaches its peak. What's more, it is not dramatically affected by the peaks of single histograms, but all elements in the histograms account for the result despite peaks still gain more weights. However, the large standard deviations shown in Tab. 4.4 demonstrate that convolution may be not suitable for subsidence estimation for dense grass covered land, or more seriously, laser scanning technology cannot produce a high precision when using convolution operator to estimate the elevation change.

Table 4.4: Subsidence estimation of survey pairs using convolution operator.

Survey pair	True subsidence [mm]	Subsidence estimate [mm]	Standard deviation [mm]
Survey 1 and survey 3	17.0	16.5	17.9
Survey 2 and survey 4	17.0	16.0	17.2
Survey 5 and survey 7	17.0	14.1	16.7
Survey 6 and survey 8	17.0	14.5	16.6
Survey 1 and survey 7	17.0	18.0	17.0
Survey 2 and survey 8	17.0	17.0	16.0

4.4. The influence of moving average (MA) operator

Moving average is a calculation to analyze data points by creating a series of averages of different subsets in a full data set. The method is described in section 3.1. The reason for applying moving average here is to reduce the grass effect which biases the values of representatives of the soils.

4.4.1. Influence on selection of soil candidates in each window

Moving average operator has an influence on the selection of soil candidates. It reduces height jumps from one window to its neighbors. The soil candidates of survey 1 and survey 3 before and after using moving average operator are shown in Fig. 4.16. The elevation value in the figure is evaluated as the height of soil candidates referencing to the reference platform. Compared with the raw height values of soils candidates, the vibration of the values after using moving average operator decreases. Furthermore, from the figures, we see that the maximal height difference of the soil candidates is reduced. Thus, the elevations have more centralized distribution, implying that the elevations of soil candidates are closer to the true ground surface elevation. As a result, the standard deviation of the elevations becomes smaller. This influence of the moving average operator can be observed in both surveys. In fact, moving average operator leads to an improvement for all surveys (see Appendix C), which results in derived soil candidates. In the rest of this section, these derived soils candidates are then be used to estimate the subsidence.

Despite the benefits of this operation, however, the number of soil candidates is reduced. This is because the moving average operator works on non-edge elements (see Fig. 3.10). Thus, those windows on the edge of the point cloud are omitted. From Fig. 4.16, it is clear that the number of window, i.e., the number of derived soil candidates, is reduced.

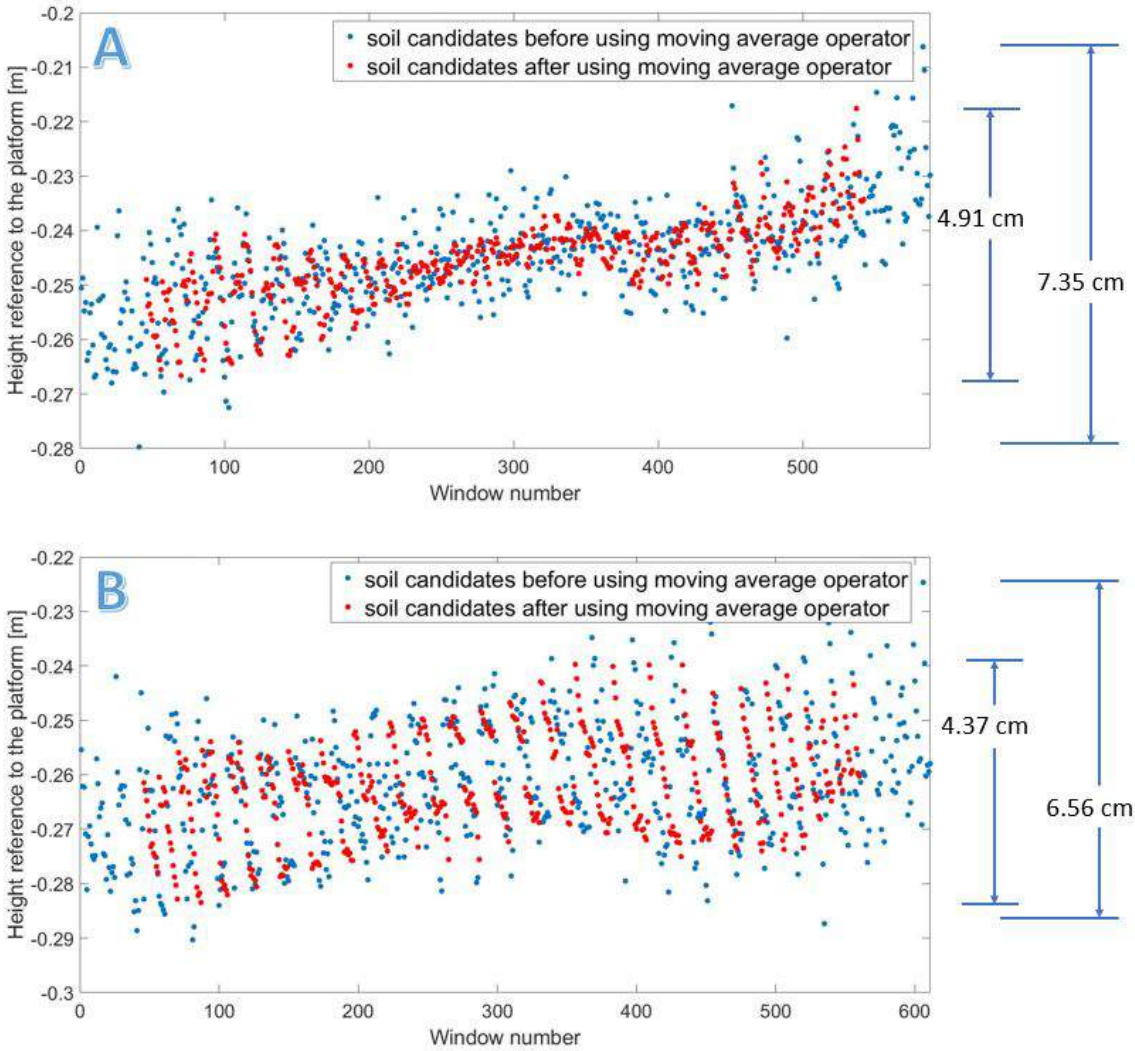

Figure 4.16: Effect of moving average operator of soil candidates selection in each window of survey 1 and survey 3. The dots in this figure are organized by traversing every non-empty windows row by row from top to bottom, thus in ordinal scale sequence (see Fig. 3.5). The red and blue colors in two figures indicate the selected soil candidates before and after using this operator respectively. (A) shows the effect of MA in survey 1, (B) shows the effect of MA in survey 3. As moving average operator works to smooth the height distribution of soil candidates, the disparity between soil candidates are reduced.

4.4.2. Influence on histograms

Since the moving average operator affects the distribution of soil candidates, the height change estimates based on the histograms are expected to be influenced. Tab. 4.5 shows the results of subsidence estimation applying this operator to the selection of soil candidates. Comparing the results in third and fourth column, we find that the moving average operator does not change the estimated subsidence obviously, with difference up to 0.1 mm. The almost same results imply that the moving average operator does not change the mean value of soil candidates in a survey.

Table 4.5: Subsidence estimation of survey pairs based on histograms using convolution operator.

Survey pair	True subsidence [mm]	Subsidence estimate without MA [mm]	Subsidence estimate with MA [mm]
Survey 1 and survey 3	17.0	16.4	16.4
Survey 2 and survey 4	17.0	16.4	16.5
Survey 5 and survey 7	17.0	13.4	13.4
Survey 6 and survey 8	17.0	13.8	13.7
Survey 1 and survey 7	17.0	17.8	17.8
Survey 2 and survey 8	17.0	17.5	17.6

However, applying moving average operator leads to smaller standard deviation of the height change, which is shown in Tab. 4.6. It is broadly seen that the standard deviation of subsidence estimate is reduced, meaning the precision is increased. This increment for each survey pair is more than 20%, which can reach 24.73% at most.

To conclude, moving average operator nearly does not vary the estimate of subsidence of the ground, but it will increase precision by 20% to 25%.

Table 4.6: Standard deviation of subsidence estimation of different survey pairs before and after applying moving average operator.

Survey pair	Standard deviation without MA [mm]	Standard deviation with MA [mm]	Percentage of increased standard deviation by MA [%]
Survey 1 and survey 3	21.4	16.5	22.90
Survey 2 and survey 4	20.6	15.9	22.82
Survey 5 and survey 7	19.0	15.1	20.53
Survey 6 and survey 8	18.3	14.4	21.31
Survey 1 and survey 7	19.2	14.5	24.48
Survey 2 and survey 8	18.2	13.7	24.73

4.4.3. Influence on convolution

We also investigated the influence of the moving average operator on convolution computation. Since the soil representatives of two surveys are expected to have less effect from the grass, the histograms of them become more centralized. As a result, the convolution between the two surveys is changed. From Fig. 4.17, we can see that

- the convolution of soil candidates of two surveys looks like a normal distribution line.
- evaluated as the elevation difference on x-axis with highest probability, subsidence estimate indicated by the red dashed line does not locate at the middle of the convolution line. This means the highest probability of elevation difference may be not found at the middle of the convolution curve.
- the subsidence estimates from some survey pairs bias a lot from the truth (17.0 mm).
- the standard deviations of convolution are similar to each other despite the subsidence estimates are quite different.

The moving-averaged convolution line of two soil sample sets is slimmer. This is explained that first, when an element in one survey subtracts the elements in another survey, the height differences between them are smaller under the effect of moving average operator. Second, the number-reduced soil candidate sizes of two surveys also make a difference on the result of the convolution.

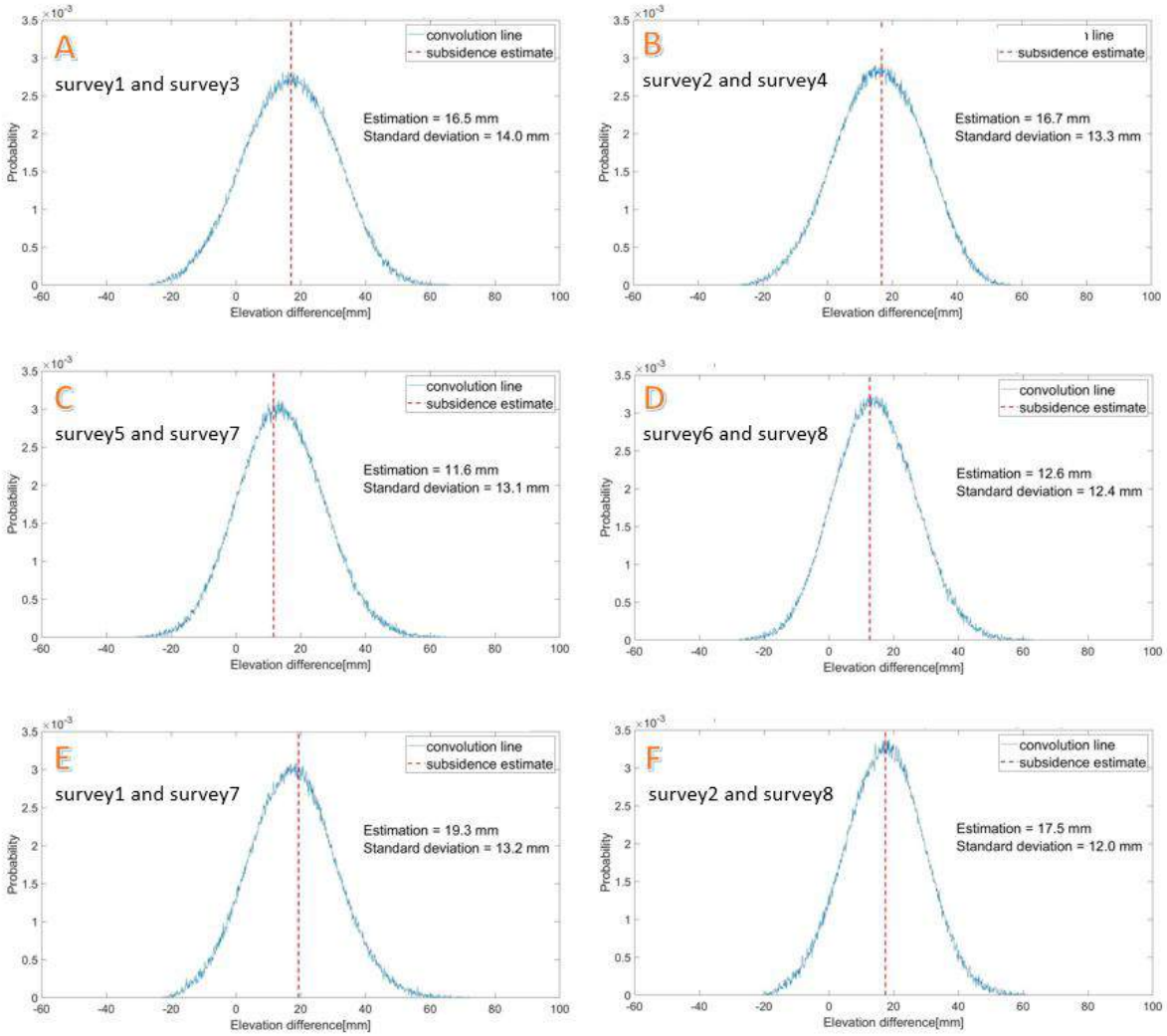

Figure 4.17: Convolution of soil candidates of different survey pairs after using moving average operator. X-axis is the height difference and y-axis the probability of the occurrence of that height difference. The red dashed line indicates subsidence estimate which reaches the peak of the probability distribution. It can be seen that the subsidence estimate may not locate at the middle of the convolution line. (A) convolution of moving-averaged survey 1 and survey 3. (B) convolution of moving-averaged survey 2 and survey 4. (C) convolution of moving-averaged survey 5 and survey 7. (D) convolution of moving-averaged survey 6 and survey 8. (E) convolution of moving-averaged survey 1 and survey 7. (F) convolution of moving-averaged survey 2 and survey 8.

Comparison between the results of convolution with and without moving average operator is shown in Tab. 4.7 and Tab. 4.8. In Tab. 4.7, it is observed that differing from the effect on histograms, moving average operator does not show a trend of changing the subsidence estimate. Nevertheless, the results of survey 1, 3 (under high scanning resolution) and survey 2, 4 (under high scanning resolution) show equal or better estimation, comparing to the results of survey 5, 7 and survey 6, 8 respectively. This implies that using moving average operator for soil candidates under short grass environment might not be a good choice. This is explained that since convolution has resulted in underestimated subsidence estimation, moving average operator could aggravate this trend due to its working way (see section 3.1.7). Besides, the reduced sample size may induce uncertainties in probability computation.

In Tab. 4.8, the standard deviations of the estimation are listed. Despite same trend is observed in histograms, moving average operator increases the precision of estimation. The increment can reach by

Table 4.7: Subsidence estimation of survey pairs based on convolution operation applying convolution operator.

Survey pair	True subsidence [mm]	Subsidence estimate without MA [mm]	Subsidence estimate with MA [mm]
Survey 1 and survey 3	17.0	16.5	16.5
Survey 2 and survey 4	17.0	16.0	16.7
Survey 5 and survey 7	17.0	14.1	11.6
Survey 6 and survey 8	17.0	14.5	12.6
Survey 1 and survey 7	17.0	18.0	19.3
Survey 2 and survey 8	17.0	17.0	17.5

21.56% to 25.30% in our experiments.

Table 4.8: Standard deviation of subsidence estimation of different survey pairs obtained from convolution. The results before and after applying moving average operator are shown.

Survey pair	Standard deviation without MA [mm]	Standard deviation with MA [mm]	Percentage of increased standard deviation by MA [%]
Survey 1 and survey 3	17.9	14.0	21.79
Survey 2 and survey 4	17.2	13.3	22.67
Survey 5 and survey 7	16.7	13.1	21.56
Survey 6 and survey 8	16.6	12.4	25.30
Survey 1 and survey 7	17.0	13.2	22.35
Survey 2 and survey 8	16.0	12.0	25.00

4.4.4. Influence on BLUE and detectability power

In this section, the effect of moving average operator on subsidence estimation using BLUE is analyzed first. Based on the results, detectability power is then computed.

The influence on BLUE

The results obtained from BLUE are affected by moving average operator. As denoted above, moving average operation produces more centralized representatives of soils. This results in less derived observations which are height differences of soil candidates of two surveys (see section 3.1) in functional model as well as smaller variances in co-variance matrix of the stochastic model. Tab. 4.9 shows the subsidence obtained using BLUE. It can be seen that the results with and without using MA operator are almost the same. The tiny difference is found mostly in the surveys under short grass environment (including survey 5 to survey 8). While for the surveys under long grass leaves, MA operator leads to same results. This may be because laser beams are occluded similarly under long grass when scanning at different positions, but the effect of occlusion varies at different scan positions when the grass is short. However, the evidence for this suppose is not sufficient as the differences between the results are so small, with only 0.1-0.2 mm.

The influence of MA operator on the statistics with respect to standard deviation is shown in Tab. 4.10. After applying moving average operator, the precision of estimation is nearly the same as that without MA, with up to 0.1 mm difference. From this table, it is difficult to draw any statements of the effect of MA operator for both scanning resolutions and length of grass. From survey 1 and survey 3, 0.1 mm larger standard deviation is obtained using MA operator while from survey 2 and survey 4, same precision are computed. This is opposite When considering the survey 5, 7 and survey 6, 8 that, same standard deviation value is observed under high scanning resolution while larger standard deviation is acquired under low scanning resolution.

MA operator alters detectability power

From these two tables, we can see that MA operator has nearly no influence on the application of BLUE. However, when considering the detectability power for assessing the estimation of the subsidence,

Table 4.9: Subsidence estimation of different survey pairs based on BLUE. The results before and after applying moving average operator are shown. The environmental factors that differ between each two survey pairs is introduced in Tab. 4.1.

Survey pair	True subsidence [mm]	Estimate without MA [mm]	Estimate with MA [mm]
Survey 1 and survey 3	17.0	17.4	17.4
Survey 2 and survey 4	17.0	17.3	17.3
Survey 5 and survey 7	17.0	14.4	14.2
Survey 6 and survey 8	17.0	14.9	14.7
Survey 1 and survey 7	17.0	19.2	19.0
Survey 2 and survey 8	17.0	18.8	18.9

Table 4.10: Standard deviation of subsidence estimation of different survey pairs obtained from BLUE. The results before and after applying moving average operator are shown. The environmental factors that differ between each two survey pairs is introduced in Tab. 4.1.

Survey pair	Standard deviation without MA [mm]	Standard deviation with MA [mm]
Survey 1 and survey 3	0.3	0.4
Survey 2 and survey 4	0.4	0.4
Survey 5 and survey 7	0.2	0.2
Survey 6 and survey 8	0.2	0.3
Survey 1 and survey 7	0.3	0.3
Survey 2 and survey 8	0.3	0.4

differences are found. It should be known that even though the distribution of the height differences of the window pairs is slimmer when MA operator is applied, i.e., the standard deviation is smaller due to the smaller jumps in z-values between neighbor windows, the null hypothesis stating no subsidence is still rejected. Tab. 4.11 shows the computed detectability power by doing hypothesis testing. From the second and third columns in this table, the moving average operator increases detectability power, and the increment is shown in the fourth column. This means the probability of detecting the subsidence estimated from BLUE goes up. The effect of MA operator can be analyzed in two aspects:

1. Grass effect – From the table, it is obvious that large increment of detectability power as a result of applying MA operator is under long grass environment, corresponding to survey 1 to survey 4. While for survey 5 to survey 8, which were captured under short grass environment, the increments of detectability power are small (2.35% and 3.65% respectively). Besides, it is not unexpected that the detectability power for the third survey pair (survey 1, 7) and the sixth survey pair (survey 2, 8) is increased in between the largest and the smallest amount.

2. Resolution – The influences of MA operator at different resolutions are seen in the table. For example, comparing to the increased detectability power in survey 1 and survey 3 (high resolution), the increased probability of detection in survey 2 and survey 4 (low resolution) is a bit smaller. However, the opposite trend is found when comparing the survey 5, 7 and survey 6, 8. This indicates that the influence of moving average operator on detectability power has no relation with scanning resolution of laser device, at least in this research.

Thus, a conclusion can be drawn to state the influence of MA operator on detectability power that, applying moving average operator on the soils candidates can increase the probability of subsidence detection. Also, it seems that long grass leads to larger increment while shorter grass leads to smaller increment. This may be explained as long grass induces more occlusion than short grass. Thus, when applying MA operator, more distinct reduction of grass effect is found in long grass environmental condition. However, the relation between resolution and moving average operator is not clear with respect to detectability power.

Detectability power provides crucial information when planning surveys to detect the subsidence on the field. It tells how possible the detected subsidence is real subsidence instead of observation errors.

After applying MA operator to soils candidates, the detectability power increases. This increment enables a better plan for field work to detect subsidence. In practice, based on the detectability power of a certain amount of subsidence during a time period, a more plausible arrangement on the plans of executing next surveys for subsidence detection can be made.

Table 4.11: Detectability power of subsidence estimation of different survey pairs obtained from BLUE. The results before and after applying moving average operator are shown. The environmental factors that differ between each two survey pairs is introduced in Tab. 4.1.

Survey pair	Detectability power without MA [%]	Detectability power with MA [%]	Power increment [%]
Survey 1 and survey 3	75.80	87.08	11.28
Survey 2 and survey 4	75.49	86.65	11.16
Survey 5 and survey 7	96.71	99.06	2.35
Survey 6 and survey 8	95.25	98.90	3.65
Survey 1 and survey 7	89.80	99.22	9.42
Survey 2 and survey 8	91.15	99.20	7.70

4.4.5. Discussion on influence of moving average operator

In a summary, MA operator has almost no influence on subsidence estimate values when using methods of histograms and BLUE, but an unclear effect on convolution with respect to the subsidence estimate. However, it increases the standard deviation of estimations from all three methods, as well as the evaluation parameter, detectability power. The standard deviation decreases with a percentage up to 25% and the detectability power increases up to 19%.

4.5. Summary of the results of different methods

For estimating subsidence using TLS data, three methods are studied, which are Best Linear Unbiased Estimator (BLUE), histograms and convolution operator, respectively. From the results, we found BLUE performs best among these three methods, with the smallest error which reaches up to 2.6 mm with respect to subsidence estimate and 0.4 mm with respect to standard deviation. While for histograms and convolution operator, the estimation error can reach up to 6.8 mm and 2.9 mm, respectively. Using the result of BLUE applying to survey 1 and survey 3, the minimal detectable subsidence with 95% confidence level and 90% detectability power is 21.1 mm. In that case, it can answer the main research question as "Yes". For the results of other methods and other survey pairs, the minimal detectable subsidence may change. But the amount of the change is expected within centimeter level. Moving average operator is applied to these three method, which results in similar subsidence estimate for all three methods but improved standard deviation and detectability power.

In the next chapter, ALS data are described and investigated at IGRS stations. As there are only one epoch of data yet, subsidence at these stations are not estimated. This is expected to be done once next generation of AHN data are available.

5

Result of investigating ALS data

In this chapter, the results of investigation on ALS data are given and discussed. The data used are AHN3 which measures the elevation of the ground of Netherlands. Focusing on IGRS and local ground surrounding IGRS, point clouds are extracted, and parameters affecting the statistics are inspected.

5.1. Outliers

Outliers of the platform and ground measurements can be found when looking at the point cloud. Taking the IGRS "Engelbert" as an example, the picture of it is shown in Fig. 5.1 (a). We can see the relative position of each part of IGRS as well as the surrounding ground surface. In the point cloud shown in Fig. 5.1 (b), different parts of IGRS, such as GPS antenna, platform, radar reflectors and ground measurements, are labeled. The labeling of the components is undertaken with an a-prior knowledge about the structure of an IGRS. Due to the point density limitation of AHN3 data and the size of antenna, only one measurement point is obtained on the GPS antenna. Eight points are collected on the platform shown in the figure. However, one individual point among them is labeled as outlier. This is because the height of this point obviously differs from the height of other platform points. Thus, it is removed, and other points are then assembled as the new platform for quality assessment. Similarly, the outlier in ground surface points is also found with respect to its elevation. However, it should be noted that at some stations the distinction between outliers and platform or ground is vague. It is not easy to decide the threshold z-value for classifying an outlier from the point cloud when the height difference is not too much. In this case, the property of the platform, which is precisely horizontal, should be considered.

One rule of determining an outlier is that if the elevation of a point in the platform measurements biases from the mean elevation value of the platform points, or the mean of the point group varies significantly when leaving the vague point out, this point is labeled as an outlier. In this study, the quantity of elevation difference for defining "significant" for the points on platform is 5 cm. This value is chosen because first, individually measured points in the point cloud have a height accuracy of no more than 5 cm standard deviation and no more than 5 cm systematic deviation according to AHN-3, thus, the accuracy of most points should be smaller than 10 cm; second, points should be in principle at the same elevation as much as possible due to precisely leveled platform; and finally, this value cannot be too small since the number of points should remain enough so that further processing can be done.

(a)

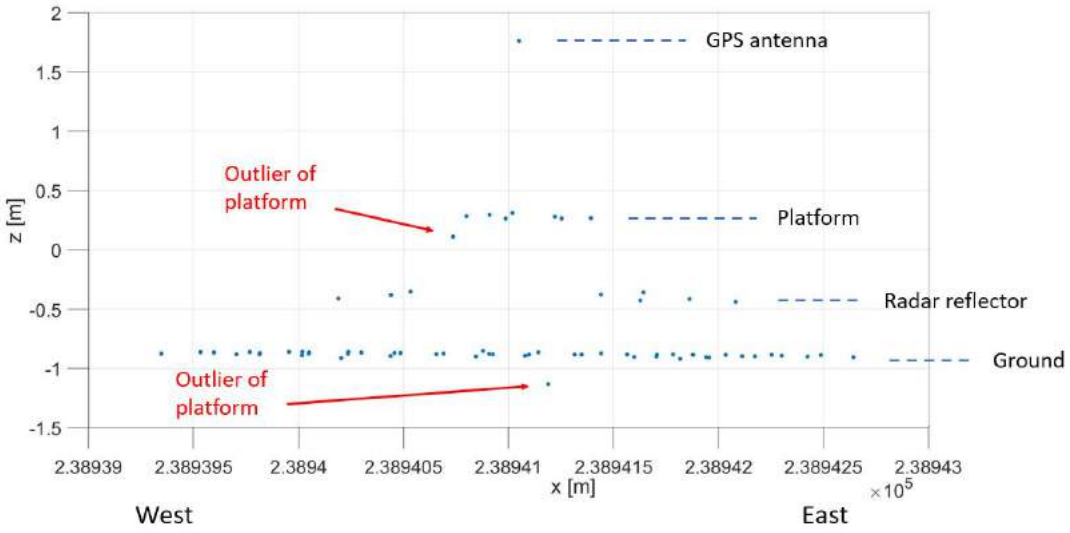

(b)

Figure 5.1: Recognition of different components of IGRS "Engelbert" based on the AHN3 point cloud. (a) shows the picture of IGRS "Engelbert" in field, (b) shows its point cloud obtained from ALS in a local scope. Outliers of platform and ground measurements are recognized because the points are away from the main point group in height dimension. This may be caused by imperfect accuracy of ALS.

For the pictures and point clouds of other IGRS, as well as classification of different components in point clouds, see Appendix D.

5.2. Elevation and uncertainty

The platforms of the IGRS and the ground are evaluated using AHN3 data. To accomplish this goal, the elevation and precision of the points on the platforms and ground of 24 IGRS are computed. As the platform is well leveled, the points that represent the platform should locate at nearly the same height. However, it is not the case at almost every IGRS due to limited ability of ALS, resulting in different height distributions. Among the platform measurements of one IGRS, those points that deviate from the majority are deemed as outliers, and they should removed from the list of platform points. Likewise, the points that are far way form the majority of the ground points are removed from ground point list. From Fig. 5.2 (a) and (b) we can see how well the platforms and ground surface at IGRS in Groningen area are measured based on AHN3 data. The standard deviations of the platform measurements vary from 0.54 cm at station Roden-1 to 2.51 cm at Norg-3, with the mean value of 1.49 cm. As the platforms for every IGRS are precisely leveled when installing, the large standard deviation may be due to less-precise airborne laser scanning. Lower precision of the AHN can be found on ground measurements (Fig. 5.2 (b)), which may due to bumpy ground and vegetation. The ground environment with respect to terrain differs from one station to another, some of them are concrete while some of them are grass land. The average standard deviation of the measurements for ground is 2.22 cm, which is 0.73 cm larger than that of platforms. We found that large standard deviations are obtained in the area with grass covered ground and uneven ground surface, while small standard deviations are obtained in areas with concrete foundation.

Referencing to the platform, the elevation differences between the platforms and ground are computed. The precision of the difference is evaluated as the addition of the standard deviation of platform measurements and ground measurements. The result is shown in Fig. 5.2 (c), where the red dots indicate the elevation difference and the line segments through the dots indicate the uncertainty range. The measurement uncertain is evaluated as $m_h \pm \sigma_h$, with m_h the mean of the height difference and σ_h the standard deviation of the height difference. This gives the information of how well the ground is measured relative to the local reference platform by AHN3 data. As calculated, the average standard deviation of the elevation difference of all investigated IGRS is 33.4 mm. This value is meaningful when planning AHN flight for detecting subsidence in these area where IGRS are located. If the standard deviation is small, there is a higher probability to detect the vertical change of the ground referencing to the platform, instead of due to measurement errors or effect of ground terrain.

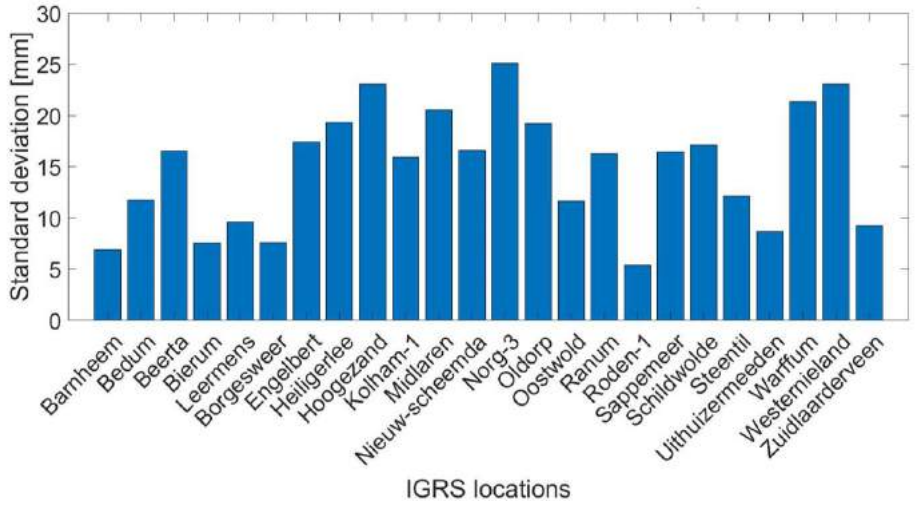

(a)

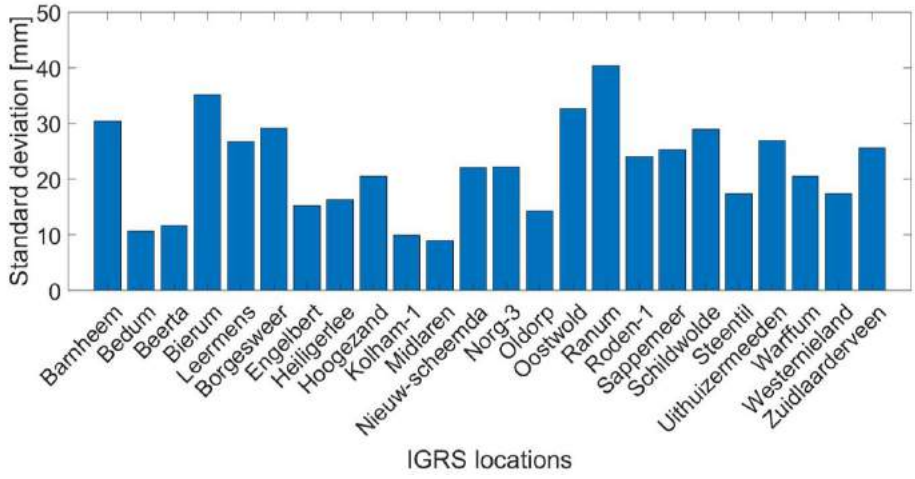

(b)

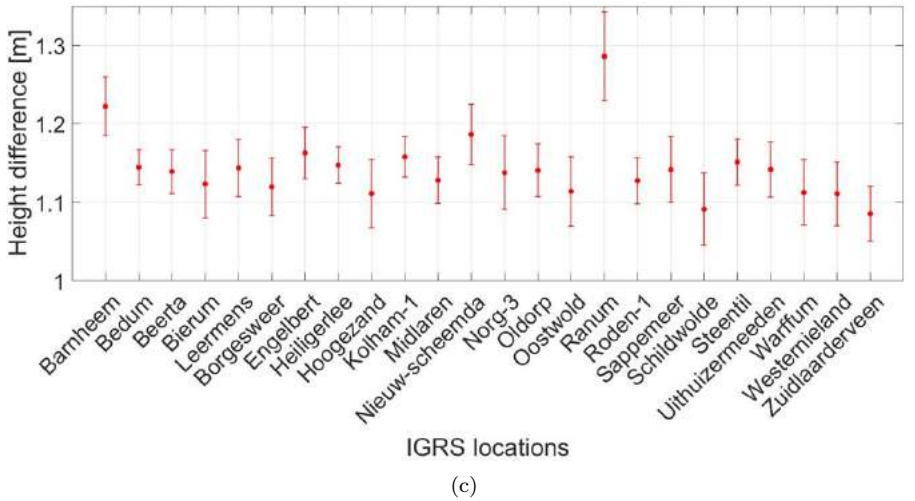

(c)

Figure 5.2: The statistics of the measurements of AHN3 data on the IGRS platform and corresponding local ground surface. (a) shows the standard deviation (precision) of the measurements on the platforms of investigated IGRS. (b) show the standard deviation of the measurements of the corresponding ground surface at different IGRS. (c) shows the height difference (shown as the dots) and its uncertainty between the platform of IGRS and local ground surface. The length of uncertainty lines corresponds to 95% confidence level. From these figures, we see how uncertainties of the ALS measurements distribute among different IGRS stations in terms of ground measurements, platform measurements and height differences between ground and platform.

From the figures, we see that the resulted standard deviation of the platforms is small when considering the scanning ability of ALS. This is because we filtered out some points which are deemed as outliers. It is supported by the a-prior knowledge that the platforms are precisely leveled, as a result, the points on it should be in principle at the same elevation level. If we take all the points that are located at the location of the platforms, much larger standard deviation would be obtained.

Fig. 5.2 gives a direct view of the quality of ALS measurements, which allows a visualized comparison among all IGRS. For more details, Tab. 5.1 lists detailed parameters of the IGRS point clouds in terms of point number, elevation value, standard deviation and minimal detectable deformation.

Table 5.1: Measurements from ALS (AHN3 data) on the IGRS platform and corresponding local ground surface. The minimal detectable deformation is computed for a detectability power of 80%.

IGRS name	# points on platform	Elevation platform [m]	Standard deviation platform [cm]	Elevation ground [m]	Standard deviation ground [cm]	Minimal detectable deformation [cm]
Barnheem	5	0.8956	0.69	-0.3267	3.04	8.73
Bedum	6	1.2242	1.18	0.0795	1.06	4.44
Beerta	9	1.0529	1.65	-0.0862	1.16	5.65
Bierum	7	2.2107	0.76	1.0874	3.52	10.09
Blijham	0	-	-	-	-	-
Borgsweer	7	0.6875	0.76	-0.4322	2.92	8.45
Engelbert	7	0.2730	1.74	-0.8898	1.53	6.49
Heiligerlee	6	0.5217	1.93	-0.6257	1.63	7.08
Hoogezand	5	2.9422	2.31	1.8311	2.05	8.65
Kolham-1	8	0.5278	1.59	-0.6303	0.99	5.25
Leermens	8	1.7544	0.96	0.6105	2.68	7.98
Midlaren	7	3.3606	2.05	2.2325	0.90	6.27
Nieuw Scheemda	8	0.7834	1.66	-0.4029	2.21	7.74
Norg-3	11	6.1845	2.51	5.0466	2.21	9.37
Oldorp	7	2.3027	1.92	1.1620	1.43	6.71
Oostwold	7	1.1011	1.16	-0.0126	3.26	9.69
Ranum	8	1.7751	1.63	0.4890	4.04	12.20
Roden-1	5	3.2220	0.54	2.0944	2.40	6.89
Sappemeer	10	2.3564	1.64	1.2148	2.53	8.45
Schildwolde	14	-0.3155	1.71	-1.4068	2.90	9.43
Steentil	6	2.9858	1.21	1.8345	1.74	5.94
Uithuizermeeden	8	2.6799	0.86	1.5380	2.69	7.91
Warffum	7	3.2507	2.14	2.1382	2.05	8.30
Westernieland	10	2.4846	2.31	1.3738	1.74	8.10
Zuidlaarderveen	6	2.2372	0.93	1.1518	2.56	7.63
Mean	8	1.9	1.5	0.8	2.2	7.8
Stand.dev.	2	1.4	0.6	1.4	0.8	1.7

As each IGRS includes GPS equipment, the height of antenna on IGRS can be calculated based on GPS data. Also, the height difference between the platform and GPS antenna is known since IGRS is mounted, the elevation of platform can be validated in accordance with GPS data because GPS is much preciser than ALS. Besides, the validation parameters is able to modify the elevation of the ground surface.

Another feature that is interesting to think about in Fig. 5.2 (a) is the different lengths of bars. Indicating the standard deviation, these bars reveal the quality of ALS points at each IGRS platform. Using the standard deviation of platform and ground measurements, the standard deviation of the height difference between platform and ground can be computed. Inputting this computed standard deviation into Eq. 3.10, and using detectability power of 80%, we can calculate the minimal detectable deformation

at each IGRS station, which is shown in Tab. 5.1. This means that based on the measurement quality of ALS in AHN3, only when the ground level vertically moves due to shallow subsurface process up to 8 cm, its movement can be detected with 80% possibility. These results relate to the mostly concrete, perfectly leveled, surroundings, so they are very likely to be worse for grass fields.

However, the reason that makes them different is not fully understood. Different from the roughness of ground, platforms at all the IGRS are made in the same way and made by the same materials. Therefore, we assume that the platforms have the same abilities for reflecting laser beams, which will result in nearly same standard deviation. One source for explaining this difference is the scan angle of each IGRS when the aircraft flies over the area. This guess is discussed in the next section.

5.3. Parameters/Attributes of the points

We have already seen that the standard deviation of the points on platform varies obviously from station to station. The distributions of the laser points on the platforms are not the same despite the designs of them are identical. This might be accounted by multiple reasons, such as incidence angle, fly height of the plane when scanning, the weather condition, time of the scanning day (thus, temperature), and the stability of the plane flying over the IGRS.

The flying height of the plane, the stability of the plane and time of the scanning day are not recorded in the data. Thus, the influence of them are unable to be explored even though the operator of AHN3 flight is likely to know. The weather condition is able to be referred as it should be recorded by weather-relate institutes. This could provide information for realizing the performance of AHN data. However it is not investigated in this study.

Incidence angle

The incidence angle of each individual measurement point is recorded as an attribute of the point. Tab. 5.2 gives the scan angles of laser beams scanning at 8 different IGRS where standard deviation of the platform points are calculated. The first column lists 8 IGRS names, the second column shows the incidence angle of the laser beam illuminating to the platform on IGRS, and the third column is calculated standard deviation of the obtained platform measurements. At some IGRS, two scan angles were recorded because they are located in the area where two fly strips overlap (see section 3.2.2). From this table, we see that large scan angles may result either large or small standard deviation. Also, similar scan angle may result in completely different standard deviations. In conclusion, we believe that there is no evidence to show clear relation between the standard deviation (thus, the elevation roughness of points) and incidence angle.

Table 5.2: The study on the influence of scan angle on the standard deviation of IGRS platforms using AHN3 data.

IGRS	scan angle	standard deviation [cm]
Barnheem	-20, 20	0.67
Bedum	16, 17	1.18
Beerta	-28, -9	1.65
Bierum	2	0.76
Borgsweer	-5, -24	0.76
Hoogezand	-5	2.31
Norg-3	-30, 7	2.51
Roden-1	-32, 7	0.54

Intensity

Another attribute recorded is the intensity of points. Unfortunately, the author does not find any relationship between elevation of the platform points and intensity. At some stations that the computed standard deviations are high, and the intensities of the points are low; while at some stations the standard deviations are low when the intensities are high.

5.4. Discussion

The vertical land motion is accounted by both deep and shallow aspects. As IGRS are installed at fundamental depth, they are considered stable with respect to the shallow ground sub-surface. Thus, the height difference between IGRS (the platform) and the ground surface is evaluated as the subsidence from shallow subsurface process. According to the precision of the AHN measurements (3.34 cm), the change of the relative height difference between the platform and the ground should be at least 3.34 cm in order to be detected reliably, i.e., reliably detecting subsidence from shallow subsurface should be at least 3.34 cm. In Groningen area, an amount of about 3.0 cm subsidence is predicted by compaction model (Rate Type Compaction Model) in the following 5 years (2020-2025) at benchmark 007E0033 (NAM, n.d.). As this value is larger than the calculated precision of AHN3 measurements for both platform on IGRS (1.17 cm) and ground (2.22 cm), the vertical land motion is able to be detected using AHN data. However, it is noted that this benchmark is near the deepest point of the subsidence bowl, implying that less subsidence would be observed at other locations. For a place where less subsidence is expected, the locally vertical land motion may not be detected in the year 2025. In that case, a longer time interval should be taken before flight for acquisition of AHN data so that subsidence is recognized instead of interference due to imprecise measurements. As laser technology develops fast, higher accuracy for scanning is expected. More points would be collected on the platform of IGRS and higher precision would be obtained.

5.5. Combine with TLS

In this research, studies on both TLS data and ALS data focus on the relationship of ground surface and local reference platform. As TLS data are acquired at multiple epochs, vertical land motion can be estimated. This searches the possibility of using TLS to estimate ground subsidence on peat soils. The results of Best Linear Unbiased Estimator suggest that a nearly 2-centimeter subsidence can be detected with 95% confidence level and 95% detectability power. While for the results of histograms and convolution, the minimal detectable subsidence is larger. The results of TLS can be combined with ALS, which scans quite area of the ground. In this research, ALS data on Integrated Geodetic Reference Stations are studied. Up to date, we only have one epoch of ALS data (AHN3) at these IGRS, so that estimation of subsidence is not possible. In this case, the performance of ALS at these stations are studied. Due to limited accuracy of ALS as well as vegetation, uncertainties of the height difference between ground and platform can reach to about 4.8 centimeters. As the fourth generation of AHN (AHN4) has been planned, it is expected to obtain AHN4 data in years later. Until then, ground subsidence can be estimated using ALS data at two epochs. By comparing the height change of ground using TLS and ALS at multiple stations, it should be possible to correct ALS estimate based on TLS estimate since we expect TLS gives a better estimate due to its higher accuracy. Also, the correction at these stations can be applied to other area where same environment with respect to vegetation and terrain. This leads to smaller uncertainties of ground subsidence estimate in other areas.

6

Conclusion and recommendation

6.1. Conclusion

The main research question of this study was formulated as: 'Is it possible to detect centimeter–level vertical surface motion of pastures on peat soils using laser scanning technology, with a predefined confidence level and a predefined detectability power?'. It can be concluded that terrestrial laser scanning is able to detect centimeter-level ground subsidence relative to the reference platform with a sub-millimeter to millimeter error and standard deviation.

Three methods of estimating ground subsidence are investigated, i.e., Best Linear Unbiased Estimation (BLUE), histogram matching, and the convolution operator. We find that BLUE performs best among these three methods, with the smallest error which reaches up to 2.6 mm and 0.4 mm standard deviation. This is adequate for the purpose of detecting centimeter to sub-centimeter vertical land motion. For the histogram method and the convolution operator, the estimation error reaches up to 6.8 mm and 2.9 mm, respectively. Even though the obtained error for the convolution operator is similar as the error using BLUE, the standard deviation resulting from the convolution operator is much larger than that from BLUE, varying from 16.0 mm to 17.9 mm. These estimate differences, as well as the differences between multiple survey pairs when applying the same method, are most likely due to the effect of grass density and length. Although it may be expected that denser and higher grass may lead to more occluded laser scanning, we find that short grass does not lead to better estimates. Even though a standard deviation of the subsidence estimate as low as 0.2 mm can be computed, the accuracy of the subsidence estimate is biased by more than 2.0 mm when the grass is short. The mechanism driving this effect is still not fully known.

The results of TLS are obtained based on field experiments carried out in Zweth, the Netherlands. Eight surveys were done by placing the laser scanner at different locations around the study area. To study the influence of the scanning resolution (either 'low', 3.1 mm at 10 m distance, or 'high', 1.6 mm at 10 m distance), both resolutions were tested at each location. We find that the resolution has negligible influence on the subsidence estimate. At each scan position, the laser scanner rotates 360° covering the study area, ensuring the whole area of interest is scanned.

A sub-question is 'How to determine the ground surface elevation on peat area where grass usually lushly grows with dense leaves?'. In this research, we define the soil surface using 0.5% local–lowest points. The results show that the estimate of the ground surface is significantly affected by the way of selecting the soil candidates. Evaluating different window sizes, we finally use a 30×30 grid to subdivide the obtained point clouds, where each cell measures $10cm \times 10cm$. In each cell, the lowest 0.5% of points are selected as being representative of the soil in this cell. Obviously, different sizes of cells, as well as different percentages of selected lowest points, will result in varying subsidence estimates. We have tested multiple selections in the cell size and n the number of local lowest points, and we find the cell size of 10 cm and the 0.5-th percentile to give the smallest error compared with the ground truth. Even though scanning from multiple positions reduces the occlusion, a bias is still found at spots where the grass cover is thick.

In order to estimate subsidence caused by shallow subsurface processes, we designed a local reference platform. For TLS surveys, the platform has a 'shoe' shape, to facilitate orientation and registration. We find that this platform works well as a reference assuming it to be stable during the period of the experiments. For ALS, the top plate of the IGRS is used as reference platform. Because the IGRS is rigidly mounted on a deep stable sand layer, it is assumed to be adequate for observing shallow subsurface relative to it.

For an given subsidence, the probability of detection can be evaluated, which provides practical information for the planning and realization of the surveys. Based on the BLUE results, we compute the minimal amount of subsidence that can be detected given a predefined significance level and detectability power. Taking the first and the third survey as an example, the minimal detectable subsidence is 21.1 mm, with a 95% confidence level and 90% detectability power. This value of 21.1 mm, supports our claim of 'centimeter level' detection capability in our main conclusion.

Regarding the ability of airborne laser scanning (ALS) data to compute subsidence relative to an idealized deep-founded reference platform (IGRS), the quality of the results is still limited. The IGRS platforms are well-visible in the AHN3 airborne laser scanning data. While the horizontal platforms are precisely leveled, guaranteeing the 'horizontalness' of the platforms, the standard deviation of the elevations of the scanning points located on the platform still reaches up to 2.51 cm. While the exact cause of this high standard deviation is not known, it may be related with (i) the metallic and smooth surface of the horizontal reference platform, combined with (ii) the oblique viewing geometry from the airborne laser, where the off-nadir angle of the incident laser pulses may be significant. Surrounding the reference platforms, measurements of the ground provide information of the terrain at a local scale. The height difference between the platform and the ground can be evaluated with a specific precision and accuracy (bias). In this research, as only one epoch of data (AHN3) is available, we are only able to estimate the height difference, and not its change over time. We find that a relative subsidence of the ground relative to the IGRS platform of almost 8 cm is needed to be detected with 80% possibility. These results relate to the mostly concrete, perfectly leveled, surroundings, so they are very likely to be worse for grass fields.

However, the next survey (AHN4) is being executed in the coming years. Once available, the vertical ground motion due to shallow subsidence can be better investigated by studying the change in the height differences between ground and local referencing platforms. Ideally, more representative areas, i.e., further away from the IGRS stations, need to be selected for practically relevant purposes.

6.2. Recommendation

Further studies are needed to thoroughly understand subsidence on peat soils in terms of time and space. This research has provided a method for using laser scanning technology to estimate the vertical ground motion as well as its quality assessment subject to detectability power and significance level. However, the results are limited by mainly two factors: first, the grass which causes an occlusion effect due to its density, length and possibly type; second, the quality of ALS data describing ground-level objects. Even though the grass effect has been investigated by some previous work, grass on peat soils are rarely studied. As the organic matters make up a large part of peat soils, the grass grows luxuriantly. This leads to the difficulties confronted when using laser scanning techniques that laser cannot penetrate the leaves of the grass. In this study, we define the soil surface as the "root surface" of the grass which adheres on the ground surface making laser completely occluded. However, it should be noticed that this "root surface" only works well when its condition remains undamaged, meaning that the roots keep covering the ground totally. Thus, every survey that scans the surface will result in a scan on the same "root surface". This definition may lose its relevance when the roots are changed by activities. Thus, a method that represents the bare ground for all the conditions should be considered in future research. When using TLS to estimate the ground surface, the setup of the laser scanner with regards to the height should be reconsidered. In this research, we placed the laser scanner as high as possible based on the knowledge that occlusion due to vegetation increases as the incidence angle increases. Besides the height of laser device, we found that variation in the position of the laser device can lead to significantly different estimates of the ground level.

To fully understand the real bare ground motion, the processing of the point clouds of laser scanning

technology should be studied so that bare ground points could be selected. The intensity of the points is an important attribute for classifying different types of objects. It could be a potential solution, but the performance of the intensity for distinguishing soil points from that of the grass still needs to be tested. Thus, a number of questions regarding point selection, grass effect and window size remain to be addressed.

Local lowest point theory has been broadly used in previous studies when extracting the elevation of soils in a vegetation-covered area. However, the accuracy of soil expression remains limited. In this research, we applied this method for extracting the soil elevation in an area with dense grass, and we found it is difficult to accurately achieve this goal even though different number of lowest points and cell sizes are tested.

Different from TLS, ALS suffers from the problem of sparse point density and systematic errors. In this research, we have seen that airborne laser scanning technology shows limitations in acquiring the elevation of the reference platform on the Integrated Geodetic Reference Stations. The elevation differences between the ground and the platforms are assessed to quantify the shallow subsurface subsidence when two elevation differences are obtained at two time epochs. However, the expression of the platforms and ground according to AHN3 (an application of ALS) data is not ideal, due to the limitations of airborne laser scanning in accuracy and point density. The points on the horizontally leveled platform exhibit a large variation in height, which is not expected. For the ground points, besides the limited measurement precision, the terrain and vegetation also contribute to the dispersion of the height measurements. Thus, an important aspect for improving the height difference quantification between the ground and reference platform for studying shallow subsurface land motion is to reduce the dispersion of the elevation estimates from the reference platform, e.g., by reducing the influence of specular reflection via a coating.

As the fourth generation of AHN (AHN4) has been planned, it is expected to obtain AHN4 data within the following years. Using the data of AHN3 and AHN4 at IGRS stations, ground subsidence may be estimated, albeit with a limited precision. As the reference platforms have a deep foundation, the points on the platforms should remain stable in elevation relative to the foundation level. In future research on ALS data at IGRS, the difference between the platform heights between two epochs should be checked. If the heights of platforms change, explanations should be given. At data acquisition epochs of ALS data, TLS experiments can be carried out at the IGRS stations. This allows the comparison of the subsidence estimate between ALS and TLS. It is expected that uncertainties in ALS can be partly corrected by TLS as TLS has higher scanning accuracy. The correction can then be applied to other areas in ALS data besides that at the IGRS stations.

Bibliography

06-GPS (2019). [Online; accessed 14-November-2020]. URL: https://www.06-gps.nl/.

AHN (n.d.). AHN: the making of. [Accessed 06-November-2020]. URL: %5Curl%7Bhttps://www.ahn.nl/ahn-making%7D.

AHN website (2020). Quality description. [Accessed 27-May-2020]. URL: %5Curl%7Bhttps://www.ahn.nl/kwaliteitsbeschrijving%7D.

Anbazhagan, S et al. (2015). "Electrical resistivity survey and shallow subsurface geological study in hard rock terrain, Southern India". In: Journal of the Geological Society of India 85.3, pp. 305–312.

Antonova, Sofia et al. (2016). "Spatio-temporal variability of X-band radar backscatter and coherence over the Lena River Delta, Siberia". In: Remote Sensing of Environment 182, pp. 169–191.

Asselen, Sanneke van et al. (2018). "The relative contribution of peat compaction and oxidation to subsidence in built-up areas in the Rhine-Meuse delta, The Netherlands". In: Science of the Total Environment 636, pp. 177–191.

Avian, Michael, Andreas Kellerer-Pirklbauer, and Arnold Bauer (2008). "Remote Sensing Data for Monitoring Periglacial Processes in Permafrost Areas: Terrestrial Laser Scanning at the Hinteres Langtalkar Rock Glacier, Austria". In: Laser 400, 180gon.

Barnhart, Theodore B and Benjamin T Crosby (2013). "Comparing two methods of surface change detection on an evolving thermokarst using high-temporal-frequency terrestrial laser scanning, Selawik River, Alaska". In: Remote Sensing 5.6, pp. 2813–2837.

Beck, Inga et al. (2015). "Vertical movements of frost mounds in subarctic permafrost regions analyzed using geodetic survey and satellite interferometry." In: Earth Surface Dynamics 3.3, pp. 409–421.

Bhardwaj, Anshuman et al. (2016). "LiDAR remote sensing of the cryosphere: Present applications and future prospects". In: Remote Sensing of Environment 177, pp. 125–143.

bodemdalingskaart (2018). bodemdalingskaart. URL: https://bodemdalingskaart.nl/nl/. (accessed: 10.23.2020).

Bramer, Isobel et al. (2018). "Advances in monitoring and modelling climate at ecologically relevant scales". In: Advances in ecological research. Vol. 58. Elsevier, pp. 101–161.

Bürgmann, Roland, Paul A Rosen, and Eric J Fielding (2000). "Synthetic aperture radar interferometry to measure Earth's surface topography and its deformation". In: Annual review of earth and planetary sciences 28.1, pp. 169–209.

Chasmer, L et al. (2011). "Fusion of airborne LiDAR and WorldView-2 MS data for classification of depth to permafrost within Canada's sub-Arctic". In: Proceedings of SilviLaser, pp. 1–7.

Coveney, Seamus and A Stewart Fotheringham (2011). "Terrestrial laser scan error in the presence of dense ground vegetation". In: The Photogrammetric Record 26.135, pp. 307–324.

Cuenca, Miguel Caro and Ramon Hanssen (2008). "Subsidence due to peat decomposition in the Netherlands, kinematic observations from radar interferometry". In: Proc. Fringe 2007 Workshop, pp. 1–6.

Cuenca, Miguel Caro, Ramon Hanssen, et al. (2011). "Surface deformation of the whole Netherlands after PSI analysis". In: Proceedings Fringe 2011 Workshop, Frascati, Italy, pp. 19–23.

Delft University of Technology (n.d.). Overall Model Test: Choosing the critical value. [Online; accessed 30-October-2020]. URL: https://ocw.tudelft.nl/course-readings/overall-model-test-choosing-critical-value/?course_id=20741.

Deltares (2017). New version of soil subsidence maps provide insight into the climate effect. URL: https://www.deltares.nl/nl/nieuws/nieuwe-versie-bodemdalingskaarten-maken-klimaateffect-inzichtelijk/.

Erkens, Gilles, Michiel J van der Meulen, and Hans Middelkoop (2016). "Double trouble: subsidence and CO 2 respiration due to 1,000 years of Dutch coastal peatlands cultivation". In: Hydrogeology Journal 24.3, pp. 551–568.

Fan, Lei et al. (2014). "The effect of short ground vegetation on terrestrial laser scans at a local scale". In: ISPRS Journal of Photogrammetry and Remote Sensing 95, pp. 42–52.

Frost, Jim (n.d.). The Gauss-Markov Theorem and BLUE OLS Coefficient Estimates. [Online; accessed 29-October-2020]. URL: https://statisticsbyjim.com/regression/gauss-markov-theorem-ols-blue/#:~:text=The%20Gauss%2DMarkov%20theorem%20states%20that%20satisfying%20the%20OLS%20assumptions,all%20unbiased%20linear%20estimation%20methods!.

Gangodagamage, Chandana et al. (2014). "Extrapolating active layer thickness measurements across Arctic polygonal terrain using LiDAR and NDVI data sets". In: Water resources research 50.8, pp. 6339–6357.

Goldberger, Arthur S (1962). "Best linear unbiased prediction in the generalized linear regression model". In: Journal of the American Statistical Association 57.298, pp. 369–375.

Hanssen, Ramon F (2001). Radar interferometry: data interpretation and error analysis. Vol. 2. Springer Science & Business Media.

Harville, David (1976). "Extension of the Gauss-Markov theorem to include the estimation of random effects". In: The Annals of Statistics, pp. 384–395.

Hoogland, T, JJH Van den Akker, and DJ Brus (2012). "Modeling the subsidence of peat soils in the Dutch coastal area". In: Geoderma 171, pp. 92–97.

Kamphuis, Jurjen (2019). "Co-location of geodetic reference points: On the design and performance of an Integrated Geodetic Reference Station". In:

Klapa, Przemysław and Bartosz Mitka (2017). "Edge effect and its impact upon the accuracy oF 2d and 3d modelling using laser scanning". In: Geomatics, Landmanagement and Landscape.

Kociuba, Waldemar, Waldemar Kubisz, and Piotr Zagórski (2014). "Use of terrestrial laser scanning (TLS) for monitoring and modelling of geomorphic processes and phenomena at a small and medium spatial scale in Polar environment (Scott River—Spitsbergen)". In: Geomorphology 212, pp. 84–96.

Kooi, Henk et al. (1998). "Geological causes of recent (100 yr) vertical land movement in the Netherlands". In: Tectonophysics 299.4, pp. 297–316.

Kraus, Karl and Norbert Pfeifer (1998). "Determination of terrain models in wooded areas with airborne laser scanner data". In: ISPRS Journal of Photogrammetry and remote Sensing 53.4, pp. 193–203.

Kuikman, PJ et al. (2003). Stocks of C in soils and emissions of CO2 from agricultural soils in the Netherlands. Tech. rep. Alterra.

Lindenbergh, Roderik and Peter Pietrzyk (2015). "Change detection and deformation analysis using static and mobile laser scanning". In: Applied Geomatics 7.2, pp. 65–74.

Liu, Lin, Tingjun Zhang, and John Wahr (2010). "InSAR measurements of surface deformation over permafrost on the North Slope of Alaska". In: Journal of Geophysical Research: Earth Surface 115.F3.

Liu, Thomas T et al. (2001). "Detection power, estimation efficiency, and predictability in event-related fMRI". In: Neuroimage 13.4, pp. 759–773.

Marlies ter Voorde (2014). Sinking coastal cities. URL: https://www.nemokennislink.nl/publicaties/zinkende-kuststeden/.

Marshall, Chris et al. (2018). "Monitoring tropical peat related settlement using isbas insar, kuala lumpur international airport (klia)". In: Engineering Geology 244, pp. 57–65.

Marx, Sabrina et al. (2017). "Terrestrial laser scanning for quantifying small-scale vertical movements of the ground surface in Arctic permafrost regions". In: Earth Surface Dynamics Discussions, pp. 1–31.

Massonnet, Didier and Kurt L Feigl (1998). "Radar interferometry and its application to changes in the Earth's surface". In: Reviews of geophysics 36.4, pp. 441–500.

Mukupa, Wallace et al. (2017). "A review of the use of terrestrial laser scanning application for change detection and deformation monitoring of structures". In: Survey review 49.353, pp. 99–116.

NAM (2019). [Online; accessed 14-November-2020]. URL: https://www.nam.nl/.

— (n.d.). Supplement to the Technical Addendum for Winningsplan Groningen 2016. [Online; accessed 02-November-2020]. URL: https://www.nam.nl/nieuws/2016/nam-supplement-technical-addendum-at-ministry-of-economic-affairs/_jcr_content/par/textimage.stream/1462205911632/9004b959cb150e564b8fd56c16031a238d48ef65/supplement-to-the-winningsplan-groningen-2016.pdf.

Nieuwenhuis, HS and F Schokking (1997). "Land subsidence in drained peat areas of the Province of Friesland, The Netherlands". In: Quarterly Journal of Engineering Geology and Hydrogeology 30.1, pp. 37–48.

Palamara, DR et al. (2007). "An evaluation of airborne laser scan data for coalmine subsidence mapping". In: International Journal of Remote Sensing 28.15, pp. 3181–3203.

Pirotti, Francesco, Alberto Guarnieri, and Antonio Vettore (2013). "Ground filtering and vegetation mapping using multi-return terrestrial laser scanning". In: ISPRS Journal of Photogrammetry and Remote Sensing 76, pp. 56–63.

Razak, Khamarrul Azahari et al. (2013). "Generating an optimal DTM from airborne laser scanning data for landslide mapping in a tropical forest environment". In: Geomorphology 190, pp. 112–125.

RECARE hub (2020). Veenweidegebied, The Netherlands. [Accessed 27-February-2020]. URL: %5Curl%7Bhttps://www.recare-hub.eu/case-studies/veenweidegebied-the-netherlands%7D.

Remkes, JW et al. (2007). Water en bodemdaling in Groot-Mijdrecht: rapport van de Onderzoekscommissie Water en Bodemdaling Groot-Mijdrecht Noord. Onderzoekscommissie.

Rietveld, H (1986). "Land subsidence in the Netherlands". In: Proceedings of the 3rd international symposium on land subsidence. Vol. 151, pp. 455–465.

Satellite Radar Lab TU Delft (2019). IGRS Integrated Geodetic Reference Stations Groningen. [Accessed 06-November-2020]. URL: %5Curl%7Bhttps://sites.google.com/d/1QB72WA362I5MqagHWzuM34h9my_ml9Dh/p/0B0KxdhVWtcF4dnpyQ1FiaHBaUjg/edit%7D.

Schothorst, CJ (1977). "Subsidence of low moor peat soils in the western Netherlands". In: Geoderma 17.4, pp. 265–291.

Short, Naomi et al. (2011). "A comparison of TerraSAR-X, RADARSAT-2 and ALOS-PALSAR interferometry for monitoring permafrost environments, case study from Herschel Island, Canada". In: Remote Sensing of Environment 115.12, pp. 3491–3506.

Smith, Steven W et al. (1997). "The scientist and engineer's guide to digital signal processing". In:

Tekno-Port (n.d.). Fly By Wire. [Accessed 06-November-2020]. URL: %5Curl%7Bhttp://elektromot.com/%7D.

Van den Born, GJ et al. (2016). Dalende bodems, stijgende kosten: mogelijke maatregelen tegen veenbodemdaling in het landelijk en stedelijk gebied: beleidsstudie. Tech. rep. Planbureau voor de Leefomgeving.

Wagner, Wolfgang et al. (2004). Robust filtering of airborne laser scanner data for vegetation analysis. na.

Wehr, Aloysius and Uwe Lohr (1999). "Airborne laser scanning—an introduction and overview". In: ISPRS Journal of photogrammetry and remote sensing 54.2-3, pp. 68–82.

Weststrate, Thijs (2018). "Urban land subsidence in the Netherlands. A case study research design at the adaptive capacity of cities in relation to land subsidence". In:

Wikipedia contributors (2020a). Area under one-tailed standard normal curve. [Online; accessed 19-November-2020]. URL: https://www.growingknowing.com/GKStatsBookNormalTable1.html.

— (2020b). Interferometric synthetic-aperture radar — Wikipedia, The Free Encyclopedia. [Online; accessed 11-November-2020]. URL: https://en.wikipedia.org/w/index.php?title=Interferometric_synthetic-aperture_radar&oldid=974866011.

— (2020c). Lidar — Wikipedia, The Free Encyclopedia. [Online; accessed 12-November-2020]. URL: https://en.wikipedia.org/w/index.php?title=Lidar&oldid=987150514.

— (2020d). List of settlements lost to floods in the Netherlands — Wikipedia, The Free Encyclopedia. [Online; accessed 9-November-2020]. URL: https://en.wikipedia.org/w/index.php?title=List_of_settlements_lost_to_floods_in_the_Netherlands&oldid=940038325.

— (2020e). Orientation (geometry) — Wikipedia, The Free Encyclopedia. [Online; accessed 13-November-2020]. URL: https://en.wikipedia.org/w/index.php?title=Orientation_(geometry)&oldid=986626016.

— (2020f). Standard normal table — Wikipedia, The Free Encyclopedia. [Online; accessed 19-November-2020]. URL: https://en.wikipedia.org/w/index.php?title=Standard_normal_table&oldid=988282836.

Wösten, JHM, AB Ismail, and ALM Van Wijk (1997). "Peat subsidence and its practical implications: a case study in Malaysia". In: Geoderma 78.1-2, pp. 25–36.

A

Supplementary data– Zweth experimental field logs

Table A.1: Survey 1 field log

Survey 1. High grass, high resolution and a low reference plate	
Date	13/8/2020, 11:00–13:00
Conditions	no wind, blue sky, drought, 30°C
Tripod position	new setup.
Instrument height	1.983 m
Minimum incidence angle	−10°
Maximum incidence angle	−55°
Resolution	1.6 mm@10m
Sensitivity	normal
Pad elevation	22.3 cm
Location pictures	link Google Photo's

Table A.2: Survey 2 field log

Survey 2. High grass, low resolution, low reference plate	
Date	13/8/2020, 11:00–13:00
Conditions	no wind, blue sky, drought, 30°C
Tripod position	same as survey 1.
Instrument height	1.983 m
Minimum incidence angle	−10°
Maximum incidence angle	−55°
Resolution	3.1 mm@10m
Sensitivity	normal
Pad elevation	22.3 cm
Location pictures	link Google Photo's

Table A.3: Survey 3 field log

Survey 3. High grass, high resolution, high reference plate	
Date	13/8/2020, 11:00–13:00
Conditions	no wind, blue sky, drought, 30°C
Tripod position	new setup.
Instrument height	1.970 m
Minimum incidence angle	−10°
Maximum incidence angle	−55°
Resolution	1.6 mm@10m
Sensitivity	normal
Pad elevation	22.3 cm
Location pictures	link Google Photo's

Table A.4: Survey 4 field log

Survey 4. High grass, low resolution, high reference plate	
Date	13/8/2020, 11:00–13:00
Conditions	no wind, blue sky, drought, 30°C
Tripod position	same as survey 3.
Instrument height	1.970 m
Minimum incidence angle	−10°
Maximum incidence angle	−55°
Resolution	3.1 mm@10m
Sensitivity	normal
Pad elevation	22.3 cm
Location pictures	link Google Photo's

Table A.5: Survey 5 field log

Survey 5. low grass, high resolution, low reference plate	
Date	17/8/2020, 9:00–12:00
Conditions	no wind, blue sky, after rain, 20°C
Tripod position	new setup.
Instrument height	1.980 m
Minimum incidence angle	−10°
Maximum incidence angle	−55°
Resolution	1.6 mm@10m
Sensitivity	normal
Pad elevation	22.3 cm
Location pictures	link Google Photo's
Comment	The following experiments were done on another day. In order to make the platform locate at the same place with the same height, we leave a iron tube inserting in the ground. It can be seen from the linked photos

Table A.6: Survey 6 field log

Survey 6. low grass, low resolution, low reference plate	
Date	17/8/2020, 9:00–12:00
Conditions	no wind, blue sky, after rain, 20°C
Tripod position	same as survey 7.
Instrument height	1.980 m
Minimum incidence angle	−10°
Maximum incidence angle	−55°
Resolution	3.1 mm@10m
Sensitivity	normal
Pad elevation	22.3 cm
Location pictures	link Google Photo's

Table A.7: Survey 7 field log

Survey 7. low grass, high resolution, high reference plate	
Date	17/8/2020, 9:00–12:00
Conditions	no wind, blue sky, after rain, 20°C
Tripod position	new setup.
Instrument height	1.971 m
Minimum incidence angle	−10°
Maximum incidence angle	−55°
Resolution	1.6 mm@10m
Sensitivity	normal
Pad elevation	22.3 cm
Location pictures	link Google Photo's

Table A.8: Survey 8 field log

Survey 8. low grass, low resolution, high reference plate	
Date	17/8/2020, 9:00–12:00
Conditions	no wind, blue sky, after rain, 20°C
Tripod position	same as survey 9.
Instrument height	1.971 m
Minimum incidence angle	−10°
Maximum incidence angle	−55°
Resolution	3.1 mm@10m
Sensitivity	normal
Pad elevation	22.3 cm
Location pictures	link Google Photo's

B

One-tailed Standard Normal Table

Areas Under the One-Tailed Standard Normal Curve

This table provides the area between the mean and some Z score.
For example, when Z score = 1.45 the area = 0.4265.

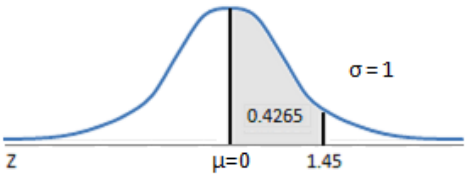

Z	0.00	0.01	0.02	0.03	0.04	0.05	0.06	0.07	0.08	0.09
0.0	0.0000	0.0040	0.0080	0.0120	0.0160	0.0199	0.0239	0.0279	0.0319	0.0359
0.1	0.0398	0.0438	0.0478	0.0517	0.0557	0.0596	0.0636	0.0675	0.0714	0.0753
0.2	0.0793	0.0832	0.0871	0.0910	0.0948	0.0987	0.1026	0.1064	0.1103	0.1141
0.3	0.1179	0.1217	0.1255	0.1293	0.1331	0.1368	0.1406	0.1443	0.1480	0.1517
0.4	0.1554	0.1591	0.1628	0.1664	0.1700	0.1736	0.1772	0.1808	0.1844	0.1879
0.5	0.1915	0.1950	0.1985	0.2019	0.2054	0.2088	0.2123	0.2157	0.2190	0.2224
0.6	0.2257	0.2291	0.2324	0.2357	0.2389	0.2422	0.2454	0.2486	0.2517	0.2549
0.7	0.2580	0.2611	0.2642	0.2673	0.2704	0.2734	0.2764	0.2794	0.2823	0.2852
0.8	0.2881	0.2910	0.2939	0.2967	0.2995	0.3023	0.3051	0.3078	0.3106	0.3133
0.9	0.3159	0.3186	0.3212	0.3238	0.3264	0.3289	0.3315	0.3340	0.3365	0.3389
1.0	0.3413	0.3438	0.3461	0.3485	0.3508	0.3531	0.3554	0.3577	0.3599	0.3621
1.1	0.3643	0.3665	0.3686	0.3708	0.3729	0.3749	0.3770	0.3790	0.3810	0.3830
1.2	0.3849	0.3869	0.3888	0.3907	0.3925	0.3944	0.3962	0.3980	0.3997	0.4015
1.3	0.4032	0.4049	0.4066	0.4082	0.4099	0.4115	0.4131	0.4147	0.4162	0.4177
1.4	0.4192	0.4207	0.4222	0.4236	0.4251	0.4265	0.4279	0.4292	0.4306	0.4319
1.5	0.4332	0.4345	0.4357	0.4370	0.4382	0.4394	0.4406	0.4418	0.4429	0.4441
1.6	0.4452	0.4463	0.4474	0.4484	0.4495	0.4505	0.4515	0.4525	0.4535	0.4545
1.7	0.4554	0.4564	0.4573	0.4582	0.4591	0.4599	0.4608	0.4616	0.4625	0.4633
1.8	0.4641	0.4649	0.4656	0.4664	0.4671	0.4678	0.4686	0.4693	0.4699	0.4706
1.9	0.4713	0.4719	0.4726	0.4732	0.4738	0.4744	0.4750	0.4756	0.4761	0.4767
2.0	0.4772	0.4778	0.4783	0.4788	0.4793	0.4798	0.4803	0.4808	0.4812	0.4817
2.1	0.4821	0.4826	0.4830	0.4834	0.4838	0.4842	0.4846	0.4850	0.4854	0.4857
2.2	0.4861	0.4864	0.4868	0.4871	0.4875	0.4878	0.4881	0.4884	0.4887	0.4890
2.3	0.4893	0.4896	0.4898	0.4901	0.4904	0.4906	0.4909	0.4911	0.4913	0.4916
2.4	0.4918	0.4920	0.4922	0.4925	0.4927	0.4929	0.4931	0.4932	0.4934	0.4936
2.5	0.4938	0.4940	0.4941	0.4943	0.4945	0.4946	0.4948	0.4949	0.4951	0.4952
2.6	0.4953	0.4955	0.4956	0.4957	0.4959	0.4960	0.4961	0.4962	0.4963	0.4964
2.7	0.4965	0.4966	0.4967	0.4968	0.4969	0.4970	0.4971	0.4972	0.4973	0.4974
2.8	0.4974	0.4975	0.4976	0.4977	0.4977	0.4978	0.4979	0.4979	0.4980	0.4981
2.9	0.4981	0.4982	0.4982	0.4983	0.4984	0.4984	0.4985	0.4985	0.4986	0.4986
3.0	0.4987	0.4987	0.4987	0.4988	0.4988	0.4989	0.4989	0.4989	0.4990	0.4990
3.1	0.4990	0.4991	0.4991	0.4991	0.4992	0.4992	0.4992	0.4992	0.4993	0.4993
3.2	0.4993	0.4993	0.4994	0.4994	0.4994	0.4994	0.4994	0.4995	0.4995	0.4995
3.3	0.4995	0.4995	0.4995	0.4996	0.4996	0.4996	0.4996	0.4996	0.4996	0.4997
3.4	0.4997	0.4997	0.4997	0.4997	0.4997	0.4997	0.4997	0.4997	0.4997	0.4998
3.5	0.4998	0.4998	0.4998	0.4998	0.4998	0.4998	0.4998	0.4998	0.4998	0.4998
3.6	0.4998	0.4998	0.4999	0.4999	0.4999	0.4999	0.4999	0.4999	0.4999	0.4999
3.7	0.4999	0.4999	0.4999	0.4999	0.4999	0.4999	0.4999	0.4999	0.4999	0.4999
3.8	0.4999	0.4999	0.4999	0.4999	0.4999	0.4999	0.4999	0.4999	0.4999	0.4999
3.9	0.5000	0.5000	0.5000	0.5000	0.5000	0.5000	0.5000	0.5000	0.5000	0.5000

Figure B.1: Area under one-tailed standard normal curve. The probability corresponding to the coefficient can be found in this table. (Source: (Wikipedia contributors, 2020f; Wikipedia contributors, 2020a))

C

Influence of moving average on soils candidates

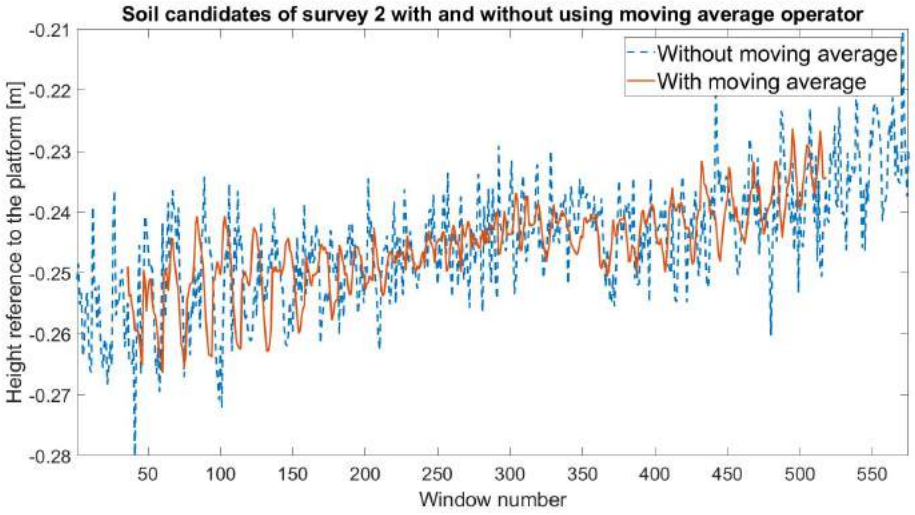
Soil candidates of survey 2 with and without using moving average operator
Without moving average
With moving average
Height reference to the platform [m]
-0.21
-0.22
-0.23
-0.24
-0.25
-0.26
-0.27
-0.28
50
100
150
200
250
300
350
400
450
500
550
Window number

(a)

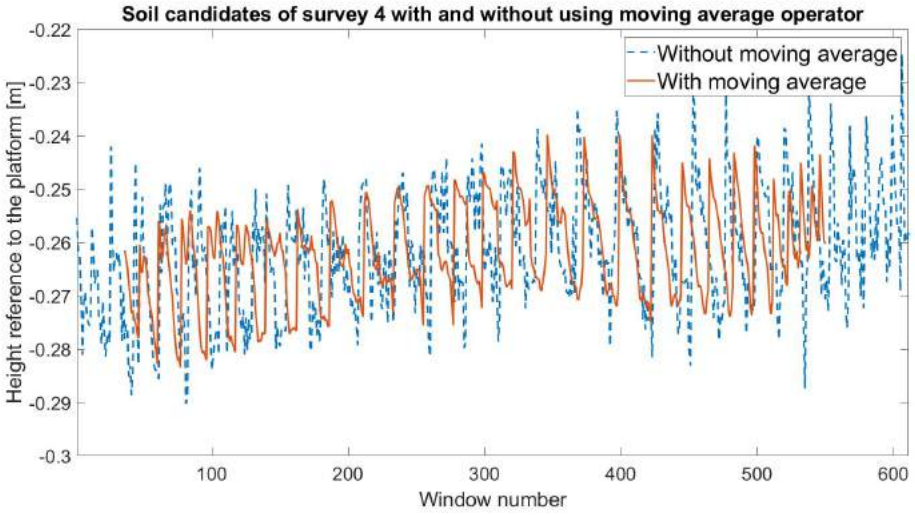
Soil candidates of survey 4 with and without using moving average operator
Without moving average
With moving average
Height reference to the platform [m]
-0.22
-0.23
-0.24
-0.25
-0.26
-0.27
-0.28
-0.29
-0.3
100
200
300
400
500
600
Window number

(b)

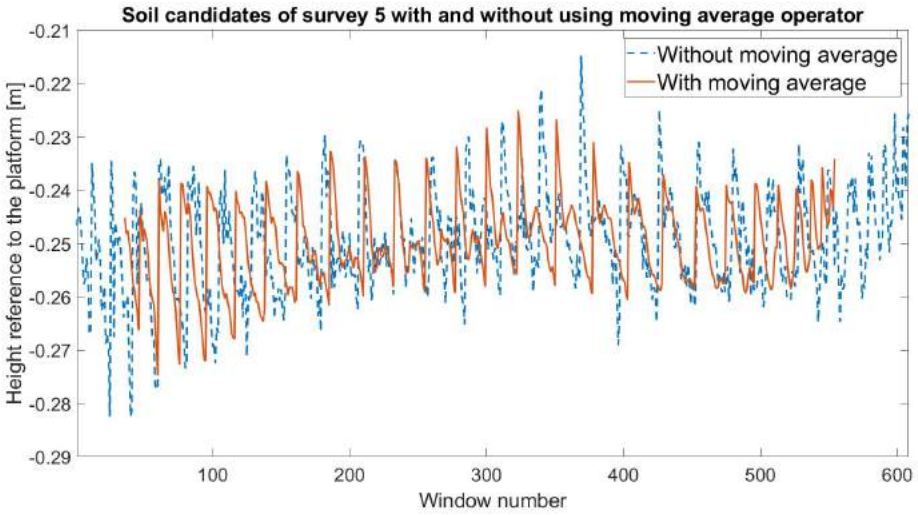
Soil candidates of survey 5 with and without using moving average operator
Without moving average
With moving average
Height reference to the platform [m]
-0.21
-0.22
-0.23
-0.24
-0.25
-0.26
-0.27
-0.28
-0.29
100
200
300
400
500
600
Window number

(c)

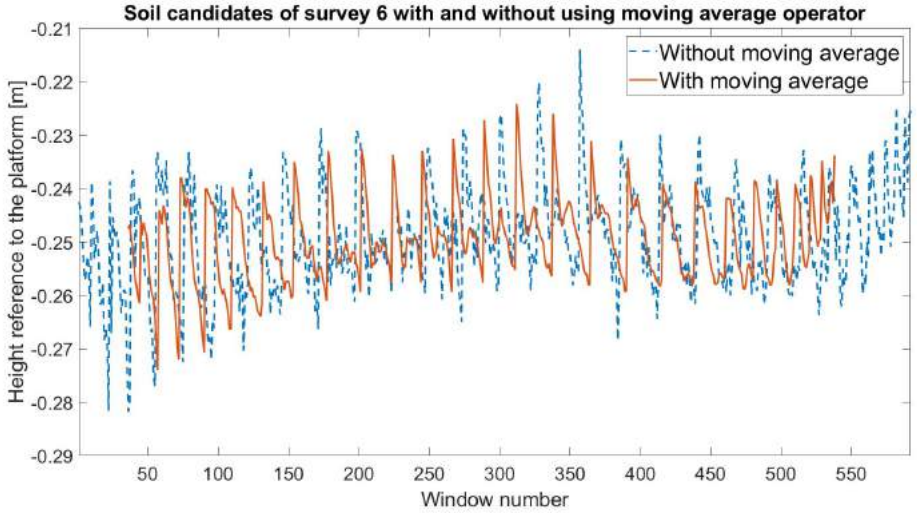

(d)

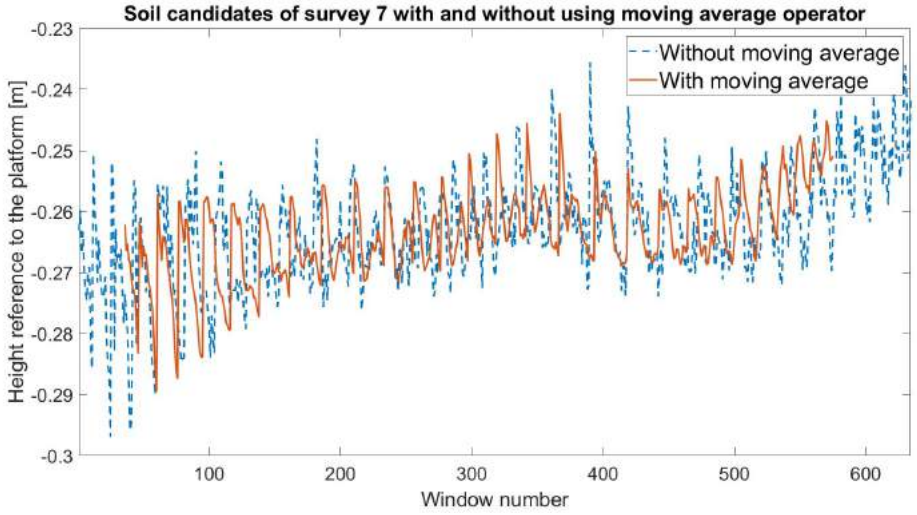

(e)

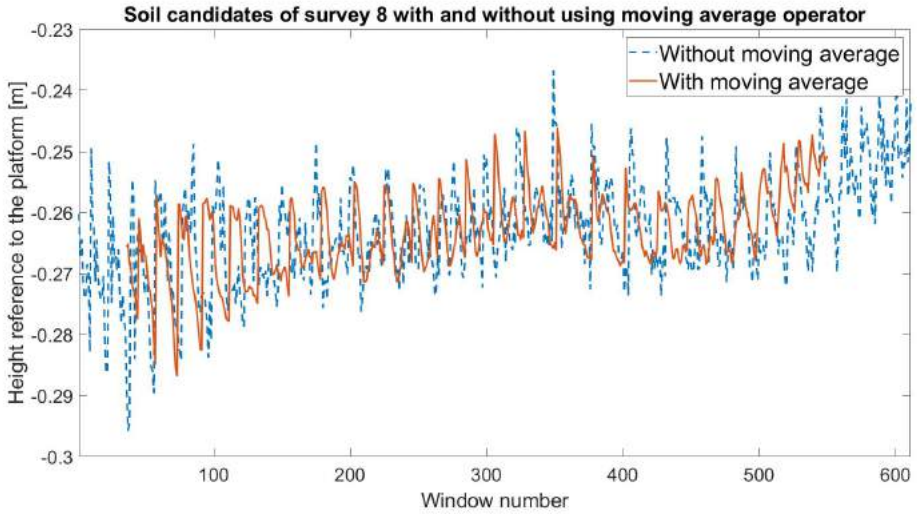

(f)

Figure C.0: Effect of moving average operator of soil candidates selection in each window of different surveys. The windows in this figure are organized by traversing every non-empty windows row by row from top to bottom (see Fig. 3.5. The height values are connected by lines in order to see the height change between two window. The red and blue lines in two figures indicate the selected soil candidates before and after using this operator respectively.

D

Pictures and point clouds of IGRS

In this appendix, field pictures of IGRS are shown in order to have a view on the environment surround each station. Corresponding to each station, a point cloud is given in $X-Z$ dimension. The combination of field picture and point cloud leads to a better understanding of the ALS measurements (points) of IGRS and ground. It is noted that the coordinates of the points are in Amersfoort / RD New - Netherlands - Holland - Dutch (EPSG:28992).

There are 25 IGRS are shown in this appendix, among 30 stations in total in Groningen area. In these IGRS, there are very few points collected on IGRS in Blijham, it is hard to distinguish platform from other objects. For the other 5 IGRS, station Eemshaven , EEXT, Ganzedijk and Haren are not visible from AHN3 as the time of installation is before AHN3 flight, thus, they are not shown here. What's more, the location of station Zernike Science Park is not known, thus, it is not studied.

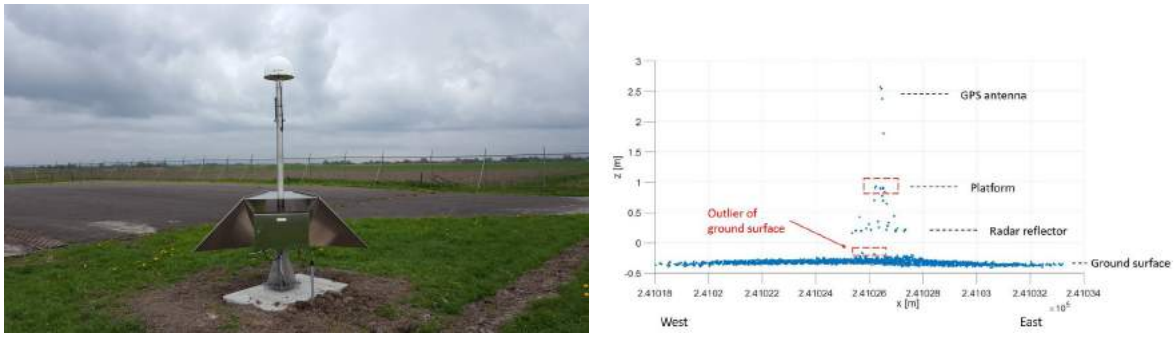

(a) (b)

Figure D.1: IGRS at Barnheem. (a) shows the picture of the station, (b) shows the point clouds of IGRS and surrounding local ground surface.

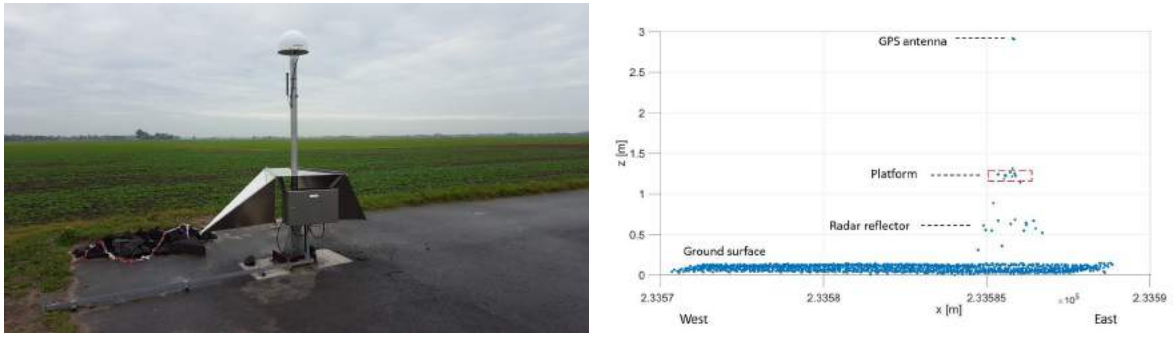

(a) (b)

Figure D.2: IGRS at Bedum. (a) shows the picture of the station, (b) shows the point clouds of IGRS and surrounding local ground surface.

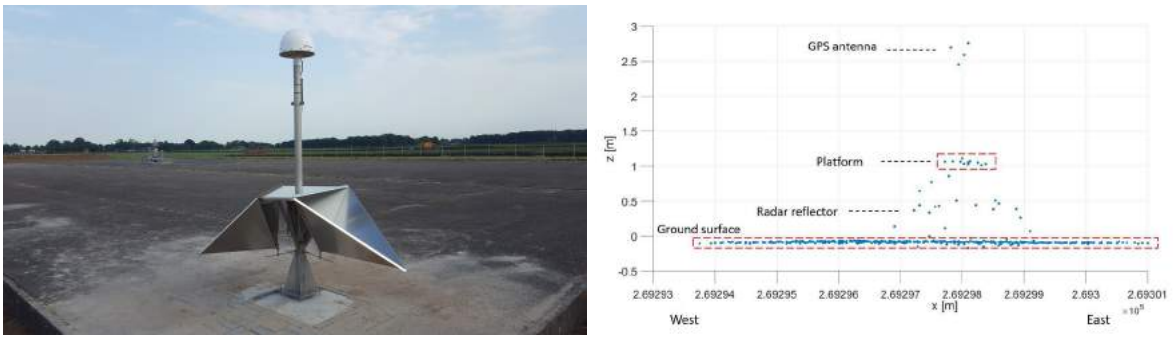

(a) (b)

Figure D.3: IGRS at Beerta. (a) shows the picture of the station, (b) shows the point clouds of IGRS and surrounding local ground surface.

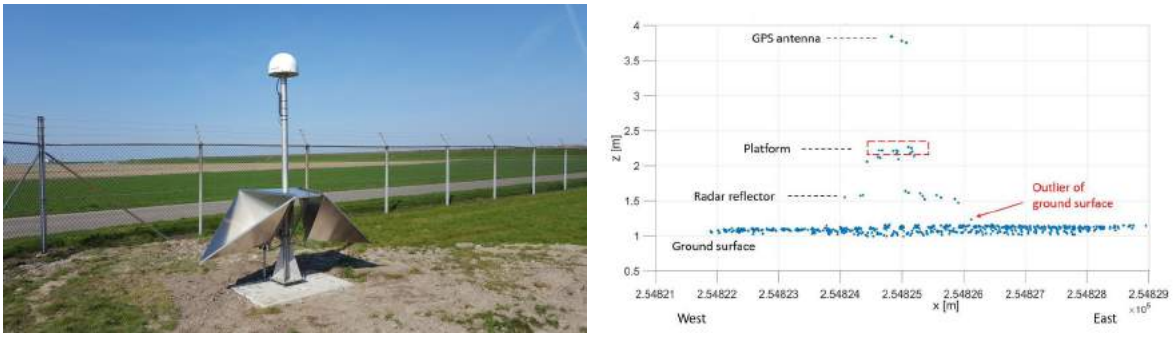

(a) (b)

Figure D.4: IGRS at Bierum. (a) shows the picture of the station, (b) shows the point clouds of IGRS and surrounding local ground surface.

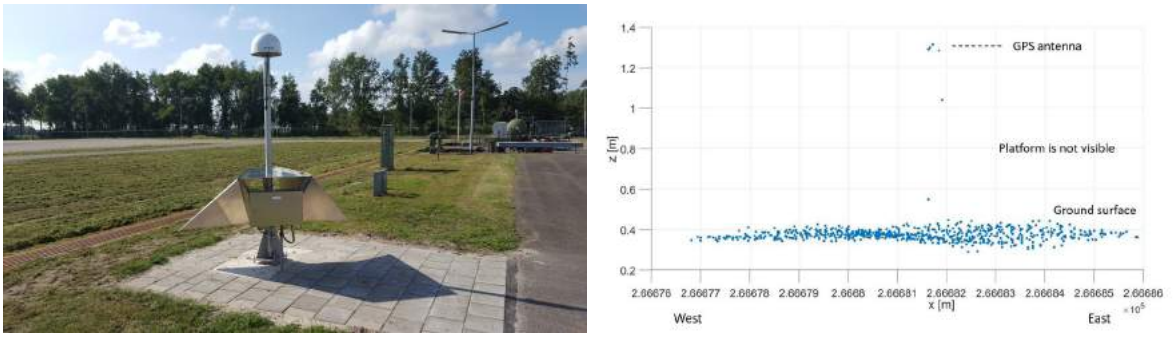

(a) (b)

Figure D.5: IGRS at Blijham. (a) shows the picture of the station, (b) shows the point clouds of IGRS and surrounding local ground surface.

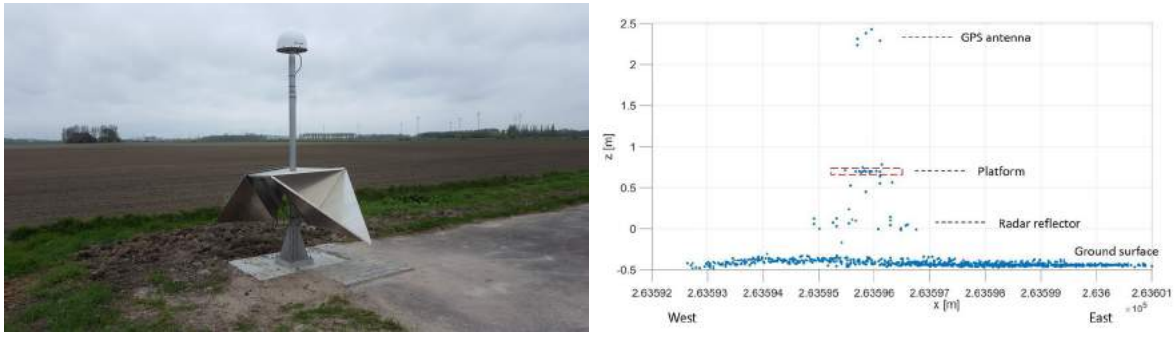

(a) (b)

Figure D.6: IGRS at Borgsweer. (a) shows the picture of the station, (b) shows the point clouds of IGRS and surrounding local ground surface.

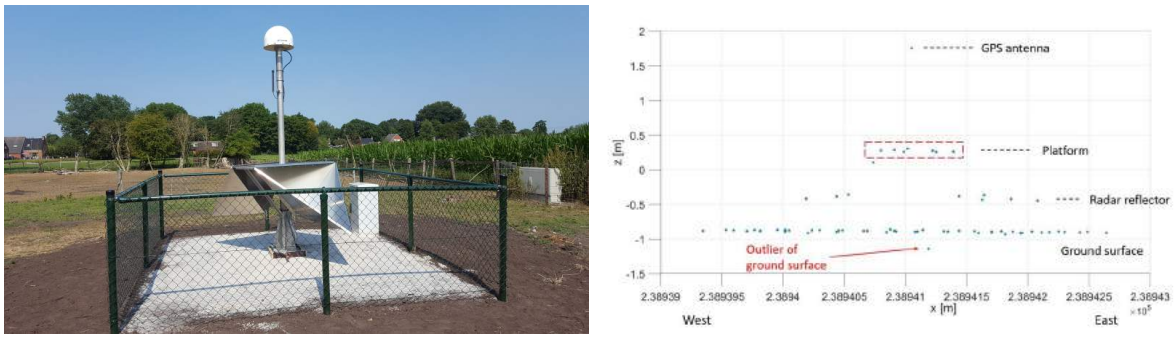

(a) (b)

Figure D.7: IGRS at Engelbert. (a) shows the picture of the station, (b) shows the point clouds of IGRS and surrounding local ground surface.

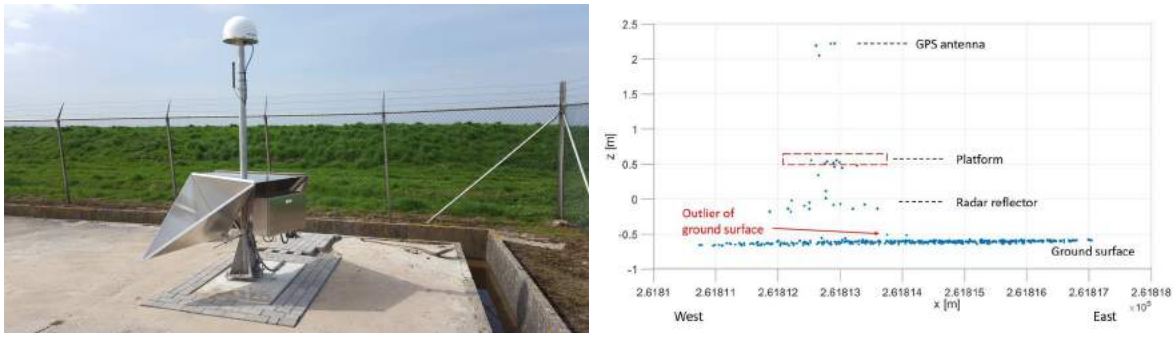

(a) (b)

Figure D.8: IGRS at Heiligerlee. (a) shows the picture of the station, (b) shows the point clouds of IGRS and surrounding local ground surface.

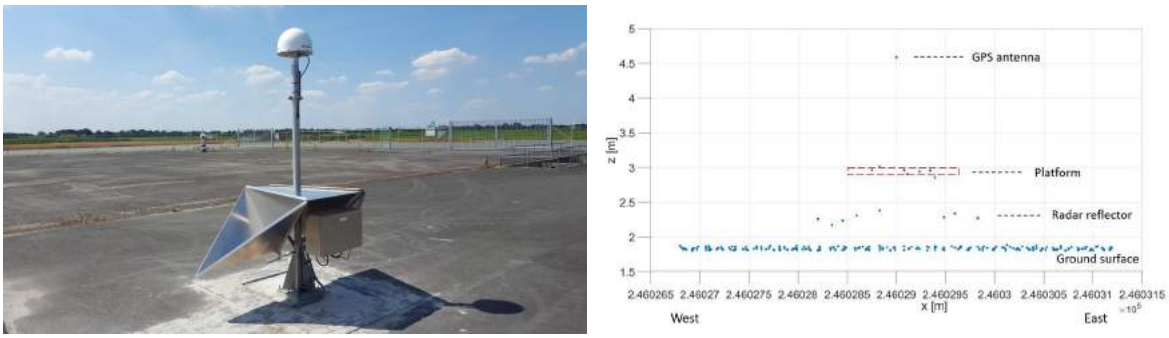

(a) (b)

Figure D.9: IGRS at Hoogezand. (a) shows the picture of the station, (b) shows the point clouds of IGRS and surrounding local ground surface.

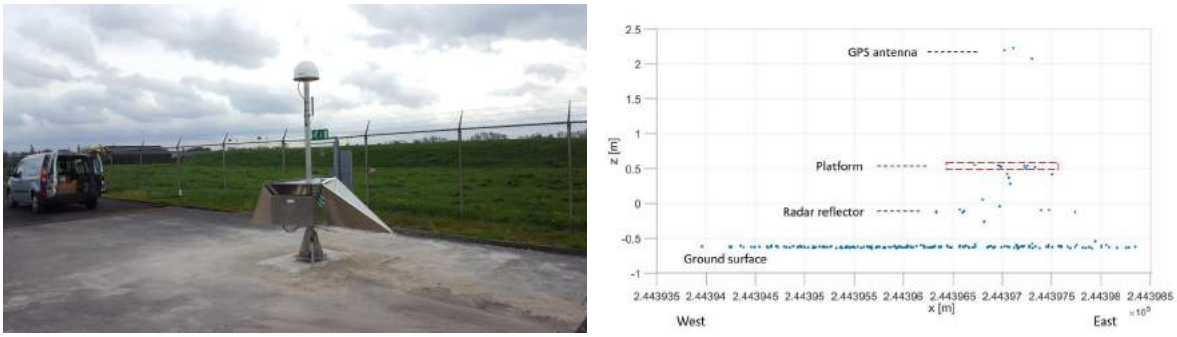

(a) (b)

Figure D.10: IGRS at Kolham-1. (a) shows the picture of the station, (b) shows the point clouds of IGRS and surrounding local ground surface.

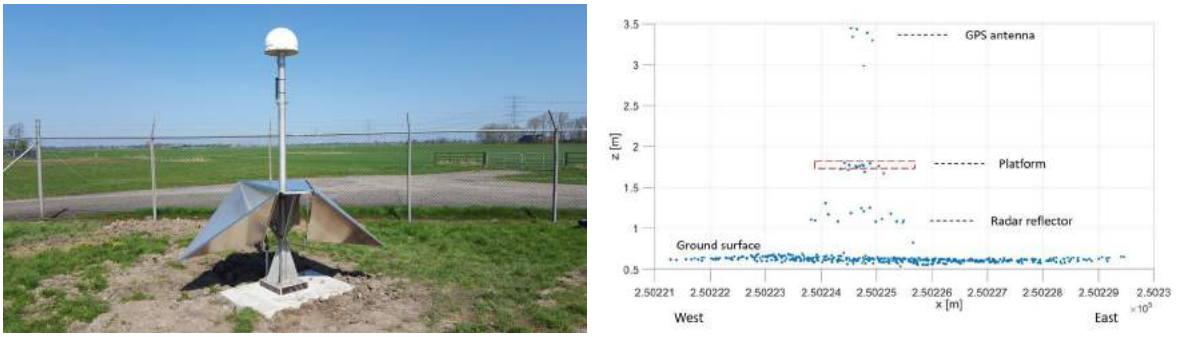

(a) (b)

Figure D.11: IGRS at Leermens. (a) shows the picture of the station, (b) shows the point clouds of IGRS and surrounding local ground surface.

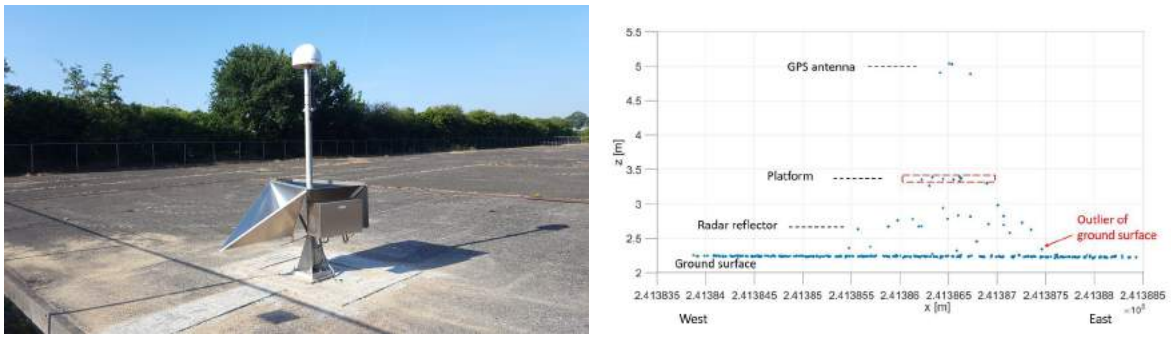

(a) (b)

Figure D.12: IGRS at Midlaren. (a) shows the picture of the station, (b) shows the point clouds of IGRS and surrounding local ground surface.

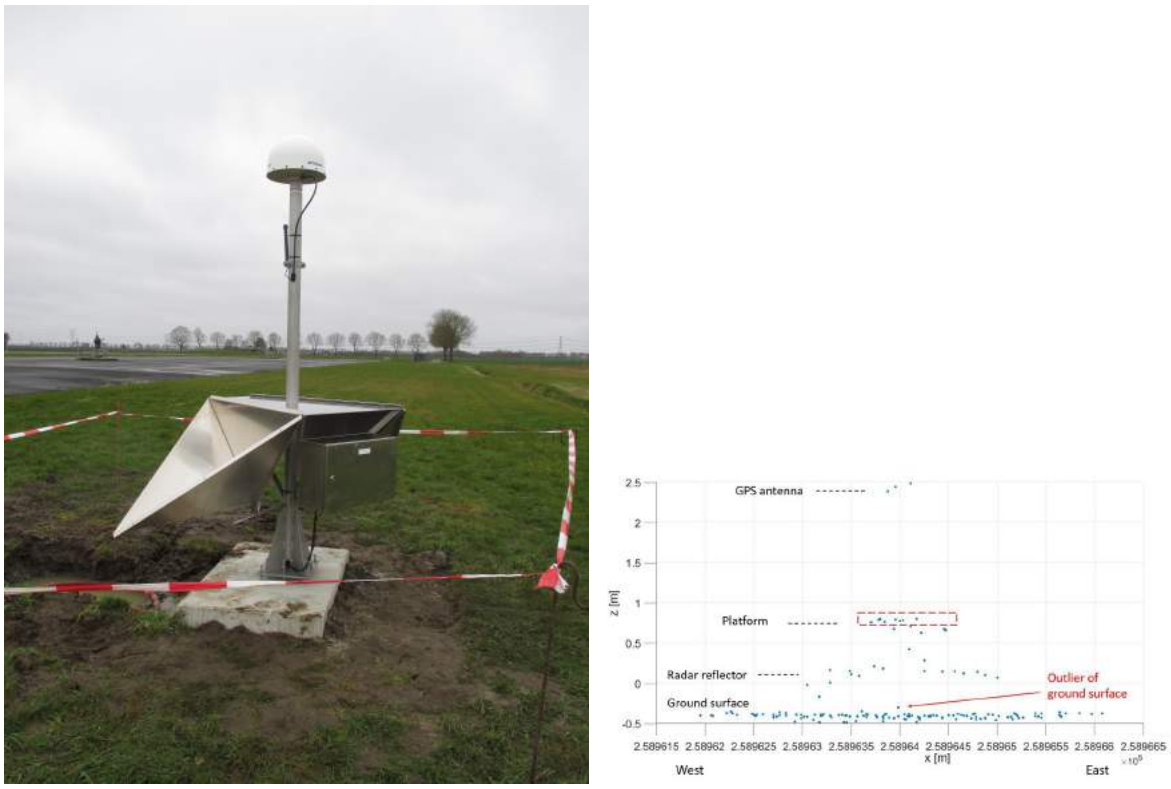

(a) (b)

Figure D.13: IGRS at Nieuw Scheemda. (a) shows the picture of the station, (b) shows the point clouds of IGRS and surrounding local ground surface.

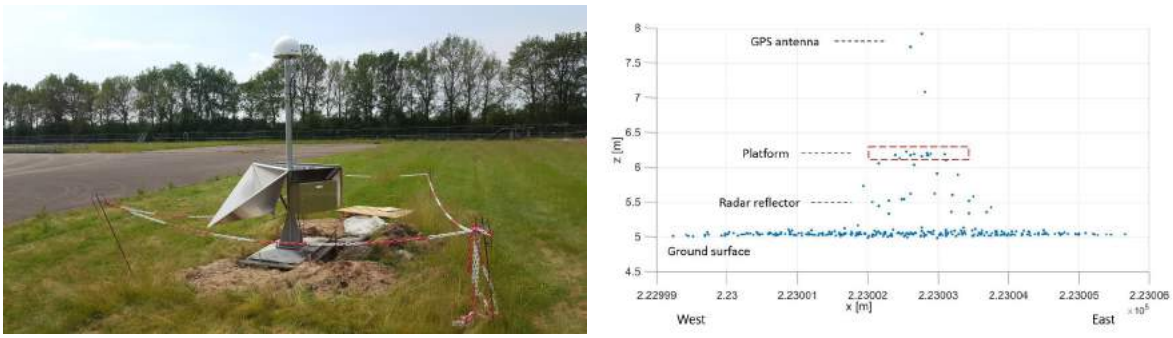

(a) (b)

Figure D.14: IGRS at Norg-3. (a) shows the picture of the station, (b) shows the point clouds of IGRS and surrounding local ground surface.

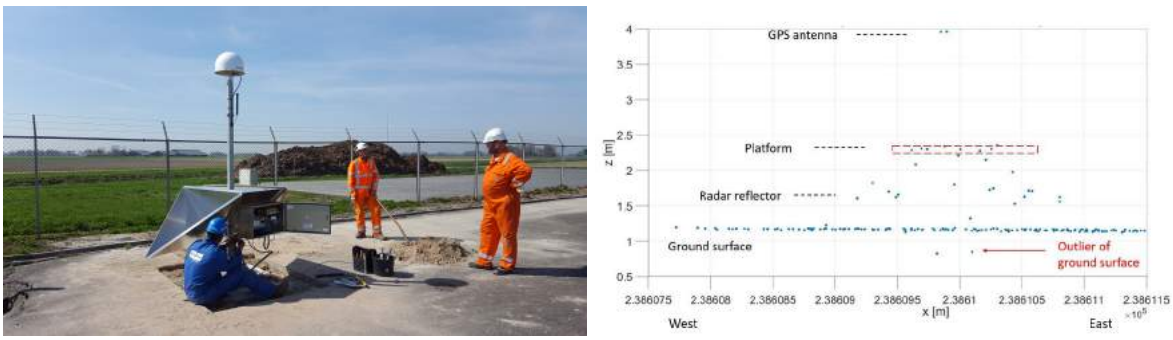

(a) (b)

Figure D.15: IGRS at Oldorp. (a) shows the picture of the station, (b) shows the point clouds of IGRS and surrounding local ground surface.

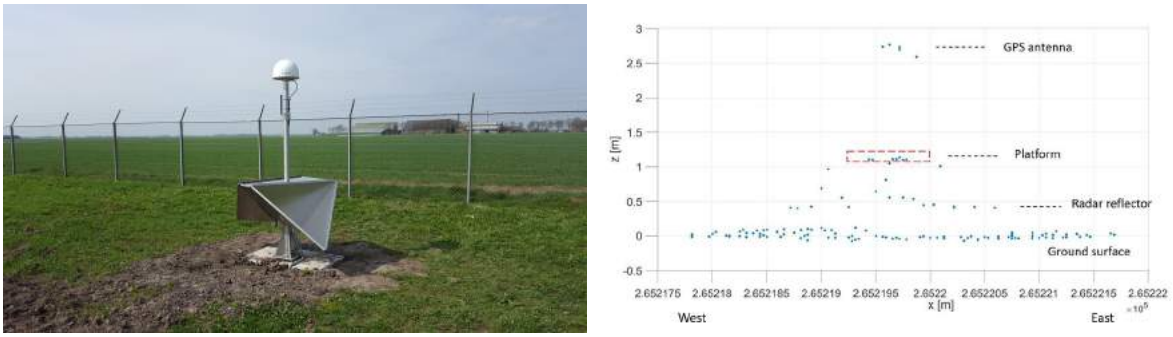

(a) (b)

Figure D.16: IGRS at Oostwold. (a) shows the picture of the station, (b) shows the point clouds of IGRS and surrounding local ground surface.

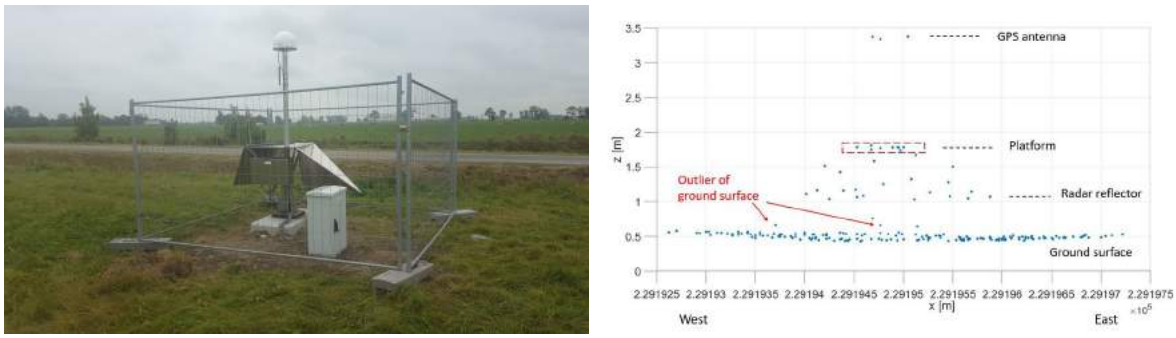

(a) (b)

Figure D.17: IGRS at Ranum. (a) shows the picture of the station, (b) shows the point clouds of IGRS and surrounding local ground surface.

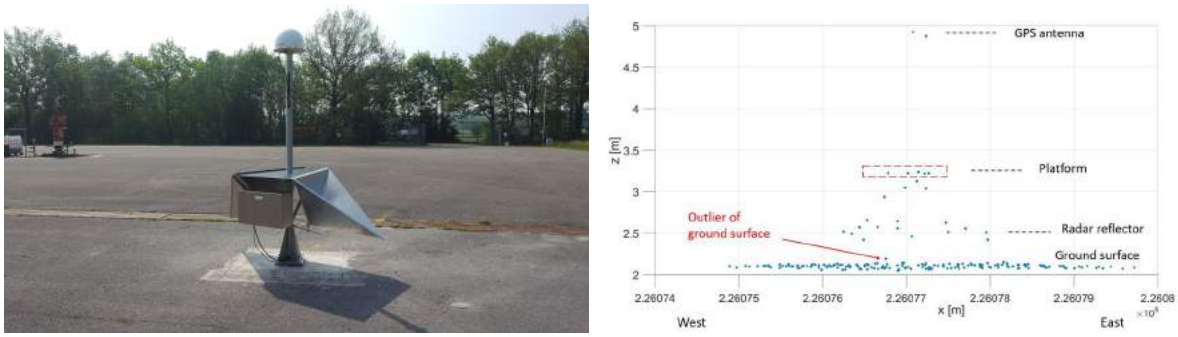

(a) (b)

Figure D.18: IGRS at Roden-1. (a) shows the picture of the station, (b) shows the point clouds of IGRS and surrounding local ground surface.

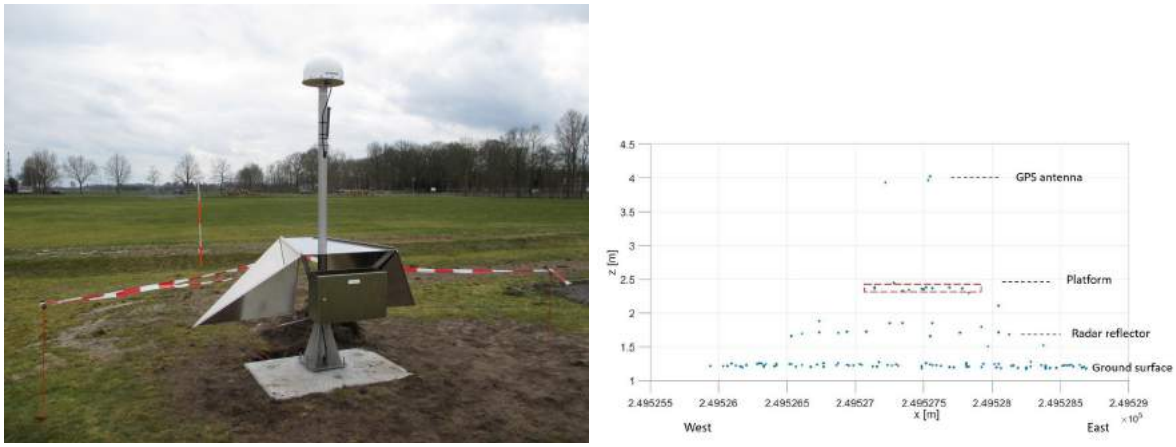

(a) (b)

Figure D.19: IGRS at Sappemeer. (a) shows the picture of the station, (b) shows the point clouds of IGRS and surrounding local ground surface.

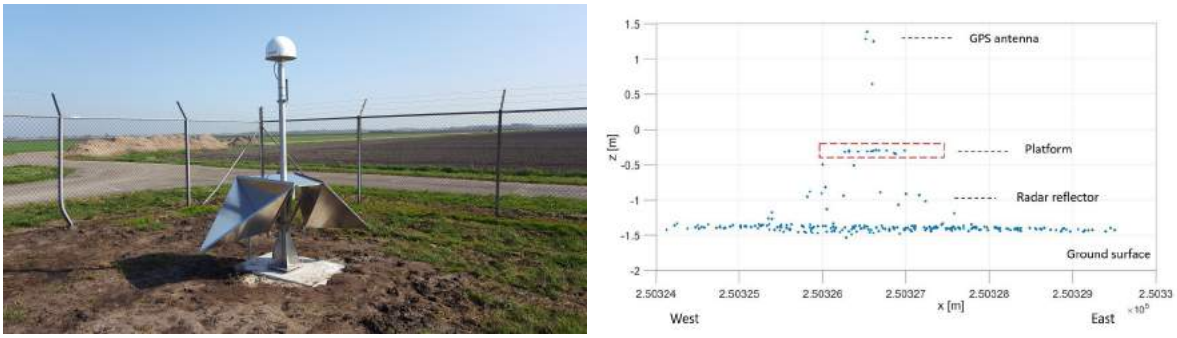

(a) (b)

Figure D.20: IGRS at Schildwolde. (a) shows the picture of the station, (b) shows the point clouds of IGRS and surrounding local ground surface.

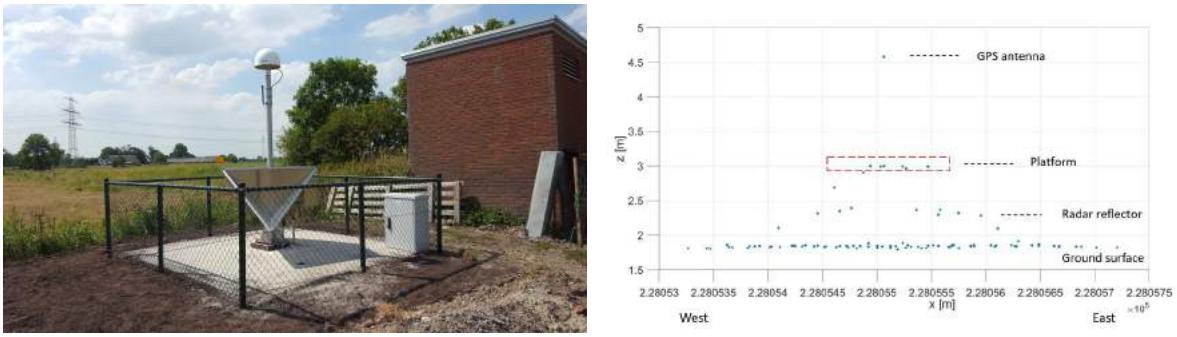

(a) (b)

Figure D.21: IGRS at Steentil. (a) shows the picture of the station, (b) shows the point clouds of IGRS and surrounding local ground surface.

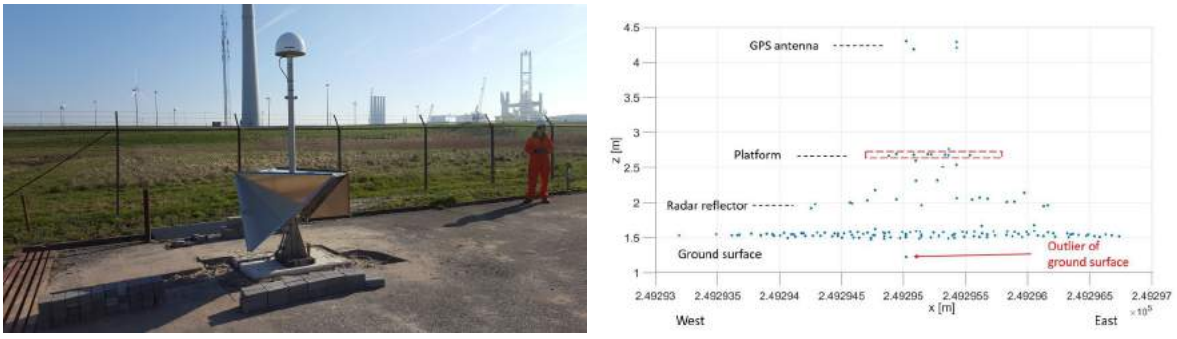

(a) (b)

Figure D.22: IGRS at Uithuizermeeden. (a) shows the picture of the station, (b) shows the point clouds of IGRS and surrounding local ground surface.

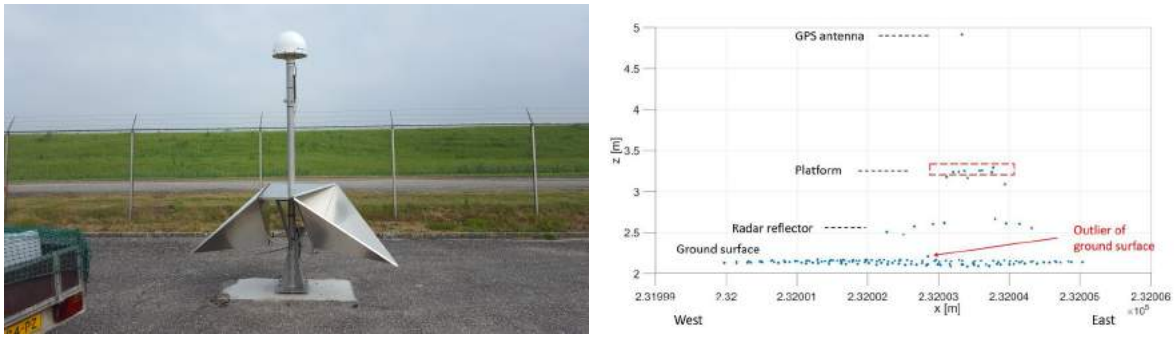

(a) (b)

Figure D.23: IGRS at Warffum. (a) shows the picture of the station, (b) shows the point clouds of IGRS and surrounding local ground surface.

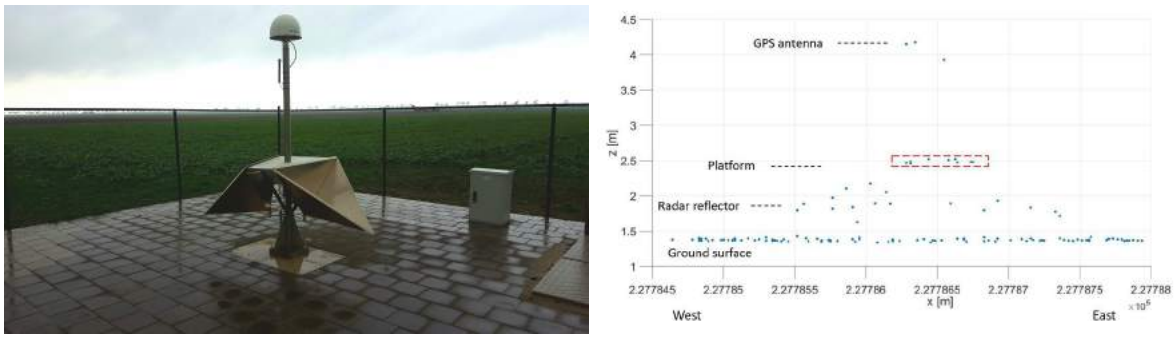

(a) (b)

Figure D.24: IGRS at Westernieland. (a) shows the picture of the station, (b) shows the point clouds of IGRS and surrounding local ground surface.

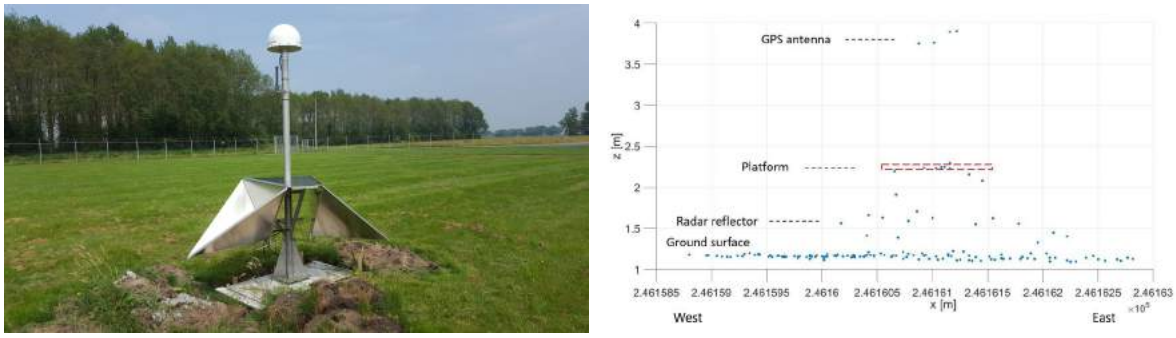

(a) (b)

Figure D.25: IGRS at Zuidlaarderveen. (a) shows the picture of the station, (b) shows the point clouds of IGRS and surrounding local ground surface.